Numerical simulation of ground surface subsidence due to coal-bed methane extraction

by Ayodeji Jayeoba

A thesis submitted in partial fulfillment of the requirements for

the degree of Doctor of Philosophy at Durham University.

Department of Earth Sciences, Durham University

April 2020

Abstract

Coal bed methane (CBM) has gained significant attention as a source of natural gas. CBM recovery is achieved through either primary production or enhanced CBM production, the later of which remains at an infant stage. Primary CBM extraction involves production of CBM reservoir fluids using production wells to facilitate pressure drawdown within the targeted formation. De-pressurization is required to release adsorbed methane within the interior surface of the coal matrix. However, de-pressurization can cause compaction within the CBM reservoir, especially in the vicinity of production wells. This, in turn, can lead to ground surface subsidence.

The objective of this project is to develop a semi-analytical solution to explore ground surface subsidence above CBM extraction wells. To achieve this, an existing analytical solution, for ground surface subsidence above a cylindrical uniform pressure change, is extended to allow for a non-uniform pressure distribution using the principle of superposition. The non-uniform effective pressure to drive the semi-analytical solution for ground surface subsidence is derived from a numerical fluid flow model describing water and methane production from a CBM formation, also developed as part of this project.

The numerical fluid flow model describes two-phase fluid flow (gas and water) in porous media in conjunction with non-equilibrium gas adsorption and stress dependent porosity and permeability. The resulting set of partial differential equations is solved using the method of lines by discretising in space using finite difference and then solving the resulting set of coupled non-linear ordinary differential equations (ODE) using MATLAB's ODE solver, ODE15s. The numerical fluid flow

model was verified by comparison with published modeling results from the literature. As a further verification, the model's ability to simulate field production and pressure data was demonstrated using field data from a CBM case study in the US.

The potential role of initial water saturation on ground surface subsidence was investigated by studying the associated spatial distributions of fluid pressure. It was found that, for a given time, the mean fluid pressure within the reservoir reduces with increasing initial water saturation. However, the spatial distribution of fluid pressure, for a given volume of produced gas, was found to be insensitive to initial water saturation. This can be attributed to the fact that the volume of water stored in the cleats of the coal-bed is very small as compared to the volume of gas stored within the coal matrix. Consequently, the presence of water in the cleats was found to have no influence on ground surface subsidence for a given gas production volume.

It was also found that ground surface subsidence for a given gas production volume is insensitive to initial coal permeability and cleat volume compressibility. A simplified analytical solution for ground surface subsidence was derived assuming that the pressure distribution within the reservoir is uniform. Sensitivity analysis showed that the simplified analytical solution is effective at predicting ground surface subsidence for a given gas production volume, predicted by the numerical model, for all of the scenarios studied. This suggests that pressure distribution within a CBM reservoir is not important for determining ground surface subsidence in this context.

Contents

List of Figures

List of Tables

Declaration

I declare that this thesis, presented for the degree of Doctor of Philosophy at Durham University, is the result of my own original research and has not been previously submitted to Durham University or any other institution.

The COMSOL simulation used for the verification of the semi-analytical model developed in chapter 4 was performed by Dr. Tore Bjornara of the Norges Geotekniske Institutt (NGI), Oslo, Norway.

Ayodeji Jayeoba

Durham University

August 2019

Acknowledgments

Without the support and influence of many other individual, this work would not have been possible. My huge thanks go to my supervisors, Prof. Simon Mathias, Prof. Stefan Nelsen and Prof. Jon G. Gluyas for giving me the opportunity to do this project and also providing me their invaluable guidance and time during my research work. They showed immense patience while I was developing my knowledge curve and gave me liberty to make mistakes so that I can express my thought more freely and with more confidence. Their passion for scientific research and their availability have been very important to the completion of the present work. As mentors and consistent source of intriguing knowledge, I could not have asked for better supervisors. I also thank the family of Prof. Simon Mathias for their hospitality over the years.

I would like to express my profound gratitude to my reviewer committee members - Prof. Edward Llewellin and Prof. Jim McElwaine - for taking out time from their busy schedule to review my research work. I also want to sincerely thank Prof. Andy Alpin for his fatherly advice when the whole situation became roller coaster.

I appreciate the support of all the faculty members and staff of the department of Earth Sciences, Durham University. Special thanks to Prof. J. Van Hunen, Prof.

R.W. Hobbs, Prof. F. Worall, Dr. C. Saville and Banner Jo.

Special thanks to Dr Tore Bjornara of the Norges Geotekniske Institutt (NGI), Oslo, Norway for performing the COMSOL simulation used for the verification of the semi-analytical model developed in Chapter 4.

I would like to thank all of Simon and Stefan's PhD students I have known whilst I have been at Durham for help with my work and general chat about related and unrelated topics: Fran, Salim, Jack, Helena, Charlotte, Simon and Ayu.

To all my fellow Nigerian students in the Department of Earth Sciences, Durham University-Munira, Kunle, Chima, Femi and Abdulwahab- I say a big thank you for your immense support, understanding and above all for providing a shoulder to lean on.

I appreciate the like of Dr Marvis Erhunmwunse, Dr Declan Amaraegbu and Mr Ehis Iredia for all their moral and financial support towards the completion of this Ph.D. programme.

Thanks also go to the friends and colleagues within and outside the Earth Sciences Department, Durham University for the memories over the years: Dawood, Nadia, Katy, Olly, Katherine, Junjie, Zeyang, Chavy, Elizabeth, Mildred, Oto Obong, and Tim of Durham University immigration office.

My sincere appreciation goes to my Dad of blessed memory and my Mum, my siblings, my wife and my children for everything you have done for me during my studies and beyond. None of this would have been possible without your continuous love and support. ***I love you all***.

Finally, I acknowledge the financial support from TETFund and University of Ibadan, Nigeria.

Dedication

To my beloved parents, ***Titus Ojo and Abigeal Ajayi***

To my wonderful wife and kids, ***Olayemi, Omodolapo, Abimbola and Shiyanbola***

Nomenclature

This is a partial list of sysmbols used in this thesis. Some sysmbols have been used to denote different things in different contexts

Greek Symbols

α Biot coefficient. [-]

$\delta(x)$ Dirac delta function. [-]

$\Delta\varepsilon_s$ Coal swelling/shrinkage strain. [-]

$\Delta\sigma$ Change in effective horizontal stress. [$ML^{-1}T^{-2}$]

ε_L Langmuir volumetric strain constant. [-]

γ A new dimensionless variable used in dimensionless transformation of equation (5.5). [-]

γ Euler-Mascheroni constant. [-]

μ Dynamic viscosity of the fluid. [$ML^{-1}T^{-1}$]

μ_g Dynamic viscosity of methane in the cleats. [$ML^{-1}T^{-1}$]

μ_w Dynamic viscosity of water in the cleats. [$ML^{-1}T^{-1}$]

ν Poisson's ratio of the coal matrix. [-]

ϕ Fracture porosity of the CBM reservoir/ aquifer porosity. [-]

ϕ_I Initial porosity. [-]

ρ Density of fluid. [ML^{-3}]

ρ_c Density of coal-bed reservoir. [ML^{-3}]

ρ_g Methane density in the cleats. [ML^{-3}]

ρ_w Density of water in the cleats. [ML^{-3}]

ρ_{g0} Density of methane at standard conditions. [ML^{-3}]

ρ_{wI} Density of water when $P = P_I$. [ML^{-3}]

τ_j Stress distribution due to non-uniform pressure distribution. [$ML^{-1}T^{-2}$]

$\tau_{\theta\theta}$ Normal total stress distribution in the angular direction. [$ML^{-1}T^{-2}$]

τ_{rr} Normal total stress distribution in the radial direction. [$ML^{-1}T^{-2}$]

τ_{rz} Tangential stress distribution. [$ML^{-1}T^{-2}$]

τ_{zz} Normal total stress distribution in the vertical direction. [$ML^{-1}T^{-2}$]

$\tilde{\tau}_j$ Stress distribution due to uniform pressure distribution. [$ML^{-1}T^{-2}$]

$d\tau$ The incremental volumetric stress. [$ML^{-1}T^{-2}$]

$d\varepsilon_{\mathbf{s}}$ The incremental sorption-induced volumetric strain. [-]

$d\varepsilon$ The incremental volumetric strain. [-]

Latin Symbols

E Young's modulus of the coal matrix/ aquifer. [$\mathrm{ML}^{-1}\mathrm{T}^{-2}$]

m Power-law exponent for the water phase. [-]

n Power-law exponent for the gas phase. [-]

$\hat{P}$ Mean fluid pressure. [$\mathrm{ML}^{-1}\mathrm{T}^{-2}$]

$\mathbf{I}$ Identity matrix. [-]

$\mathrm{Ei}(x)$ Exponential integral function. [-]

$\tilde{u}_j$ Displacement due to uniform pressure distribution. [L]

$\tilde{w}$ Ground surface subsidence due to uniform pressure distribution. [L]

c_c Coal-bed compressibility. [$\mathrm{M}^{-1}\mathrm{LT}^2$]

c_f Cleat volume compressibility. [$\mathrm{M}^{-1}\mathrm{LT}^2$]

c_g Methane compressibility. [$\mathrm{M}^{-1}\mathrm{LT}^2$]

C_m Vertical (oedometric) bulk compressibility as measured in an oedometer with lateral expansion. [$\mathrm{M}^{-1}\mathrm{LT}^2$]

c_w Compressibility of the water. [$\mathrm{M}^{-1}\mathrm{LT}^2$]

D Depth of the center of the aquifer from the ground surface. [L]

D_A Apparent diffusion coefficient. [$\mathrm{L}^2\mathrm{T}^{-1}$]

$F(x)$ Heaviside step function. [-]

g Acceleration due to gravity. [LT^{-2}]

H Thickness of coal-bed methane reservoir/ thickness of the aquifer. [L]

$IGIP$ Initial gas in place. [Mscf]

j Relates to direction where r represents radial direction and z represents vertical direction. [L]

K Bulk modulus of the rock. [$ML^{-1}T^{-2}$]

k Coalbed methane reservoir/ aquifer permeability. [L^2]

K_f Bulk modulus of the fluid. [$ML^{-1}T^{-2}$]

k_I Initial coal permeability. [L^2]

k_{rg0} End-point relative permeability of gas. [-]

k_{rg} Relative permeability of gas. [-]

k_{rw0} End-point relative permeability of water. [-]

k_{rw} Relative permeability of water. [-]

L Cleat spacing. [L]

M Molar mass of methane. [kg mol^{-1}]

M_c Mass of the coalbed. [M]

N Number of nodes node. [-]

P Reservoir pressure. [$ML^{-1}T^{-2}$]

P_I Initial reservoir pressure. [$ML^{-1}T^{-2}$]

P_i Uniform initial pressure of the aquifer prior to fluid production. [$ML^{-1}T^{-2}$]

p_I A dimensionless form of initial reservoir pressure. [-]

P_L Langmuir pressure constant. [$ML^{-1}T^{-2}$]

P_m Pressure in coal matrix. [-]

P_s Effective pressure that accounts for both the pore-pressure and the swelling strain associated with methane adsorbtion. [$ML^{-1}T^{-2}$]

$P_{L,\varepsilon}$ Langmuir pressure constant for coal swelling strain. [$ML^{-1}T^{-2}$]

$p_{L,\varepsilon}$ A dimensionless form of Langmuir constant. [-]

P_w Bottom-hole pressure. [$ML^{-1}T^{-2}$]

Q Constant fluid production rate. [L^3T^{-1}]

q_g Volumetric flux of methane. [LT^{-1}]

Q_w Volumetric rate of gas production at standard conditions. [L^3T^{-1}]

q_w Volumetric flux of water. [LT^{-1}]

R Radius of the reservoir/ radial extent of the aquifer. [L]

r Radius distance from the production well. [L]

r_e Radius of influence of the production well. [L]

R_g Gas constant. [Nm $mol^{-1}K^{-1}$]

r_i The value of r at the ith node. [L]

r_w Well radius. [L]

S Specific storage coefficient of the aquifer. [$M^{-1}LT^2$]

s Drawdown of the piezometric surface within the aquifer. [L]

s Mass of adsorbed methane per unit mass of coal-bed. [-]

S_g Volume fraction of the fracture porosity containing methane (Gas saturation). [-]

S_w Volume fraction of the fracture porosity containing water (Water saturation). [-]

S_{gc} Critical gas saturation. [-]

S_{wI} Initial volume fraction of water in fracture porosity. [-]

S_{wr} Residual water saturation. [-]

T Temperature of the CBM reservoir. [K]

t Time. [T]

t_c Characteristic time. [T]

t_r Mass transfer coefficient. [T]

u_j Displacement due to non-uniform pressure distribution. [L]

u_r Displacement in the radial direction. [L]

u_z Displacement in the vertical direction. [L]

V_g Volume of gas produced. [L^3]

v_g A dimensionless form of volume of gas produced. [-]

V_L Langmuir volume constant. [$M^{-1}L^3$]

w Subsidence at the surface directly above the production well. [L]

w Ground surface subsidence due to non-uniform pressure distribution. [L]

w_D A dimensionless form of ground surface subsidence above the production well. [-]

Chapter 1

Introduction

1.1 Coal-bed methane extraction

The commercial development of coal-bed methane (CBM) arguably started in United States of America during the early 1980s following the energy crises of the 1970s (Hamawand et al., 2013). CBM extraction has since gathered momentum worldwide and is now widely considered to be a commercially well established valuable source of energy. CBM is particularly important in the US, Australia, Canada, China, India and Russia.

CBM reservoirs are classified as unconventional gas reservoirs. Although procedures required for CBM reservoir development are similar to those associated with conventional gas reservoirs, CBM reservoirs are distinct because they serve as both the source rock and the reservoir rock (similar to shale gas reservoirs). CBM reservoirs also exhibit unconventional fluid flow behavior due to the coal shrinkage effects associated with gas desorption (Harpalani and Chen, 1995; Levine, 1996; Robertson and Christiansen, 2006; Mitra et al., 2012). As will subsequently be de-

scribed in more detail, coal shrinkage leads to an increase in formation permeability with continued pressure depletion and gas production, and therefore CBM reservoirs commonly exhibit a "negative" declining trend (Liu and Harpalani, 2014). Gas desorption induced coal shrinkage also leads to an additional volumetric strain. Therefore, geomechanical processes associated with CBM extraction are unconventional as well.

CBM extraction results in a reduction in the reservoir pressure. This decrease in pressure is referred to as a depletion response (Addis, 1997). Reservoir depletion is an important component of standard CBM extraction, which involves de-pressurization of CBM reservoirs. De-pressurization leads to desorption of adsorbed gas as well as coal shrinkage, which, in turn, leads to volumetric reduction of the reservoir rock.

A procedure for CBM recovery enhancement includes CO_2 and/or N_2 co-injection (Mazzotti et al., 2009). In this technique, methane desorption occurs due to competitive adsorption of CO_2 and/or N_2 on the surface area of coal particles within the coal mineral. Because CO_2 and N_2 are preferentially adsorbed to the surface of coal particles compared to CH_4, injection of CO_2 and/or N_2 leads to CH_4 desorption without the need for pressure depletion. Enhanced CBM recovery is not yet a mature technology, in spite of the increasing number of pilot and field test worldwide that have shown its potential and technical challenges (Gunter et al., 2005; Reeves, 2005; Van Bergen et al., 2006; Wong et al., 2006; Yamaguchi et al., 2006; Li and Fang, 2014). A potential consequence of pressure depletion driven CBM production is ground surface subsidence above and around CBM production wells. This thesis focuses on the mathematical modeling of ground surface subsidence due to

pressure depletion CBM extraction.

1.2 Problem statement

CBM reservoirs are unconventional reservoirs in that they play the role of both source rock and reservoir formation. Coal formations are frequently intersected by a network of orthogonal fractures, referred to as cleats (Laubach et al., 1998). Coal formations are therefore often conceptualized as a dual-porosity system with a primary porosity (micropores) associated with the coal matrix and a secondary porosity (macropores) associated with the cleat system (fractures). The matrix domain provides a large internal surface area with a strong affinity for specific gases, such as methane, ethane, and carbon dioxide (Pillalamarry et al., 2011).

The fracture domain surrounds the matrix blocks of CBM reservoirs and provides the flow paths for CBM to production wells (Fig. 1.1) (Laubach et al., 1998; Liu et al., 2011). Gas flow in the fractures is generally assumed to be controlled by Darcy's law. In contrast, gas migration in the matrix is assumed to be controlled by Fick's law of diffusion.

The dominant gas storage mechanism in a CBM reservoir is adsorption, and CBM is produced by reducing pore pressure through groundwater production (Pashin, 2007; Moore, 2012). During the removal of CBM and groundwater, the pressure depletion creates an increase in the effective stress and a decrease in fracture permeability (Moore, 2012) due to the loss of fluid in the pores and cleats. The reduction in the fracture permeability has a net effect of reducing the gas flow (Seidle et al., 1992; Palmer and Mansoori, 1996; Cui and Bustin, 2005; Shi and Durucan, 2005; Moore, 2012). Similarly, the decline in pore-pressure causes the reservoir pressure

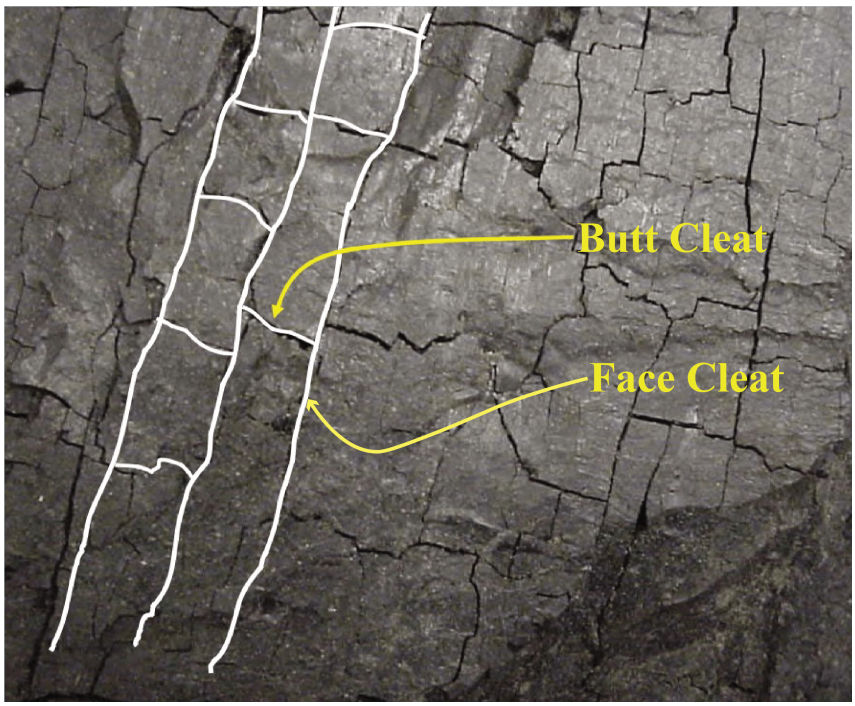

Figure 1.1: A picture of coal sample showing the face and the butt cleats. The face cleat is longer and continuous than the butt cleat. (Adapted from Underground COAL (2013))

.

to reduce more than the surrounding geological formations, which leads to a strain disparity. This causes the reservoir formation to compact more than the surrounding rocks, thereby increasing the stress on the solid skeleton (Segall, 1992).

However, the desorption of CBM within the coal matrix causes matrix shrinkage, which favours the opening of open-mode fractures, with resultant effect resulting in increased cleat porosity and formation permeability. With continued production, there is an associated gas pressure reduction, which, in turn, leads to changes in the stress environment in the reservoir. Researchers have reported a decrease of horizontal stress in CBM reservoirs due to reservoir pressure drawdown (Mitra et al., 2012; Liu and Harpalani, 2013; Singh, 2014). The rate of decline has been ob-

served to be 50% higher than the corresponding drop in pore pressure (Saurabh et al., 2016). A considerable amount of theoretical and experimental work has been undertaken to derive permeability-effective stress relationships to be used in numerical reservoir simulation software for CBM extraction (Harpalani and Schraufnagel, 1990; Levine, 1996; Gu and Chalaturnyk, 2006; Moore, 2012).

Permeability-effective stress relationships associated with CBM imply that fluid flow in a CBM reservoir is strongly coupled with associated geomechanical processes (Connell, 2009). That is, fluid pressure drawdown leads to an increase in the effective stress, which in turn, results in a reduction in the pore volume of the CBM reservoir. This reduction leads to a decrease in the fracture domain permeability, which in turn will affect fluid movement. This direct fluid-to-solid hydromechanical coupling is particularly evident when considering ground surface subsidence initiated by underground fluid extraction (Rutqvist and Stephansson, 2003).

Conversely, the matrix domain shrinks with gas desorption, thereby imposing an additional volumetric strain on the poroelastic behavior of the CBM reservoir (Levine, 1996). A significant increase in coal permeability during CBM reservoir depletion is sometimes followed by a sudden decrease in coal permeability, which is accompanied by the production of coal fines (Okotie and Moore, 2011; Moore et al., 2011). A common cause of coal fine production is due to anisotropy and shearing in the vicinity of uncased wells or perforations due to loss of radial support (Espinoza et al., 2015). This is because, under the well-accepted uniaxial strain conditions in CBM reservoirs, a significant decrease in horizontal stress results in anisotropic loading conditions of coal and ultimately failure (Singh, 2014; Espinoza et al., 2015).

The reduction in horizontal stress as a result of continuous CBM production may lead to shear failure within a CBM reservoir (Liu and Harpalani, 2014). During the CBM reservoir drawdown, the effective vertical stress increases, especially for deeper coals, which are subjected to significant vertical stresses while the effective horizontal stresses decrease. This, in turn, leads to a highly anisotropic stress loading condition, which is conducive to shear failure of the CBM reservoir (Saurabh et al., 2016). Consequently, the outcome of the two primary phenomena that control the internal framework of the CBM reservoirs, that is, pore pressure drawdown and gas desorption, may lead to rock structure deformation within and around the reservoir formation. Rock structure deformation may lead to significant ground surface subsidence due to the relatively shallow depths of many CBM reservoirs ($<$ 1000 m).

The concept and requirement of subsidence due to CBM extraction is somewhat in contrast to that of subsidence as a result of coal mining. While the removal of CBM involves extensive depressurization of a CBM reservoir, which may cover a large area, the depressurization generated from dewatering in most coal mining operations is mainly focused around the mine. Also, subsidence associated with CBM extraction is a function of depressurization and the matrix compressibility of the CBM reservoir and adjoining formations (Freij-Ayoub, 2012; Moore, 2012; Nelson, 2000). However, coal mining-induced subsidence is also strongly influenced by the physical collapse of strata at depth (Shen et al., 2010; Nelson, 2000; Poulsen and Shen, 2013).

Interestingly, published discussions on the environmental effects of CBM production mostly focus on issues associated with chemical interaction between co-

produced water and groundwater aquifers. The reviews of these articles centre on the quality of CBM co-produced water (Rice et al., 2002; McBeth et al., 2003; Jackson and Reddy, 2007; Dahm et al., 2011), the effect of coal-bed methane discharge water on vegetation and soil ecosystem (Stearns et al., 2005; Hamawand et al., 2013) and the management of the CBM co-produced water (Frost et al., 2002; Patz et al., 2004; Nghiem et al., 2011; Jackson et al., 2013). Other areas of interest include CBM well failure and methane leakage from CBM reservoirs (Okotie and Moore, 2011; Liu et al., 2012) and the effect of artificial hydraulic fracturing on adjacent horizons (Mooney, 2011; Bishop et al., 2012). However, little attention is given to the possible risks associated with subsidence due to CBM production (Pitman et al., 2003; Batley and Kookana, 2012; Hamawand et al., 2013).

Thus far, there has been no report of ground surface subsidence resulting from CBM production. Consequently, our fundamental understanding of the practical and technical risks posed by CBM production and uncertainties associated with ground surface subsidence due to CBM production remains rudimentary (Commonwealth of Australia, 2014a). Nevertheless, recent numerical work has indicated that CBM production may lead to possible ground surface subsidence problems in the future (Fanchi, 2002; Chamani and Rasouli, 2011; Freij-Ayoub, 2012; Brown et al., 2014; Commonwealth of Australia, 2014a; Wu et al., 2018a).

Therefore, all the relevant aspects of fluid flow processes in CBM reservoir (two-phase fluid flow, non-equilibrium sorption gas adsorption, and stress-dependent porosity, and permeability) must be taken into account during the development of a suitable performance assessment tools that describes the behaviour of the CBM reservoir and its surrounding geological layers during CBM production.

1.3 Ground surface subsidence due to fluid withdrawal from subsurface

Ground surface subsidence can be caused by both natural and anthropogenic activities (ground fluids withdrawal, excavation, indirect factors, e.t.c.), but the impacts of both occur at different time and spatial scales. While natural subsidence is a relatively slow phenomenon, anthropogenic related subsidence is typically much faster (Nauroy, 2011).

Subsidence as a result of fluid withdrawal from reservoirs/aquifers is an issue of great significance in environmental geosciences and environmental geomechanics. The extraction of groundwater can aggravate the issue of subsidence without prior consideration of aquifer recharge and the challenges associated with climate change (Selvadurai and Kim, 2015). Ground surface subsidence resulting from fluid extraction have been observed and reported (Hu et al., 2004) with examples abound in the literature (Poland and Davis, 1969; Gambolati, 1972; Saxena, 1979; Harada and Yamanouchi, 1983; Poland, 1984; Hsi and Small, 1992; Forth, 2004; Phien-Wej et al., 2006; Calderhead et al., 2011; Mahmoudpour et al., 2016; Gambolati and Teatini, 2015).

The process of fluid extraction to the manifestation of ground surface subsidence is a complicated process influenced by a large number of factors including the amount of fluid extracted, the pore pressure decline, size and depth of the exploited aquifer/reservoir, volume, compressibility and permeability of the pumped aquifer/reservoir, and geomechanical properties of the formation and the overburden, and coupling between flow and stress that develop within the aquifer/reservoir

(Rutqvist and Stephansson, 2003; Teatini et al., 2011). When fluid is produced from a confined aquifer, the fluid pressure continually reduces as production progresses. The depletion of fluid pressure during fluid extraction transfers the stress relief in the pore fluid pressures to the deformable porous skeleton (solid phase). This leads to an increase in effective stress within the aquifer, which in turn may lead to compaction of the aquifer, which can subsequently translate to ground surface subsidence (Gambolati et al., 2005; Galloway and Burbey, 2011; Loáiciga, 2012; Pujades et al., 2017).

Subsidence has become a growing concern worldwide as a result of its potential impact on natural resources, infrastructure, and environment (Gambolati et al., 2005; Galloway and Sneed, 2013). Consequently, studying and predicting subsidence due to fluid extraction is imperative to forestall the destructive potential of subsidence and its occurrences. It will also enable the specification of suitable constraints to aid the sustainable use of subsurface fluids.

Terzaghi (1925) was the first to develop a coupled diffusion-deformation model with an application to one-dimensional soil consolidation. Biot (1941) extended Terzaghi's model to a general theory of a three-dimensional coupled poroelastic system to describe the dynamics of flow in porous media. The model coupled a flow-diffusion equation for the interstitial fluid with a stress equilibrium equation for the porous medium. The model recognizes consolidation as a direct response of a compressible porous medium to a change in the fluid flow operating within it (Gambolati et al., 2005). Since then, several numerical simulations have been developed to better understand ground surface subsidence due to fluid withdrawal from the subsurface (Sandhu and Wilson, 1969; Christian and Boehmer, 1970; Hwang et

al., 1971; Gambolati and Freeze, 1973; Gambolati et al., 1991; Small et al., 1976; Lewis and Schrefler, 1978; Hsi and Small, 1992; Hsi et al., 1994; Lewis and Schrefler, 1998; Gambolati et al., 2005; Gambolati and Teatini, 2015).

For instance, a coupled three-dimensional three-phase fluid flow and geomechanical model for simulating a deformable saturated oil reservoir was developed by Lewis and Sukirman (1994) to study ground surface subsidence above a compacting hydrocarbon reservoir. Chen et al. (2003) proposed a coupled three-dimensional groundwater flow and soil consolidation model to investigate the mechanisms of ground settlement. They found that excessive groundwater withdrawal may not only lead to ground settlement but also have an adverse effect on sustainable water resources of deeper aquifers. Wu et al. (2010) developed a non-linear regional ground surface subsidence model, which coupled a three-dimensional groundwater flow model and a one-dimensional vertical deformation model based on visco-elastoplastic constitutive laws. Wang et al. (2018) developed a numerical model of a coupled one-dimensional multi-layered aquifer system to simulate ground surface subsidence due to hydraulic head variation in a pumped layered aquifer.

Numerical modelling can handle complicated material rheology, reservoir geometry and structures, distribution of stress within the stratigraphy, and heterogeneity within the reservoirs and subsurface formations (Du and Olson, 2001). However, the shortcomings of numerical modeling include the effort required to adequately develop, implement, and compute complicated formulations. This, in turn, limits the conduct of more comprehensive sensitivity analysis to understand the processes involved in ground surface subsidence and the significance of each parameter for predicting ground surface subsidence.

Analytical solutions offer a more efficient but straightforward approach to estimate ground surface subsidence. It can provide satisfactory results when studying ground surface subsidence (Verruijt, 1969), if the linear poroelasticity theory is appropriate to describe the study area (Ketelaar, 2009). The advantages of this approach are that they require fewer physical parameters and less data to be determined, they allow a more intuitive understanding to be developed, and they are computationally less laborious as compared to numerical counterparts (Du and Olson, 2001).

McCann and Wilts (1951) developed an analytical solution to estimate ground surface subsidence above the oil field in the Long Beach-San Pedro area California by representing the oil reservoirs as a set of hollow cavities. The cavities were located within a linear elastic semi-infinite porous medium in an attempt to reproduce the measured subsidence observations. The pore pressure drawdown was set equal to the field pressure depletion at the internal boundary of each cavity. However, the model was found to not correspond well with field observations. This is because the model can only effectively function under the uniform pressure assumption (Gambolati, 1972). McNamee and Gibson (1960) attempted to derive analytical solutions for Biot consolidation of anisotropic porous medium with a different sets of boundary conditions. However, the method is complex to evaluate, which renders it beyond the application for most practical purposes. This is because the successful implementation of the process depends on the possibility of evaluating integrals in the complex plane, which possess a finite number of poles and branch-points.

Based on a simple nucleus-of-strain concept from thermoelastic strain theory in a half-space with a traction-free surface (Mindlin and Cheng, 1950), Geertsma

(1973) estimated the magnitude and distribution of surface subsidence resulting from reservoir depletion. The model derived the stress field, and the surface subsidence emanated from the extraction of gas from a subsurface reservoir. The major shortcoming of the model was the requirement of a geomechanically homogeneous and isotropic half-space embedding the reservoir. Gambolati (1972) extended Gertsma's model to deal with a heterogeneous tension center and showed that the earlier solution of McCann and Wilts (1951) was a special case of this solution.

1.4 Attempts to simulate subsidence associated with coal-bed methane extraction

Subsidence associated with oil and gas production from a cylindrical reservoir has been estimated using analytical solutions derived by Geertsma (1973). Other methods include semi-analytical models (Fokker, 2002; Fokker and Orlic, 2006) and numerical models (Fredrich et al., 2000; Sroka and Hejmanowski, 2006). However, such models may not be suitable to estimate subsidence associated with CBM extraction. This is because the analysis of problems involving ground surface subsidence due to CBM extraction needs to account for gas desorption induced coal shrinkage, which was ignored in the models.

There have been many sophisticated attempts to simulate both CBM and enhanced CBM production. Most studies focus on the complicated relationship between coal fracture permeability, effective stress and gas sorption and its implication on gas productivity (Seidle et al., 1992; Levine, 1996; Palmer and Mansoori, 1996; Gilman and Beckie, 2000; Cui and Bustin, 2005; Shi and Durucan, 2005; Mitra et

al., 2007; Robertson et al., 2008, e.g.). However, a few studies are reporting to investigate the associated effect of ground surface subsidence (Fanchi, 2002; Chamani and Rasouli, 2011; Freij-Ayoub, 2012; Brown et al., 2014; Wu et al., 2018a).

Fanchi (2002) coupled a black oil simulator with a CBM algorithm and uniaxial compaction model to investigate ground surface subsidence due to CBM production. Their focus was on the Fruitland coal formation in San Juan, United States of America. However, their model is likely to have underestimated ground surface subsidence because they assumed porosity and permeability were constant throughout. In practice, CBM formation porosity and permeability are highly sensitive to effective stress changes, giving rise to large rock deformations during gas production (Chin et al., 2000). In contrast, their uniaxial compaction model is limited to one-dimensional strain and is therefore likely to lead to an overestimate in ground surface subsidence because it ignores the lateral distribution of strain within the overburden above the CBM reservoir (Wu et al., 2018a).

Chamani and Rasouli (2011) studied production-induced stress, displacement, and ground surface subsidence due to CBM extraction in the San Juan Basin, United States of America, using a three-dimensional finite element model, which overcomes the limitation of the uniaxial compaction model. However, their model also assumed constant porosity and permeability. Furthermore, their model did not account for desorption shrinkage strain. Consequently, their model was also likely to underestimate ground surface subsidence. Note that coal shrinkage leads to greater levels of ground surface subsidence (Commonwealth of Australia, 2014a). Freij-Ayoub (2012) coupled their fluid flow model with the geomechanical model, FLAC3D (a finite difference code), to examine the possibilities of land surface sub-

sidence as a result of CBM extraction in the Gippsland Basin in Victoria, Australia. However, they also assumed a constant porosity and permeability within the CBM formation. Two coal seams of thicknesses 50 m and 44 m, respectively, separated by a non-coal bearing sedimentary layer with a thickness of 12 m, were simulated. The top of the shallowest coalbed was set at a depth of 100 m. The author considered three scenarios vis-a-vis: (1) coal confined between clay; (2) coal bounded top and bottom with sand; (3) coal bounded top and bottom with sand with an intermediate sedimentary formation designated as clay. The simulations involved extraction of water between 500 and 1500 m^3/day for 5 days. For Case 1, estimated subsidence varied between 100 and 110 mm while subsidence predicted for Cases 2 and 3 varied from 10 to 16 mm, respectively.

Brown et al. (2014) sought to quantify ground surface subsidence due to CBM extraction within the Surat Basin Australia using Geertsma's (1973) land subsidence analytical solution, which assumes uniform pressure within the CBM formation. The study analyzed three regions and predicted the maximum surface deformation to be approximately 0.1 m. However, the assumption of uniform pressure change adopted in Geertsma's model may have resulted in an underestimate in surface deformation because of the pressure gradient at the vicinity of the production well is higher than the pressure gradient at the far-edge of the reservoir (Wu et al., 2018a). In a recent article, Wu et al. (2018a) compared the suitability of the analytical solution of Geertsma (1973), the uniaxial compaction model, and a three dimensional hydro-mechanical model for modeling ground surface subsidence due to CBM extraction. They implemented stress-dependent permeability model, which Chamani and Rasouli (2011) and Freij-Ayoub (2012) ignored in their models. They

found that Geertsma's model underestimates ground surface subsidence induced by CBM extraction because the model ignores the pressure gradient within the CBM formation. The uniaxial compaction model is restricted to one-dimensional strain, thereby ignoring the lateral extent of the CBM reservoir and treated the overlying formations as soft clay overburden, which offers negligible resistance to displacement, which in turn leads to an overestimate in ground surface subsidence. Wu et al. (2018a), therefore, recommends the use of a fully coupled three-dimensional hydro-mechanical models.

However, apart from the fact that fully coupled models are computationally expensive (Du and Olson, 2001), Wu et al. (2018a) model assumes the reservoir area is equivalent to the horizontal extension of the outer domain. Therefore, the numerical model was unable to properly account for how fluid production induced-deformations propagate out into a laterally extensive CBM reservoir and other geological formations surrounding the CBM reservoir region, thereby underestimating surface subsidence. This is because accurate simulation of numerical stress solutions requires the discretized domain to be far more extensive than the reservoir (Yin et al., 2007).

Interestingly, most of the above simulations (Fanchi, 2002; Chamani and Rasouli, 2011; Freij-Ayoub, 2012; Wu et al., 2018a) implemented an equilibrium sorption rate approach, which influences the production time and production profile (Freij-Ayoub, 2012). The equilibrium sorption rate approach is attractive because it enables a coalbed methane reservoir to be treated as single porosity system, which invariably ignores the transient effects associated with gas diffusion from the micropores (Manik, 1999; Manik et al., 2002). Furthermore, a number of the simulations

adopted constant porosity and permeability within the CBM formation; therefore, the models will underestimate ground surface subsidence. This is because CBM porosity and permeability are highly sensitive to effective stress and pressure, leading to large rock deformations during CBM production (Chin et al., 2000). Thus, these models are not always appropriate for the description of the CBM recovery process (Wei et al., 2007) and, in turn, ground surface subsidence associated with coalbed methane extraction. Therefore, further efforts are needed to investigate where relevant simplifications can be justified for reliably estimating the level of subsidence that may occur within the life span of a productive CBM reservoir.

To correctly capture the intricate behaviour of ground surface subsidence due to CBM production, the CBM reservoir response should be modelled in conjunction with non-equilibrium gas desorption and stress-dependent porosity and permeability. It is also necessary that the model can capture a larger drainage area but at the same time remain computationally inexpensive. There are currently no models to explore ground surface subsidence as a result of CBM production that takes into account all the coupled aspects of fluid flow in conjunction with the stated attributes. Consequently, this project seeks to develop a computationally inexpensive but accurate, effective, and efficient model, which will adopt stress-dependent permeability with the ability to model a larger drainage area.

1.5 Coal permeability

CBM reservoirs are unconventional reservoirs, and several numerical simulations have been developed to get a better understanding of the complex processes involved in CBM production. The models range from simple (Gilman and Beckie,

2000) to complex (Fan, 2019) based on the number of physical and chemical processes incorporated into the models. Furthermore, these numerical models can be categorized based on the number of phases in the reservoir (whether the flow in the reservoir is considered one phase or two phases) (Liu et al., 2014; Ma et al., 2017a), the thermal conditions of the reservoir, whether it is an isothermal or non-isothermal (Connell, 2009; Li et al., 2016), the sorption rate implemented (single-porosity, dual-porosity or triple-porosity) (Reevs and Pekot, 2001; Wei and Zhang, 2010; Bertrand et al., 2017), and the gas components (pure gas or multi-component gases) (Zhu et al., 2011; Thararoop et al., 2012). However, irrespective of the category the models belong, an important controlling factor that will determine the outcome of a model is the coal permeability model implemented in the simulation (Moore, 2012).

Coal permeability is one of the most critical parameters that control the efficiency of CBM production (Cui and Bustin, 2005). It determines the ability of the CBM reservoir to transmit fluid within the coalbed methane reservoir to the wellbore, and it can vary within up to four orders of magnitudes (Durucan and Edwards, 1986). This property makes the fluid flow in CBM reservoirs different from most conventional reservoirs. The permeability of a CBM reservoir is caused primarily by the network of the cleats. Cleats comprise well-developed, extensive, roughly planar fractures that run parallel to one another known as face cleats. Orthogonal to these are the butt cleats, which are not well-developed and terminate at the intersections with face cleats (Fig. 1.2) (Shi and Durucan, 2005; Liu et al., 2011). The effect of reservoir pressure on the permeability of coal samples has been investigated by several researchers (Somerton et al., 1975; Durucan and Edwards, 1986; Sparks et

al., 1995; Enever and Henning, 1997). Experimental measurement and theoretical studies indicate that the permeability of coal has an exponential relationship with the effective confining pressure (McKee et al., 1988; Seidle et al., 1992). Also, there is the presence of bedding planes or surfaces in coal. However, these planes play only a small role in fluids movement in CBM reservoirs due to overburden weight (Ma et al., 2011).

Apart from the effect of confining stress on the permeability of CBM reservoirs, studies have also shown that structural deformation of the coal matrix, caused by matrix swelling/shrinkage due to gas adsorption/desorption, has a direct impact on the dynamic response of the permeability of CBM reservoirs, which in turn, affects CBM production (Seidle and Huitt, 1995; Levine, 1996; Mavor et al., 2004; Siriwardane et al., 2009). During CBM production, the CBM reservoir pressure will gradually decrease, and the effective stress will increase as methane is extracted from the coal. The coal permeability will decrease as a result of this process (compaction). However, the diffusion of the adsorbed methane from the matrix to the cleats will cause the coal matrix to shrink, and the coal permeability to increase. Therefore, the effective stress and the sorption-induced matrix deformation has the opposite effect on the coal permeability (Gray et al., 1987).

The primary attribute of coal permeability is its ability to increase with time during the primary CBM production. This observation was first reported by Kissell (1972), who found that regions of a coalbed adjacent to old areas of a mine were considerably more permeable than regions adjacent to freshly mined areas. Kissell (1972) suggested that the increase in the coal permeability may be a direct result of either the weakening resulting from the strata movements as a result of coal mining,

which in turn, leads to depressurization or the coal shrinkage effect resulting from the loss of methane (Moffat and Weale, 1955). Sequel to Kissell (1972)'s observation, Kissell and Edwards (1975) formulated a two-phase flow model to simulate the flow of methane and water in coalbeds. They concluded that the permeability increase is a result of an increase in gas relative permeability in the coal.

However, it has since been understood that the increase of coal permeability during primary production of CBM is mainly caused by the matrix shrinkage effect (Palmer and Mansoori, 1996; Shi and Durucan, 2004). Once the significant gas desorption starts, the coal permeability begins to increase, and the increment continues dramatically with continuing gas desorption (Harpalani and Schraufnagel, 1990). Mavor and Vaughn (1998) reported that the absolute permeability of coal increased significantly with continuing gas production in the San Juan Basin Fruitland Formation. The coal permeability is sensitive to both effective stress and sorption induced strain (Liu et al., 2011b; Pan and Connell, 2012). Thus, for a reliable description of fluid flow behaviour in a CBM reservoir, porosity and permeability models should adequately account for the effects of stress and matrix domain shrinkage/swelling.

There are several published coal permeability models in the literature. While a number of these models are emprically based (Somerton et al., 1975; Dabbous et al., 1976; Durucan and Edwards, 1986; Harpalani and McPherson, 1986; Gray et al., 1987; Seidle and Huitt, 1995), other models are derived analytically to described how the porosity and permeability of coal changes due to change in pore pressure (Sawyer et al., 1990; Gray et al., 1987; McKee et al., 1988; Seidle et al., 1992; Levine, 1996; Palmer and Mansoori, 1996; Gilman and Beckie, 2000; Pekot and Reeves, 2003; Cui and Bustin, 2005; Shi and Durucan, 2005; Mitra et al.,

2007; Robertson et al., 2008; Zhang et al., 2008; Wang et al., 2009; Connell et al., 2010; Gu and Chalaturnyk, 2010; Wei and Zhang, 2010; Wu et al., 2010,b; Liu and Rutqvist, 2010; Izadi et al., 2011; Ma et al., 2011; Chen et al., 2012). For detailed review readers are referred to palmer (2009); Pan and Connell (2012).

Analytical models have been developed by several researchers to describe the dynamic change in coalbed permeability (Sawyer et al., 1990; Gray et al., 1987; Palmer and Mansoori, 1996; Cui and Bustin, 2005; Shi and Durucan, 2005; Ma et al., 2011). These models are developed based on the simplification of coal structure into regular geometries such as a spherical model, a capillary tube model, a matchstick model, and a cube model (Lu et al., 2012), assuming uniaxial strain with constant vertical stress (Palmer and Mansoori, 1996; Cui and Bustin, 2005), constant volume assumption (Ma et al., 2011) and tri-axial stress assumption (Robertson et al., 2008; Wang et al., 2011).

The two most widely implemented models, *P&M* and *S&D* (Palmer and Mansoori, 1996; Shi and Durucan, 2004), are developed based on a geomechanical approach with uniaxial strain assumption using matchsticks model. In the *P&M* model, desorption of methane results in a volumetric strain, which in turn, results in changes in the fracture domain porosity and permeability. However, *S&D* development is based on stress changes; that is, desorption of methane results in volumetric strain; thus, changes in the effective horizontal stress (Ma et al., 2011). The *P&M* model has the capability to calculate negative permeability ratios because it may give negative porosity (Robertson and Christiansen, 2007). However, *S&D* is comparable to *P&M* with low sorption induced gas. The permeability ratio in the *S&D* model is always greater than zero, thus describes that actual permeability data mod-

elled by *S&D* are more accurate than that of *P&M* (Robertson and Christiansen, 2007).

1.6 Research objective

The objective of this project is to develop a semi-analytical solution to explore ground surface subsidence above CBM extraction wells. A problem with the analytical solution of Geertsma (1973) in this context is that it assumes a uniform pressure distribution within the CBM reservoir (Wu et al., 2018a), which is the main shortcoming of Brown et al. (2014) model. However, because ground surface subsidence is a linear function of fluid pressure, it is argued that Geertsma's analytical solution can be extended to account for arbitrary pressure distributions using the principle of superposition (Jayeoba et al., 2019). In this thesis, relevant pressure distributions are achieved by developing a two-phase (gas and water) CBM reservoir simulator within the MATLAB environment. The model incorporates gas adsorption/desorption model, dynamic permeability changes, and coal shrinkage, which are the main limitations of Fanchi (2002), Chamani and Rasouli (2011) and Freij-Ayoub (2012). The advantage of this approach is that subsidence can be calculated more efficiently as compared to fully coupled numerical models such as the one proposed by Wu et al. (2018a). It follows that a more comprehensive sensitivity analysis is possible, and further insight about parametric controls on CBM extraction-induced ground surface subsidence can be obtained.

1.7 Thesis outline

The outline of this thesis is as follows:

Chapter two describes the development of a basic set of equations for single-phase gas flow in a CBM reservoir, taking into account gas desorption kinetics along with stress dependent porosity and permeability model. The set of equations are solved using a method of lines (MoL) approach by discretizing the equations in space using finite differences and solving the resulting set of ordinary differential equations (ODE) in time using MATLAB's ODE solver, ODE15s. The numerical solution is compared with numerical results previously presented by Ye et al. (2014). The model is also calibrated to field data from the Horseshoe Canyon CBM reservoir in Canada.

Chapter three extends the numerical model developed in Chapter 2 to account for two-phase flow and the presence of water. The presence of water leads to three coupled non-linear differential equations, which are solved simultaneously, again using MoL and the MATLAB solver, ODE15s. The numerical solution is compared to relevant published numerical results (Mora and Wattenbarger, 2009) obtained using the commercial software packages GEM and ECLIPSE. The effect of initial water saturation on gas production and reservoir pressure drawdown is then investigated.

Chapter four involves extending the analytical solution, for ground surface subsidence derived by Geertsma (1973), to account for non-uniform pressure distributions using the principle of superposition. A closed-form equation is derived to describe subsidence above a groundwater production well. Results from the analytical solution are compared to results from a fully coupled hydro-mechanical finite

element model developed using COMSOL.

In chapter 5, the pressure distributions from the CBM model developed in Chapters 2 and 3 are used to derive an effective pressure to drive the semi-analytical solution for ground surface subsidence developed in Chapter 4. A sensitivity analysis is then performed to investigate how different model parameters affect ground surface subsidence during CBM production.

Chapter 6 summarizes the findings and conclusions from the thesis and provides suggestions for further work in the future.

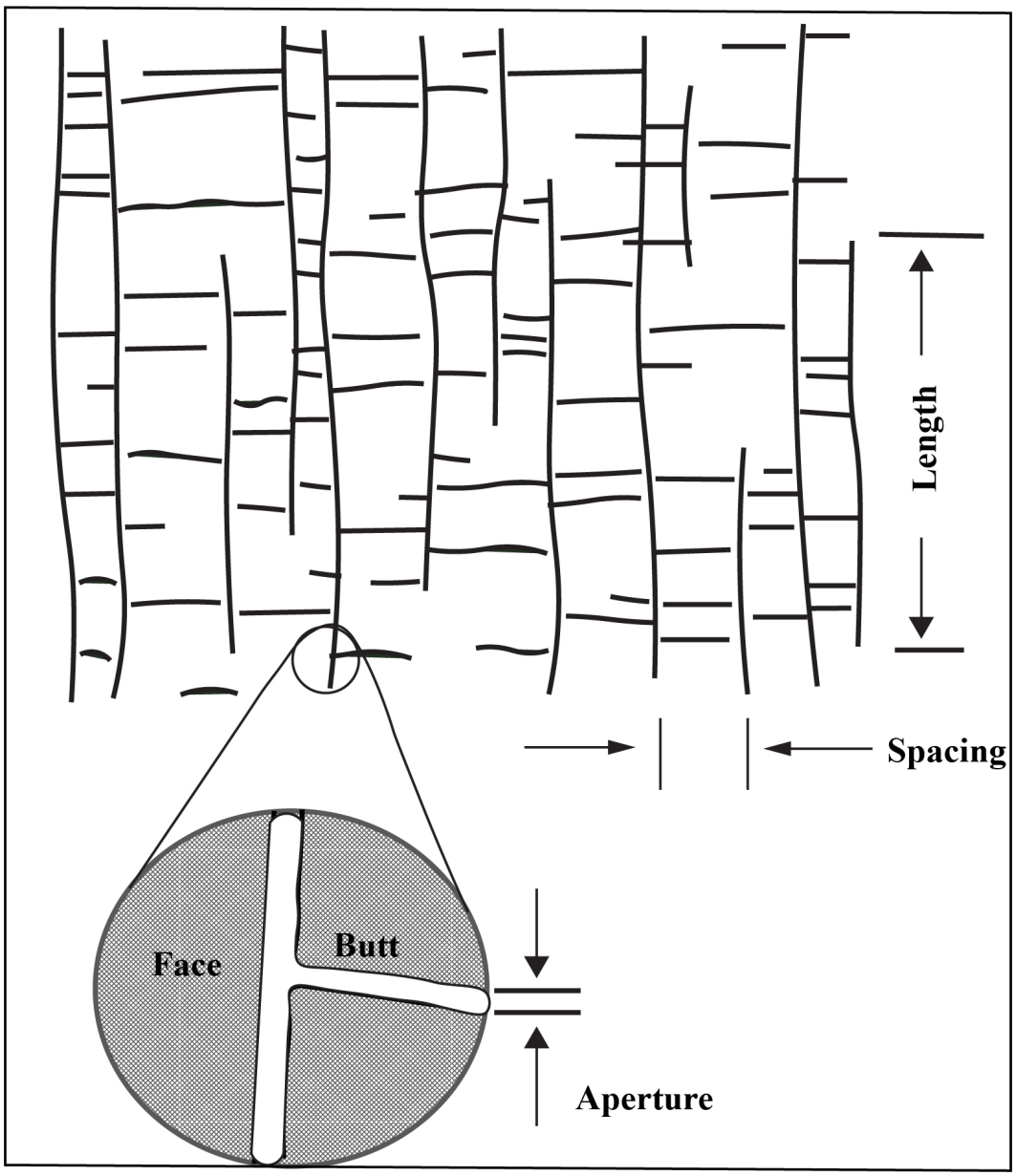

Figure 1.2: Schematic illustration of coal cleat pattern. (Adapted from Laubach et al. (1998))

.

Chapter 2

Coal-bed methane production in the absence of water

Summary

This chapter describes the development of a basic set of equations for single-phase gas flow in a coalbed methane reservoir, taking into account gas desorption kinetics along with stress dependent porosity and permeability model. The main objective of the work is:

- To solve the set of equations using method of lines (MoL) approach by discretizing the equations in space using finite differences and solving the resulting set of ordinary differential equations (ODE) in time using MATLAB's ODE solver, ODE15s.
- To build a MATLAB code capable of modelling single-phase gas flow in CBM reservoir.

The model is a single-phase gas flow model in a CBM reservoir. The decision to build a model in MATLAB instead of using any of ECLIPSE, GEM or COMSOL,

was to enable us to model a simplified situation and concentrate solely on the single-phase flow, without the influence of any multiphase effects.

The single-phase MATLAB model was built by myself with assistance from Simon Mathias and Stefan Nielsen. All simulations were run and analyzed by myself. The parameter values for the verification of the model were presented in Ye et al. (2014), and the parameter values for model calibration were presented in Gerami et al. (2008). The bottom hole pressure and observed production rate data used in the model calibration were digitally extracted from Fig. 3 of Gerami et al. (2008). A COMSOL model was not run at this stage of the work, but our numerical model results were compared with the COMSOL finite element model presented by Ye et al. (2014).

2.1 Introduction

Coalbed methane (CBM) is a natural gas that resides in coal. Coal serves as both the source rock and the reservoir for methane production. It is typically conceptualized as a dual-porosity/permeability continuum system with a primary porosity (micropores) associated with the coal matrix (the matrix domain) and a secondary porosity (macropores) associated with the cleat system (the fracture domain) (see Fig. 2.1).

The matrix domain provides a large internal surface area, which contains the vast majority of the gas-in-place volume, with a strong affinity for certain gases, such as methane, ethane, and carbon dioxide (Pillalamarry et al., 2011). Gas storage in the coal matrix is dominated by adsorption. Furthermore, pore sizes in the matrix are very small, rendering it close to impermeable. The fracture domain consists

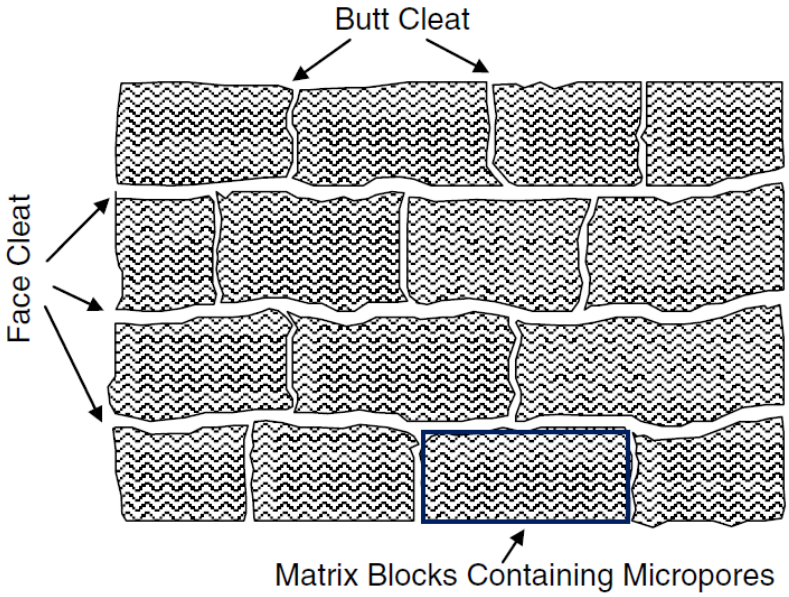

Figure 2.1: Schematic diagram illustrating the matrix-cleat system associated with coal (after Harpalani and Ouyang (1996)).

of a naturally occurring network of fractures. These fractures are known as face cleats or butt cleats (Laubach et al., 1998). The fracture domain surrounds the matrix blocks of CBM reservoirs and provides the flow paths for coalbed methane to production wells (see Fig. 2.2) (Laubach et al., 1998; Law et al., 2002; Liu et al., 2011). Gas flow in the fractures is generally assumed to be controlled by Darcy's law. In contrast, gas migration in the matrix is assumed to be controlled by gas diffusion.

In this way, gas migration is thought to be controlled by pressure gradients in the macropores and concentration gradients in the micropores. Gas diffusion in micropores is thought to comprise of three simultaneous processes: (1) molecular diffusion and (2) Knudsen diffusion of the non-adsorbed gas and (3) surface diffu-

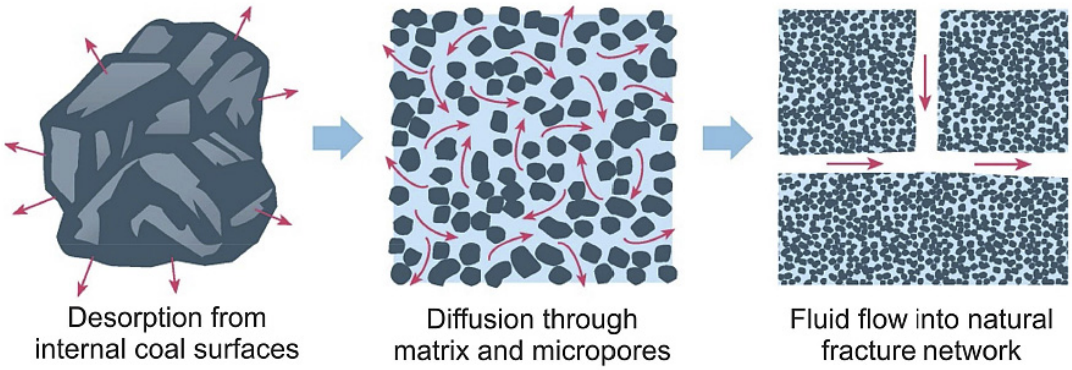

Figure 2.2: Schematic diagram illustrating gas migration in a coal-bed methane reservoir (after Al-Jubori et al., 2009)

sion of the adsorbed gas layer (Thimons and Kissell, 1973; Shi and Durucan, 2005; Pillalamarry et al., 2011).

Primary production of CBM leads to a reduction in gas pressure in the cleat system, which causes gas to desorb at the cleat face of the coal matrix. This, in turn, leads to a concentration gradient in the adsorbed gas within the coal matrix, giving rise to surface diffusion of gas from the centre of the coal matrix to the cleat faces (Liu et al., 2011; Moore, 2012). Molecular diffusion and Knudsen diffusion in the coal matrix are generally thought to be significant as compared to surface diffusion (Pillalamarry et al., 2011).

A strong interaction is thought to exist between permeability, gas desorption induced shrinkage, and stress-induced deformation (Zhu et al., 2007; Liu et al., 2014). As stated earlier, the matrix is largely thought to be impermeable, with almost all permeability attributed to an orthogonal cleat system. Cleats that run parallel to the main flow direction are referred to as face cleats. The orthogonal cleats, commonly referred to as butt cleats, are less well connected and often terminate at the intersections of the face cleats (Shi and Durucan, 2005; Liu et al., 2011). Many

researchers have investigated the influence of confining stress on the permeability of coal samples (Somerton et al., 1975; Durucan and Edwards, 1986; Sparks et al., 1995; Enever and Henning, 1997). Experimental measurement and theoretical studies indicate that the permeability of coal has an exponential relationship with effective stress (McKee et al., 1988; Seidle et al., 1992).

Experimental and field studies have shown that structural deformation of the matrix domain, caused by matrix shrinkage due to gas desorption, also has a significant impact on CBM formation permeability (Seidle and Huitt, 1995; Levine, 1996; Mavor et al., 2004; Siriwardane et al., 2009).

Based on the above understandings about CBM migration in CBM reservoirs, a series of mathematical models in the form of a set of partial differential equations (PDEs) with initial and boundary conditions have been developed(King et al., 1986; Gilman and Beckie, 2000; Zhu et al., 2007; Thararoop et al., 2012; Wei and Zhang, 2010; Bertrand et al., 2017; Ma et al., 2017a). King et al. (1986) developed a conventional mathematical and numerical model for coal seam degasification. The multi-mechanistic model, which considers the CBM reservoir as dual-porosity single permeability porous medium with a single well in rectangular, cylindrical, and elliptical coordinate geometry, follows two driving mechanisms including flow through the pressure field (Darcian flow) and flow through the concentration field (Fickian flow). Remner et al. (1986) proposed a two-dimensional (Cartesian coordinate system), two-phase (gas-water), multi-mechanistic flow model in coal-seams. The model also conceptualized coal seams as a dual-porosity, single-permeability system and utilized a quasi-steady kinetic-type state model developed by King et al. (1986) and Langmuir isotherm to calculate the desorption rate. Sung et al. (1986)

extended the model of Remner et al. (1986) by developing a numerical model that described the simultaneous flow of methane and water in hydraulically fractured coal seams. The hydraulic fracture was represented by superimposing fracture nodes on the matrix nodes. While flow within the fractures was assumed to be one-dimensional, flow in the matrix was in two-dimensional. The fracture and matrix domains were connected by a term referred to as ”fluid loss”.

A mathematical model to simulate methane flow in the borehole coal mining system was developed by Balla (1989). The model considered the sorption phenomenon of methane as a function of pressure. He found that variation in methane pressure during production created a change in the stress distribution of the rock and, subsequently, a change in the permeability of the coal. The idea of improving a ”conventional black oil” model to simulate coalbed methane reservoir extraction was first suggested by Amoco (Seidle and Arri, 1990). The model treated adsorption gas on the surface of coal as gas dissolved in immobile oil. The assumption here is that gas desorbed instantaneously from the coal matrix domain to the fracture domain so that the phase equilibrium in the fracture domain and the micropores is maintained. Sawyer et al. (1990) presented a fully three-dimensional, two-phase (gas-water) flow model in CBM reservoirs. The model, which described the mechanism of gas transport by a quasi-steady-state formulation, accounted for changes in fracture domain permeability due to matrix shrinkage/swelling.

Kolesar et al. (1990a) developed a single-phase, one-dimensional model in radial coordinates. The model is based on a non-equilibrium model using the unsteady-state formulation, and the authors concluded that the sorption rate predicted by the unsteady-state model is higher than that of quasi-steady-state model at early

stage of simulation (Kolesar et al., 1990a,b). Meanwhile, a description of multi-component gas sorption is needed for effective prediction of gas-in-place, gas rate, and reserve in CBM reservoirs by the existing compositional reservoir simulator. Therefore, Arri et al. (1992) developed a description of binary gas sorption on coal referred to as extended Langmuir isotherm and incorporated this into a compositional reservoir simulator for effective prediction of primary and enhanced recovery of coalbed methane. Gilman and Beckie (2000) proposed a simplified mathematical model of methane diffusion and movement in a coal seam. The model utilized dual-porosity, single permeability model for coal seam, and took account of a relatively slow mechanism of methane released from the coal matrix into cleats. The authors found that the reference time of methane released from the coal matrix into cleat exerts a critical influence on the overall methane production with a significant change of permeability due to desorption.

Reevs and Pekot (2001) developed a specialized triple-porosity and dual-permeability compositional model by modifying dual-porosity representation to incorporate another porosity in the form of a gas storage system within the coal matrix domain to provide needed free gas (and in some circumstances water). The desorbed gas from the internal matrix block surfaces migrates via Darcy flow through matrix permeability into the fractures and subsequently to the wellbore. Similarly, Wei and Zhang (2010) presented a two-dimensional, two-phase, triple-porosity and dual permeability, coupled fluid flow and geomechanical CBM model for simulating water and gas production. The authors investigated the coupling effects of effective stress and shrinkage/swelling with the coupled fluid flow and geomechanical approach. The overall effect of introducing the new porosity system is to slow the process of

gas migration from the micropores into the fracture domain (Hower, 2003). However, these models (Reevs and Pekot, 2001; Wei and Zhang, 2010) differ from conventional CBM simulator and the bidisperse model (triple-porosity) concept of Shi and Durucan (2005c) in that the desorbed gas, instead of undergoing diffusion process through the matrix domain to the fracture domain, moves via Darcy flow, upon establishing a relative permeability to gas (Shi and Durucan, 2005c), through micropermeability of the matrix domain to the cleats. Thararoop et al. (2012) developed a compositional flow mathematical model for coalbed methane reservoirs. The model treated coal seams as dual-porosity, dual-permeability system, and made use of non-equilibrium sorption rate model proposed by King et al. (1986). The model incorporated water in the coal matrix with the inclusion of coal shrinkage and swelling effects.

In a recent article, Bertrand et al. (2017) proposed a fully coupled hydro-mechanical model for CBM production modeling. The model adopted dual-continuum approach for both mechanical and hydraulic behaviour, and shape factors are employed to consider the geometry of the matrix blocks in the mass exchange between fractures and matrix. Similarly, Ma et al. (2017a) developed a fully coupled two-phase and poromechanics numerical model for the analysis of the geomechanical impact on coalbed methane production. The model incorporated the equilibrium sorption model and considered changes in fluid flow properties through variations in cleats fractures instigated by changes in the effective stress and desorption-induced shrinkage. Besides, Touzani et al. (2017) presented a numerical model that predicts the gas extraction processes from a CBM reservoir using a finite element method.

However, most of the above numerical simulations employed conventional fi-

nite difference and finite element methods for space discretization. Spatial schemes in finite difference method give rise to either stability problems or numerical diffusion due to truncation terms associated with Taylor's expansion, and it has the tendencies to generate numerical dispersion when applied to problems with sharp fronts. Finite element methods do not conserve mass over a cell and can generate numerical oscillations (known as the Gibbs effect) when applied to problems with discontinuities. The handling of the temporal variable, which has been adjudged to be critical (Dale, 2010) to resolving the non-linear nature of the problem, generally revolves around the low-order time-stepping such as backward Euler, implicit Crank-Nicholson, and explicit Euler algorithms. While fully explicit time-stepping can run to severe time-step limitations due to Courant-Friedrichs-Lewy (CFL) condition, fully implicit time-stepping leads to additional numerical diffusion. These show that the approximation of the spatial and time derivatives are the primary sources of errors in the solution of partial differential equations (Dale, 2010, p.35). However, the fundamental objective when computing a numerical approximation to the solution of a differential equation is to obtain a result that indeed approximates the true solution (Dale, 2010).

Meanwhile, there exist adaptive multi-step-multi-order time integration algorithms (Shampine and Reichelt, 1997), which treat the temporal variable more accurately. These time integration algorithms implement sophisticated variable-order and variable-step-size time discretization. These techniques maintain a specific time integration error while maximizing the time-step size. One of these techniques to solve the relevant partial differential equations is the method of lines, MOL(Wouwer et al., 2005; Haq et al., 2012; Schiesser, 2012).

MOL approximates the spatial derivatives of PDEs but not the temporal derivative (Schiesser, 2012). The basic principle of MOL involves the replacement of the spatial (boundary value) derivatives present in PDEs with algebraic approximations. Once the spatial derivative replacement process is completed, the spatial derivatives are no longer expressed explicitly in terms of the spatial independent variables. Therefore, only the initial value variable (the temporal derivative) in a physical problem persists. Furthermore, with only one persisting independent variable, the physical problem now transforms into a system of ODE that approximates the original PDE as an initial value problem (IVP). MOL is an attractive approach to solve PDE because of its simple implementation, and it allows the solution to take advantage of the advanced general-purpose methods and the wide availability of high-quality ODE solvers designed for IVPs (Wouwer et al., 2005) e.g., $FORTRAN$ with *NAG*, $FORTRAN$ with $DSS/2$, $MATLAB$ (Shampine and Reichelt, 1997; Lee et al., 1996; Sharaf and Bakodah, 2003; Wouwer et al., 2005).

MATLAB *(matrix laboratory)* is a multi-paradigm numerical computing environment. It contains a built-in suite of solvers that use multi-step multi-order schemes to solve ordinary differential equations (ODEs) (Shampine et al., 2003). The solvers herein, referred to as MATLAB ODE solvers, provide users with a selection of higher-order solvers using an array of methods of varying accuracies and time-stepping schemes. MATLAB's ODE solvers are designed for solving a single first-order IVP and a system of first-order IVPs. The MATLAB ODE solvers include $ODE23$, $ODE45$ and $ODE113$ for nonstiff equations, and $ODE23s$ and $ODE15s$ for stiff equations. These techniques allow the use of optimal step size and, in some cases, adjust the step size for error minimization in each step (Esfandi-

ari, 2017). These ODE solvers can solve across a finite interval of the independent variable (Shampine et al., 2003).

ODE 15s is a multi-step multi-order (from 1^{st} to 5^{th} order accurate time) stiff solver which uses the so-called Numerical Differentiation Formulas (NDFs), which are modified version of Backward Differentiation Formulae (BDFs) (Shampine and Reichelt, 1997) that anticipate a backward difference order $(k+1)$ when working in order k. By default, ODE 15s uses NDF methods (Shampine and Reichelt, 1997), but users have the opportunity of choosing between NDF or BDF methods. In our simulation, we use the default setting, which is the NDFs because they are more accurate than BDFs due to the positive impact of backward difference on local truncation error (Celaya et al., 2014). ODE 15s uses local truncation error as the error estimation while it uses backward differences to calculate an approximation. The approximation can be obtained by using the backward interpolating polynomial of the Newton method (Celaya et al., 2014). ODE 15s uses a variable time-stepping scheme, which changes the step size in relation to the stability and accuracy requirement/specification of the problem being solved. It can automatically set a trial first step size, and it is also possible to define the size of the initial step the solver tries to potentially help it better to recognise the scale of the physical problem (Hairer et al., 1993). However, the step can be repaired through the control of the step of the algorithm in case it fails. Besides, the user has the option of specifying an upper bound on the size of the time step if necessary.

MOL has recently been applied to immiscible two-phase and two-component two-phase flow problems (Amaziane et al., 2012; Bourgeat et al., 2012; Vohralík and Wheeler, 2013). Mathias et al. (2006, 2008a) and Ireson et al. (2009) pre-

sented MOL solutions of Richards' equation (RE) using the MATLAB ODE solver, ODE15s, which is suitable for stiff systems of ODEs (Shampine and Reichelt, 1997). ODE15s has also been successfully applied to modelling two-phase immiscible flow problems (Mathias et al., 2009) and non-Darcy flow problems (Mathias et al., 2008a; Wen et al., 2009). The method has hitherto been applied to multicomponent, multiphase problems in porous media (Mathias et al., 2014; Goudarzi et al., 2016; Hardwick and Mathias, 2018). However, we have not found any paper considering MOL for the gas flow problem in CBM reservoirs.

In this chapter, a numerical model for a dry gas (i.e., free of water) CBM reservoir is developed. The governing equations include a mass conservation statement, a gas desorption model, and a permeability function to account for the dependence of permeability on effective stress and matrix shrinkage in a uni-axial strain setting. The equations are discretized in space using finite differences. The resulting set of ordinary differential equations are then solved using one of MATLAB's ODE solvers. Numerical results are then verified by comparison to finite element simulations previously published by Ye et al. (2014). The model is also calibrated to CBM production data from Horseshoe Canyon reservoir.

2.2 Mathematical model

Consider methane production from a cylindrical, homogenous, isotropic and horizontally oriented, CBM reservoir. The CBM reservoir is overlain and underlain by impermeable geological formations. Furthermore, the CBM reservoir is purely comprised of coal and methane. The coal-bed initially exhibits a uniform pressure, P_I [$\mathrm{ML^{-1}T^{-2}}$], and free methane is initially in equilibrium with the adsorbed

methane in the coal matrix. Gas production is stimulated by holding the production well at a fixed pressure, P_w [$ML^{-1}T^{-2}$]. The mass conservation statement for methane in the CBM reservoir takes the form

$$\phi\rho_g(c_c+c_g)\frac{\partial P}{\partial t}+\rho_c\frac{\partial s}{\partial t}=-\frac{1}{r}\frac{\partial(r\rho_g q_g)}{\partial r} \tag{2.1}$$

where ϕ [-] is the cleat porosity, ρ_g [ML^{-3}] is the methane density in the cleats, c_c [$M^{-1}LT^2$] is the coal-bed compressibility, c_g [$M^{-1}LT^2$] is the methane compressibility, P [$ML^{-1}T^{-2}$] is pressure, t [T] is time, ρ_c [ML^{-3}] is the density of the coal-bed, s [-] is the mass of adsorbed methane per unit mass of coal-bed, r [L] is radial distance from the methane production well and q_g [LT^{-1}] is the volumetric flux of methane found from Darcy's law:

$$q_g=-\frac{k}{\mu_g}\frac{\partial P}{\partial r} \tag{2.2}$$

where k [L^2] is the permeability of the formation and μ_g [$ML^{-1}T^{-1}$] is the dynamic viscosity of methane.

The initial and boundary conditions take the form:

$$\begin{aligned} &P=P_I, && r_w\le r\le R, && t=0\\ &P=P_w, && r=r_w, && t>0\\ &\partial P/\partial r=0, && r=R, && t>0 \end{aligned} \tag{2.3}$$

where r_w [L] is the well radius and R [L] is the radius of the CBM reservoir.

The coal-bed and fluid compressibilities are found from:

$$c_c=\frac{1}{\phi}\frac{\partial\phi}{\partial P} \tag{2.4}$$

$$c_g=\frac{1}{\rho_g}\frac{\partial\rho_g}{\partial P} \tag{2.5}$$

The density of methane is assumed to obey the ideal gas law

$$\rho_g=\frac{PM}{R_gT} \tag{2.6}$$

where $M = 0.016$ kg mol^{-1} and $R_g = 8.31432$ Nm mol^{-1} K^{-1} with P and T being pressure and temperature in Pa and K, respectively. It follows that the gas compressibility, $c_g = 1/P$. Through out this thesis, the viscosity of gas is determined using a correlation due to Lee et al. (1996) as reported by Ahmed (2001, p. 73). See Appendix A for details.

The volumetric rate of gas production at standard conditions (i.e., 14.7 psi and 60^oF or 0.1014 MPa and 288.7 K), Q_w [L^{3}T^{-1}], is found from

$$Q_w(t) = \frac{2\pi H r_w \rho_g q_g(r = r_w, t)}{\rho_{g0}} \tag{2.7}$$

where H [L] is the CBM reservoir thickness and ρ_{g0} [ML^{-3}] is the density of methane at standard conditions.

2.2.1 Gas adsorption kinetics

The adsorbed gas is assumed to be controlled by the following kinetic equation (Ye et al., 2014):

$$\frac{\partial s}{\partial t} = \frac{s_0 - s}{t_r} \tag{2.8}$$

where t_r [T] is a mass transfer coefficient, describing surface diffusion of adsorbed gas within the blocks of coal matrix, and s_0 is found from the Langmuir isotherm (Ye et al., 2014):

$$s_0 = \frac{\rho_{g0} V_L P}{P_L + P} \tag{2.9}$$

where V_L [-] [M^{-1}L^3] is the Langmuir volume constant and P_L [ML^{-1}T^{-2}] is the Langmuir pressure constant.

Because the CBM reservoir is initially in equilibrium:

$$s = \frac{\rho_{g0} V_L P_I}{P_L + P_I}, \quad r_w \leq r \leq R, \quad t = 0 \tag{2.10}$$

It is possible to equate Eq. (2.8) with a Fickian diffusion model at large times to show that (Mathias and Zimmerman, 2003)

$$t_r = \frac{L^2}{\pi^2 D_A} \tag{2.11}$$

where D_A [L^2T^{-1}] is the apparent diffusion coefficient of the adsorbed gas in the coal matrix and L [L] is the cleat spacing.

2.2.2 Cleat permeability and porosity model

The cleat permeability is often thought to be a cubic function of the cleat porosity

$$k = k_I \left(\frac{\phi}{\phi_I} \right)^3 \tag{2.12}$$

where k_I [L^2] and ϕ_I [-] are the initial permeability and porosity, respectively. This equation is widely accepted and commonly used in conventional and unconventional oil and gas industry to describe the permeability change with respect to porosity variation (Palmer and Mansoori, 1996; Shi and Durucan, 2005; Liu et al., 2011b). The equation can be derived by applying the cubic law for permeability (Snow, 1968), which assumes the cleats are bounded by parallel smooth impermeable surfaces and flow in the cleats is laminar and fully developed. It has also been supported by experimental results on fractures rocks (Jones, 1975).

Shi and Durucan (2004) suggest that

$$\phi = \phi_I \exp(-c_f \Delta\tau'_h) \tag{2.13}$$

where c_f is the cleat volume compressibility due to variation of effective horizontal stress, $\Delta\tau$ [$ML^{-1}T^{-2}$].

Under uniaxial strain conditions (Shi and Durucan, 2004)

$$\Delta\tau'_h = -\left(\frac{\nu}{1-\nu} \right)(P - P_I) + \frac{E}{3(1-\nu)}\Delta\varepsilon_s \tag{2.14}$$

where ν [-] and E [$ML^{-1}T^{-2}$] are the Poisson's ratio and Young's modulus of the coal matrix, respectively, and

$$\Delta\varepsilon_s = \varepsilon_L \left(\frac{P_m}{P_{L,\varepsilon} + P_m} - \frac{P_I}{P_{L,\varepsilon} + P_I} \right) \tag{2.15}$$

where ε_L [-] is the Langmuir volumetric strain constant and $P_{L,\varepsilon}$ [$ML^{-1}T^{-2}$] is the Langmuir pressure constant for coal swelling strain (following Ye et al. (2014), it is assumed that $P_{L,\varepsilon} = 2.082 P_L$) and P_m [$ML^{-1}T^{-2}$] is the pressure in coal matrix.

Considering Eqs. (2.8) and (2.9) it can be understood that

$$P_m = \frac{P_L s}{\rho_{g0} V_L - s} \tag{2.16}$$

Furthermore, substituting Eq. (2.13) into Eq. (2.4) leads to

$$c_c = \frac{c_f \nu}{1 - \nu} \tag{2.17}$$

2.2.3 Numerical solution

The above set of equations (Eqs (2.1) and (2.8)) can be solved using the method of lines. This can be achieved by discretising the equations in space using finite differences and solving the resulting set of ordinary differential equations (ODE) in time using MATLAB's ODE solver, ODE15s (Goudarzi et al., 2016).

We start by discretizing the radial axis r into N number of nodes such that $r_w < r_i < r_e$ for $i = 1 \ldots N$ where, r_i is the value of r at the ith node. The pressure, P, and adsorbed methane mass fraction, s, are approximated at each node by P_i and s_i, respectively. Having discretized in space, the above problem reduces to the following set of ordinary differential equations with respect to time:

$$\phi_i \rho_{g,i} (c_{c,i} + c_{g,i}) \frac{dP_i}{dt} + \rho_c \frac{ds_i}{dt} = \frac{r_{i-1/2} \rho_{g,i-1/2} q_{g,i-1/2} - r_{i+1/2} \rho_{g,i+1/2} q_{g,i+1/2}}{r_i (r_{i+1/2} - r_{1-1/2})}, \quad i = 1 \ldots N \tag{2.18}$$

and

$$\frac{ds_i}{\partial t} = \alpha(s_{0,i} - s_i), \quad i = 1 \ldots N \tag{2.19}$$

where

$$q_{i+1/2} = -\frac{k_{i+1/2}}{\mu_g}\left(\frac{P_{i+1} - P_i}{r_{i+1} - r_i}\right), \quad i = 2 \ldots N \tag{2.20}$$

Due to the convergence of flow lines at the well, it is a good idea to space the nodes logarithmically in the r direction such that (Mathias et al., 2008a)

$$r_i = (r_{i-1/2} + r_{i+1/2})/2, \quad i = 1 \ldots N \tag{2.21}$$

where

$$\log_{10}(r_{i+1/2}) = \log_{10}(r_w) + i\left[\frac{\log_{10}(R) - \log_{10}(r_w)}{N}\right], \quad i = 0 \ldots N \tag{2.22}$$

For all the simulations in this chapter, N was set to 200 and values of variables at $r_{i+1/2}$ are obtained from values at r_i by linear interpolation.

2.3 Results

2.3.1 Model verification with finite element results

Ye et al. (2014) provides a comprehensive set of numerical results that describe numerical solutions of the above set of equations using the finite element package, COMSOL. Ye et al. (2014) was primarily interested in the role of non-Darcy effects on CBM production. However, they also present results for two base case scenarios where flow is assumed to be Darcian, as in Eq. (2.2). In this section we will compare results from our own numerical solution to those from Ye et al. (2014) for the two Darcian scenarios. The parameters describing these scenarios are presented in Table 2.1.

Fig. 2.3 shows a comparison of modeling results from our numerical model, described above, and the finite element simulation results presented by Ye et al. (2014). The parameters used were derived from information provided by Ye et al. (2014) and are shown as Case 1 and Case 2 in Table 2.1. Subplots a and c show comparisons of pressure profiles at different times. There is excellent agreement between both models for this aspect. Subplots b and d show comparisons of methane production as a function of time. There is a good correspondence between the two models although our numerical model slightly underestimates the magnitude as compared to Ye et al. (2014). However, this discrepancy is probably due to the very high grid resolution we provided around the well-bore in our model. Looking at the grid adopted by Ye et al. (2014) it is possible to assume that our results represent a more accurate numerical solution. Also note, that Ye et al. (2014) simulated a quarter-space, therefore it was necessary to divide our production rate by four to achieve correspondence.

2.3.2 Calibration to observed production data at Horseshoe Canyon

Fig. 2.4 shows wellbore pressure and production data from a well producing methane from the Horseshoe Canyon coal bed of the Western Canadian Sedimentary Basin. Of particular interest is that the gas was dry and very little water was present (Gerami et al., 2008), making the data suitable for calibrating our numerical model. Measured gas adsorption parameters and other physical properties for this site are presented by Gerami et al. (2008) and reported in Table 2.1. However, there is uncertainty with regards to the initial permeability, k_I, cleat volume compressibility, c_f, and the radial extent of the connected CBM reservoir, R.

Table 2.1: Parameter values used for the numerical simulations. Case 1 and 2 are the Darcy flow scenarios looked at by Ye et al. (2014). Case 3 uses the same parameters as Case 2 with the exception of those parameters indicated by a * and +. Parameters indicated by a * were obtained from a description of the Horseshoe Canyon case study provided by Gerami et al. (2008). Parameters indicated by a + were obtained by calibration of the model to the observed production data from Horseshoe Canyon.

Parameter	Case 1	Case 2	Case 3
Initial permeability, k_I $(m^2)^+$	1.8×10^{-15}	3.9×10^{-15}	13×10^{-15}
Cleat volume compressibility, c_f $(MPa^{-1})^+$	0.36	0.15	0.01
Initial porosity, ϕ_I (-)*	4.6×10^{-4}	4.6×10^{-4}	5×10^{-3}
Radius of the CBM reservoir, R (m)*	454	454	264.8
CBM reservoir thickness, H (m)*	1.0	1.0	8.99
Langmuir pressure constant, P_L (MPa)*	2.070	2.070	4.652
Langmuir volume constant, V_L $(m^3\ kg^{-1})^*$	0.0243	0.0243	0.00919
Density of coal, ρ_c $(kg\ m^{-3})^*$	1330	1330	1468
Initial pressure, P_I (MPa)*	9.6	9.6	1.413
Wellbore pressure, P_0 (MPa)*	2.0	2.0	0.6 to 0.2
CBM reservoir temperature, T (K)*	318	318	289
Langmuir volumetric strain constant, ε_L (-)	0.0127	0.0127	0.0127
Well radius, r_w (m)	0.1	0.1	0.1
Mass transfer coefficient, t_r (days)	0.83	0.83	0.83
Young's modulus, E (MPa)	2900	2900	2900
Poisson's ratio, ν (-)	0.35	0.35	0.35

However, the estimated IGIP available to the CBM well is 6.36 million standard (i.e., at standard conditions) cubic meters (Gerami et al., 2008). A value of R can therefore be determined from the material balance equation

$$R = \left[\frac{\text{IGIP}}{\pi H} \left(\frac{\rho_c V_L P_I}{P_L + P_I} + \frac{\rho_g \phi_I}{\rho_{g0}} \right)^{-1} \right]^{1/2} \tag{2.23}$$

which turns out to be 264.8 m.

By manual calibration it is then found that a good correspondence between the numerical model and the observed production data is achieved when $k_I = 14 \times 10^{-15}$ m^2 and $c_f = 0.01$ MPa^{-1}. A comparison of our modeled production data with the observed data is also shown in Fig. 2.4. Note that the boundary pressure, P_w, for the numerical model was forced to be the observed wellbore pressure data presented in Fig. 2.4.

2.4 Conclusions

The governing equations for methane production from a CBM well in the absence of water were presented. These were solved by discretising in space using finite differences and integrating the resulting set of ordinary differential equations (ODE) with respect to time using MATLAB's ODE solver, ODE15s. A model verification exercise was performed against published simulation results from the literature, obtained using the finite element model, COMSOL. The ability of the model to simulate natural observed behavior was demonstrated by calibrating the model to observed field data from the Horseshoe Canyon coal field in Canada.

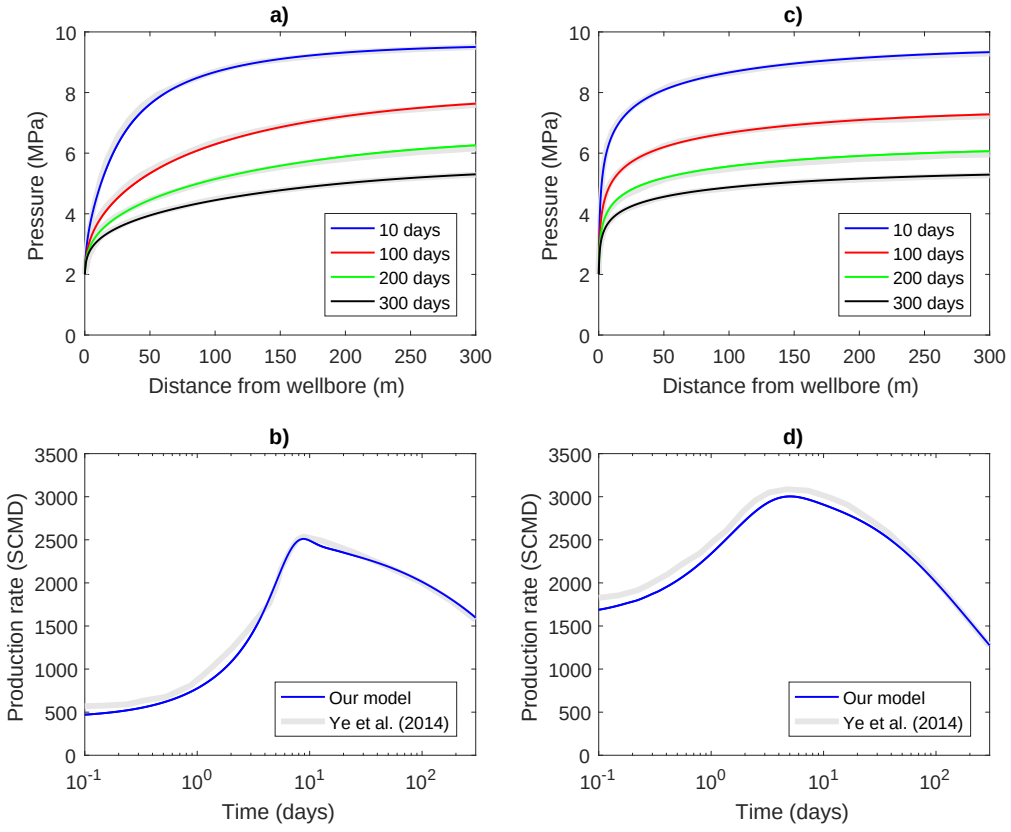

Figure 2.3: Plots of numerical modeling results showing a comparison of our numerical model with the COMSOL finite element model presented by Ye et al. (2014). Note that SCMD is a standard SPE (Society of Petroleum Engineering) acronym for Standard (i.e., at standard conditions) Cubic Meters per Day. Subplots a) and b) represent Case 1 in Table 2.1. Subplots c) and d) represent Case 2 in Table 2.1. The thick grey lines represent the results from Ye et al. (2014).

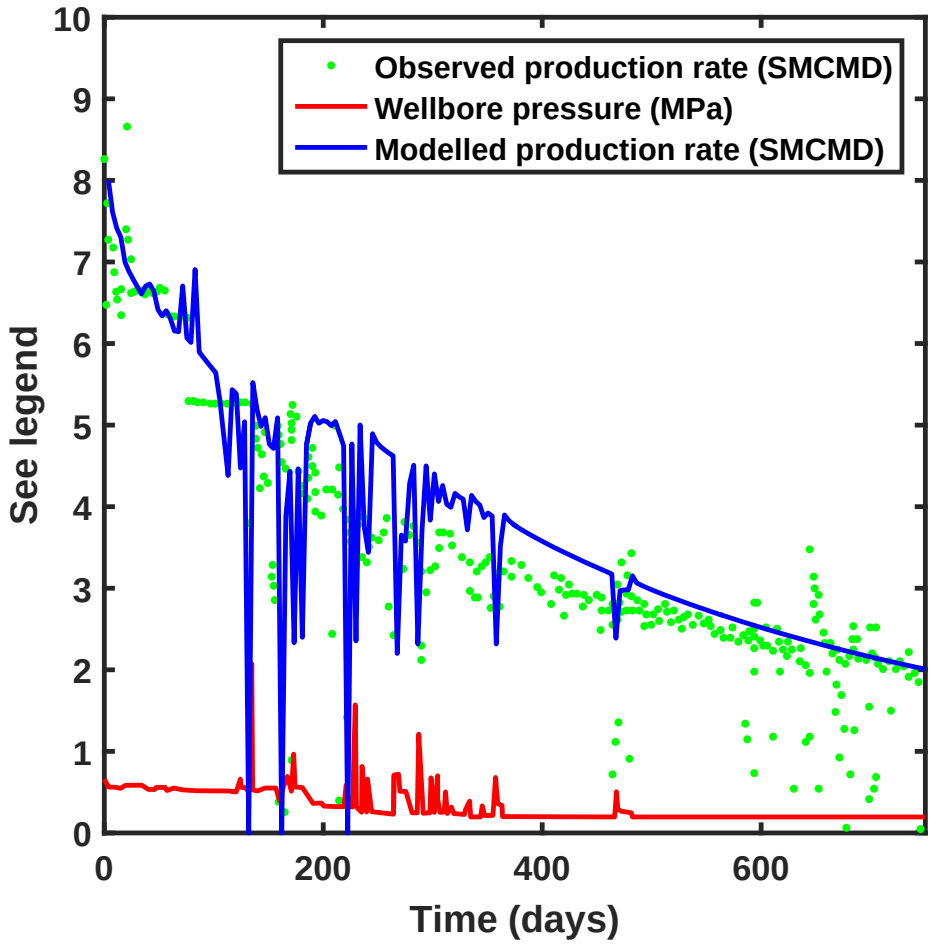

Figure 2.4: Plot of production rate and wellbore pressure as a function of time from the Horseshoe Canyon CBM production site. The observed data was digitally extracted from Fig. 3 of Gerami et al. (2008). The modeled production data was obtained from our numerical model with P_w driven by the observed wellbore pressure. The parameters used in the model are given as Case 3 in Table 2.1. The SPE acronym, SMCMD, stands for Standard Thousand Cubic Metres per Day.

Chapter 3

Coal-bed methane production in the presence of water

Summary

This chapter describes the development of mathematical model for two-phase (water-gas) flow in a CBm reservoir. The objectives are:

- To Solve a set of equations for two-phase fluid flow in the CBM reservoir using MATLAB ODE solver, ode 15s, and method of lines (MoL).
- To build a MATLAB code capable of modelling two-phase (water-gas) flow in a CBM reservoir.
- To investigate the impact of initial water saturation on pressure drawdown after a specified amount of gas has been produced.

The model is a two-phase (water-gas) immiscible flow model for modelling coal-bed methane recovery in a CBM reservoir. The choice to build a model in MATLAB instead of adopting any of the suite of commercial and/or open-source

available that can handle CBM flow in a CBM reservoir (COMSOL, TOUGH2, GEM, ECLIPSE) was to enable us model simplified situation without the interference of any multiphase effects. Also, the benefit of building the model was to have a deeper understanding of the mechanics behind CBM movements in coal formation. Furthermore, this could lead to more considerable experimentation with mathematical description of the CBM flow processes and allowed us to give more attention to the dominating functions and less to those which seemed to have a minor impact on the results, thus streamlining the model.

The MATLAB model used was built by myself with assistance from Simon Mathias and Stefan Nielsen. All simulations were run and analyzed by myself. Ye et al. (2014) and Mora and Wattenbarger (2009) presented the parameter values used in this chapter. GEM and ECLIPSE models were not run in this work; however, the gas production curves from my model were only compared with gas production results obtained from GEM and ECLIPSE as presented by Mora and Wattenbarger (2009).

3.1 Introduction

As discussed in the previous chapter, coal-bed methane (CBM) is mostly stored as an adsorbed phase on the surface of micropores within the coal matrix. In contrast, gas storage in conventional reservoirs comprises mostly free gas compressed within the pore-space. Therefore gas and water production time-series from CBM reservoirs are significantly different as compared to those from conventional gas reservoirs (McKee and Bumb, 1987; Shi et al., 2016) (see Fig. 3.1). The important distinction is that in conventional gas reservoirs (see Fig. 3.1a), gas production rate

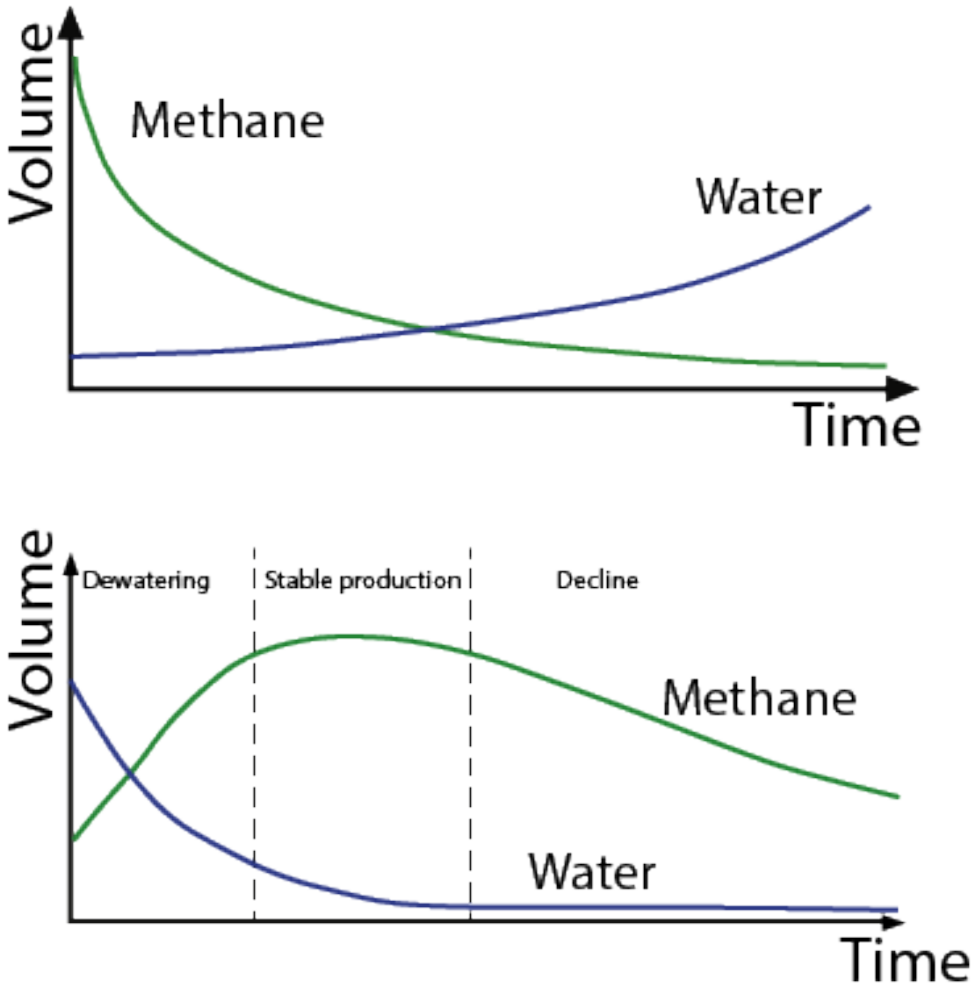

Figure 3.1: Schematic of production time-series in a) a typical conventional gas well from a clastic reservoir and b) a typical CBM reservoir (modified after Bertrand et al., 2017).

is at its highest level at the start of production and gradually declines with the final phase being accompanied by an increase in water production. In contrast, CBM production gives rise to water production rate peaking at the start of production, followed by a continuous rise in methane production caused by decompression induced gas desorption (Fig. 3.1b).

In almost all cases, methane production from CBM reservoirs is preceded by the production of a significant amount of water, which is a necessary precursor to

lower reservoir pressure. This is because CBM is trapped in the coal matrix due to pressure exerted both by water present in the fracture domain and hydrostatic pressure. The methane gas desorption initiates once the reservoir pressure in the fracture domain reduces to the critical desorption pressure such that gas can desorb from coal particles (Schraufnagel, 1993). Methane gas molecules then diffuse through the matrix domain toward the fracture domain where the flow becomes viscous and migrates through the cleat system, and finally reaches the production well (Ayoub et al., 1991) (see Fig. 3.2).

Some modeling attempts have treated fluid flow in the fracture domain of a CBM reservoir with initial water saturation of 100% at the start of production as a single-phase flow system, obtaining some useful simulations results (Bumb and McKee, 1988; Aminian et al., 2005). However, such models do not conform with reality because many CBM wells co-produce water with at least a small amount of gas when production starts (Sun et al., 2017), It is, therefore, essential to treat fluid flow in coal fracture systems as a two-phase flow process, which explicitly acknowledges the coexistence of water and gas (Seidle, 2011, p. 247).

Initial water saturation is a significant factor concerning CBM production performance (Roadifer, 2003; Moore, 2012). A decrease in the initial water saturation increases the gas production rate in CBM reservoirs (Moore, 2012). Water saturation affects fluid mobility within CBM reservoirs due to associated variations in relative permeability. Relative permeability is the fraction of permeability available to a particular fluid phase in the presence of multiphase flow in porous media. Several authors have proposed different formulations to determine relative permeability from fluid saturation in CBM reservoirs and porous media in general (Brooks and

Corey, 1966; Van Genuchten, 1980; Orr, 2007; Zhou, 2012; Durucan et al., 2013; Chen et al., 2013a; Xu et al., 2014).

Some studies have attempted to derive relative permeability from reservoir history-matching (Zhou, 2012). Others have focused on acquiring relative permeability from core analysis (Ham and Kanzas, 2008). Chen et al. (2013b) applied a theoretical matchstick model to estimate relative permeability, analogous to the use of capillary bundle models, which are common in conventional porous media settings. For more detail on relative permeability models for CBM, readers are referred to Shen et al. (2011) and Zhang et al. (2015).

The two-phase fluid flow in the CBM reservoir is a complex nonlinear system that cannot be solved analytically must instead be solved analytically. Several numerical fluid flow models in CBM reservoirs (Yound et al., 1998; Thararoop et al., 2012; Unsal et al., 2010; Liu et al., 2014) have developed and obtained some useful computational and simulation results. Most of the existing numerical model resolved the temporal term around the choice of explicit or implicit low-order time stepping.

Alternatively, multi-step, multi-order schemes, which treat the temporal term more accurately, have been presented before for two-phase immiscible fluid flow in porous media (Mathias et al., 2006, 2008b). These techniques conserve a specific time integration error despite maximizing the time-step size. The good thing is that there is no need to redevelop the time-integration algorithms because they are available in the form of high-quality solvers (MATLAB, Python, or FORTRAN with NAG) and are very simple to implement.

In this chapter, a mathematical model is developed to describe two-phase im-

miscible flow (water and methane gas) within a CBM reservoir during methane production. As in the previous chapter, the relevant mathematical equations are presented, followed by a description of the numerical solution process. A verification example is then presented whereby results from the developed model are compared to previously published results from existing commercial software packages. The dry-gas case study of Ye et al. (2014) is then revisited to explore the effect of initial water saturation on gas production and corresponding fluid pressure evolution.

3.2 Mathematical model

Consider the co-production of methane and water from a cylindrical, homogenous, isotropic and horizontally oriented, CBM reservoir. The CBM reservoir is overlain and underlain by impermeable geological formations. Furthermore, the CBM reservoir is purely comprised of coal, methane and water. The CBM reservoir initially exhibits a uniform pressure, P_I [$\mathrm{ML^{-1}T^{-2}}$], and uniform water saturation, S_{wI} [-], and free methane is initially in equilibrium with the adsorbed methane in the coal matrix. Gas production is stimulated by holding the production well at a fixed pressure, P_w [$\mathrm{ML^{-1}T^{-2}}$]. Additional relevant assumptions include that capillary pressure (i.e., the difference between the gas pressure and water pressure) is negligible and that the gas and water are immiscible.

The mass conservation statements for methane and water in the CBM reservoir take the form:

$$\frac{(\phi \rho_g S_g)}{\partial t} + \rho_c \frac{\partial s}{\partial t} = -\frac{1}{r}\frac{\partial (r \rho_g q_g)}{\partial r} \tag{3.1}$$

$$\frac{(\phi \rho_w S_w)}{\partial t} = -\frac{1}{r}\frac{\partial (r \rho_w q_w)}{\partial r} \tag{3.2}$$

where ρ_w [ML^{-3}] is the density of water in the cleats, S_g [-] and S_w [-] are volume fractions of the fracture porosity containing gaseous methane and water, respectively (referred to hereafter as the gas and water saturations, respectively), and q_g [LT^{-1}] and q_w [LT^{-1}] are the volumetric fluxes of methane and water, respectively, found from the following modified forms of Darcy's law:

$$q_g = -\frac{kk_{rg}}{\mu_g}\frac{\partial P}{\partial r} \tag{3.3}$$

$$q_w = -\frac{kk_{rw}}{\mu_w}\frac{\partial P}{\partial r} \tag{3.4}$$

where μ_w [$ML^{-1}T^{-1}$] is the dynamic viscosity of water in the cleats, k_{rg} [-] and k_{rw} [-] are the relative permeabilities of gas and water, respectively, and everything else is as defined in the previous chapter.

Throughout this thesis, the density, compressibility and viscosity of water are calculated using correlations due to Batzle and Wang (1992).

The relevant initial and boundary conditions take the form:

$$\begin{aligned}
&P = P_I, && r_w \leq r \leq R, && t = 0 \\
&S_w = S_{wI}, && r_w \leq r \leq R, && t = 0 \\
&P = P_w, && r = r_w, && t > 0 \\
&\partial P/\partial r = 0, && r = R, && t > 0
\end{aligned} \tag{3.5}$$

where r_w [L] is the well radius and R [L] is the radius of the CBM reservoir.

3.2.1 Phase saturation

Saturation of a fluid phase is defined as the fraction of the void volume of a porous medium filled by this phase. The coal cleats are assumed to be under-saturated due to the presence of free water in the cleat system. The fact that methane gas and

water jointly fill the coal cleats implies that the sum of the degree of saturation of the liquid phase, S_w, and the gas phase, S_g, is always equal to unity:

$$S_w + S_g = 1 \tag{3.6}$$

3.2.2 Relative permeability

During primary recovery, the production of CBM first requires dewatering to reduce the reservoir pressure. This reduction in pressure in the coal-bed methane reservoir pressure is followed by desorption of methane from the coal matrix domain. Once the desorbed methane that diffuses into the fracture domain reaches the threshold of irreducible gas saturation, simultaneous gas and water flow occurs in the domain. In the presence of multiple phases flow in the fracture domain, the permeability for one phase is reduced due to the presence of other phases within the fracture domain.

Relative permeability, which is the ratio of the effective permeability to the absolute permeability of the porous media, is commonly used for characterizing the flow capacity for one fluid during a simultaneous filtration of multiphase system. It depends on all the phase saturation and always less than absolute permeability. For example, if only single phase is present in a pore, its relative permeability is 1, but when two or more phases flow in a pore, they interfere with each other and their relative permeabilities decreases. For two phase flow, without loss of generality, the relative permeabilities are assumed to be power law functions of saturation as follows (e.g. Orr, 2007):

$$k_{rw} = k_{rw0}\left(\frac{S_w - S_{wr}}{1 - S_{gc} - S_{wr}}\right)^m, \quad S_{wr} \leq S_w \leq 1 - S_{gc} \tag{3.7}$$

$$k_{rg} = k_{rg0}\left(\frac{S_g - S_{gc}}{1 - S_{gc} - S_{wr}}\right)^n, \quad S_{gc} \leq S_g \leq 1 - S_{wr} \tag{3.8}$$

where S_{wr} [-] is the residual water saturation, S_{gc} [-] is the critical gas saturation, and k_{rw0} [-], k_{rg0} [-], m [-] and n [-] are the end-point relative permeabilities and power-law exponents for the water and gas phases, respectively.

3.2.3 Solving for pressure instead of gas saturation

It is useful to solve for pressure head instead of gas saturation because pressure is needed to determine the effective stress and also the gas mass transfer from the matrix into the fracture system (see Chapter 2). The first step to achieving this involves recognizing that

$$\frac{\partial(\phi\rho_g S_g)}{\partial t} = \phi\rho_g\left[S_g(c_c + c_g)\frac{\partial P}{\partial t} + \frac{\partial S_g}{\partial t}\right] \tag{3.9}$$

$$\frac{\partial(\phi\rho_w S_w)}{\partial t} = \phi\rho_w\left[S_w(c_c + c_w)\frac{\partial P}{\partial t} + \frac{\partial S_w}{\partial t}\right] \tag{3.10}$$

where c_w [$\mathrm{M^{-1}LT^2}$] is the compressibility of the water found from

$$c_w = \frac{1}{\rho_w}\frac{\partial \rho_w}{\partial P} \tag{3.11}$$

The compressibility is generally taken to be a constant and therefore

$$\rho_w = \rho_{wI}\exp[c_w(P - P_I)] \tag{3.12}$$

where ρ_{wI} [$\mathrm{ML^{-3}}$] is the density of water when $P = P_I$.

The next step is to recognize that $S_g + S_w = 1$, (Recall (3.6)), and therefore

$$\frac{\partial(\phi\rho_g S_g)}{\partial t} = \phi\rho_g\left[S_g(c_c + c_g)\frac{\partial P}{\partial t} - \frac{\partial S_w}{\partial t}\right] \tag{3.13}$$

Considering again Eqs. (3.1) and (3.2) it can be realized that

$$\phi\rho_g\left[S_g(c_c + c_g)\frac{\partial P}{\partial t} - \frac{\partial S_w}{\partial t}\right] + \rho_c\frac{\partial s}{\partial t} = -\frac{1}{r}\frac{\partial(r\rho_g q_g)}{\partial r} \tag{3.14}$$

and

$$\phi\rho_w\left[S_w(c_c+c_w)\frac{\partial P}{\partial t}+\frac{\partial S_w}{\partial t}\right]=-\frac{1}{r}\frac{\partial(r\rho_w q_w)}{\partial r} \tag{3.15}$$

from which it follows that

$$\phi(c_c+S_g c_g+S_w c_w)\frac{\partial P}{\partial t}=-\frac{1}{r\rho_g}\frac{\partial(r\rho_g q_g)}{\partial r}-\frac{1}{r\rho_w}\frac{\partial(r\rho_w q_w)}{\partial r}-\frac{\rho_c}{\rho_g}\frac{\partial s}{\partial t} \tag{3.16}$$

and

$$\frac{\partial S_w}{\partial t}=-\frac{1}{r\phi\rho_w}\frac{\partial(r\rho_w q_w)}{\partial r}-S_w(c_c+c_w)\frac{\partial P}{\partial t} \tag{3.17}$$

Recall $\frac{\partial s}{\partial t}$ is given in Eq. (2.8) as

$$\frac{\partial s}{\partial t}=\frac{s_0-s}{t_r} \tag{3.18}$$

3.2.4 Numerical solution

Numerical solution of the above set of Eqs (3.16), (3.17) and (3.18) is achieved in exactly the same way as in Chapter 2, with finite differences and the MATLAB ODE solver, ODE15s. However, instead of just two partial differential equations, we now have three (one for P, S_w and s). The discretised form of the relevant equations takes the form (similar to as in Chapter 2):

$$\phi_i(c_{c,i}+S_{g,i}c_{g,i}+S_{w,i}c_{w,i})\frac{dP_i}{dt}=R_{g,i}+R_{w,i}-\frac{\rho_c}{\rho_{g,i}}\frac{ds_i}{dt},\quad i=1\ldots N \tag{3.19}$$

$$\frac{dS_{w,i}}{dt}=\frac{R_{w,i}}{\phi_i}-S_{wi}(c_c+c_w)\frac{dP_i}{dt},\quad i=1\ldots N \tag{3.20}$$

and

$$\frac{ds_i}{\partial t}=\alpha(s_{0,i}-s_i),\quad i=1\ldots N \tag{3.21}$$

where

$$R_{g,i} = \frac{r_{i-1/2}\rho_{g,i-1/2}q_{g,i-1/2} - r_{i+1/2}\rho_{g,i+1/2}q_{g,i+1/2}}{\rho_{g,i}r_i(r_{i+1/2} - r_{1-1/2})} \tag{3.22}$$

$$R_{w,i} = \frac{r_{i-1/2}\rho_{w,i-1/2}q_{w,i-1/2} - r_{i+1/2}\rho_{w,i+1/2}q_{w,i+1/2}}{\rho_{w,i}r_i(r_{i+1/2} - r_{1-1/2})} \tag{3.23}$$

and

$$q_{g,i+1/2} = -\frac{k_{i+1/2}k_{rg,i+1/2}}{\mu_g}\left(\frac{P_{i+1} - P_i}{r_{i+1} - r_i}\right), \quad i = 2\ldots N \tag{3.24}$$

$$q_{w,i+1/2} = -\frac{k_{i+1/2}k_{rw,i+1/2}}{\mu_w}\left(\frac{P_{i+1} - P_i}{r_{i+1} - r_i}\right), \quad i = 2\ldots N \tag{3.25}$$

3.3 Results

3.3.1 Model comparison with GEM and ECLIPSE

As a first verification example, results from the above model are compared to results from two existing commercial software packages, namely GEM and ECLIPSE, previously presented by Mora and Wattenbarger (2009). Both GEM and ECLIPSE are compositional reservoir simulators that use finite differences to solve the governing equations of multi-phase flow in porous media. GEM is developed and owned by Computer Modeling Group (CMG) Ltd. ECLIPSE is developed and owned by Schlumberger. All three models (including the two-phase flow model described above) were used to simulate methane gas and water production from a cylindrical CBM reservoir. The model parameters used are shown in Table 3.1. Note that, along with Mora and Wattenbarger (2009), the pore-space is assumed to be initially saturated with water (i.e., $S_{wI} = 1$) and the porosity of the domain is assumed to be constant throughout (i.e., $c_f = 0$).

Unfortunately, Mora and Wattenbarger (2009) do not describe the relative permeability model used. Therefore we have chosen to adopt Eqs. (3.7) and (3.8)

with $k_{rg0} = k_{rw0} = 1$, $S_{gc} = S_{wr} = 0$ and $n = m = 1$ for one of the simulations and $n = m = 2$ for another simulation. Furthermore, Mora and Wattenbarger (2009) do not specify the radius of their injection well, therefore we have chosen to set this equal to 0.2 m.

Fig. 3.3a shows a comparison of numerically simulated gas production rate as a function of time from GEM, ECLIPSE and the present model with $n = m = 1$ and $n = m = 2$. Here it can be seen that when $n = m = 2$, the present model significantly underestimates the amount of gas produced. In contrast when $n = m = 1$ the results are very similar. Fig. 3.3b shows a plot of water production rate during the same time, which is shown to relatively insensitive to the relative permeability exponent. The reason that less gas is produced with high values of n and m is that this greater non-linearity in the relative permeability model leads to a reduced relative permeability at low gas saturations. Unfortunately, Mora and Wattenbarger (2009) do not present their water production results and therefore no further comparison can be made.

3.3.2 Revisiting the Ye et al. (2014) study with water

To explore the effect of water on gas production and pressure distribution in the presence of stress dependent porosity and permeability, the Case 1 (recall Table 2.1) from Ye et al. (2014) is revisited with varying initial water saturations. In this case we have chosen to adopt Eqs. (3.7) and (3.8) for relative permeability again with $k_{rg0} = k_{rw0} = 1$ and $S_{gc} = 0$ but also with $S_{wr} = 0.1$ and $n = m = 2$, which is perceived to be more realistic for gas and water systems in geological formations (consider Mathias et al., 2013).

Table 3.1: Parameter values for the GEM and ECLIPSE simulations presented by Mora and Wattenbarger (2009). Note that the radius, R, of the model is found from $\sqrt{A/\pi}$.

Parameter	Field units	Metric units
Initial permeability, k_I	5 mD	5×10^{-15} m^2
Cleat volume compressibility, c_f	0	0
Initial porosity, ϕ_I (-)	0.01	0.01
Area of the CBM reservoir, A	80 acres	323,800 m^2
CBM reservoir thickness, H	12.5 ft	3.810 m
Langmuir pressure constant, P_L	100 psi	0.6895 MPa
Langmuir volume constant, V_L	591 ft^3 ton^{-1}	0.01845 m^3 kg^{-1}
Density of coal, ρ_c	1500 kg m^{-3}	1500 kg m^{-3}
Initial pressure, P_I	700 psi	4.826 MPa
Wellbore pressure, P_0	50 psi	0.3447 MPa
CBM reservoir temperature, T	70 ^{o}F	294.3 K
Langmuir volumetric strain constant, ε_L	N/A	N/A
Well radius, r_w	unspecified	0.2 m
Mass transfer coefficient, t_r	200 days	200 days
Young's modulus, E	N/A	N/A
Poisson's ratio, ν	N/A	N/A

Fig. 3.4a shows a plot of gas production rate against time for different initial water saturations. As the initial water saturation increases, the gas production rate is reduced, due to an associated reduction in gas relative permeability. The time at which peak gas production rate occurs (around 20 days) is insensitive to initial water saturation for $S_{wI} < 0.6$. However, for $S_{wI} > 0.6$, a second rise in gas production occurs later on at around 100 days. Inspection of the plots of associated water production rate against time (Fig. 3.4b) suggests that this second gas production peak corresponds with a steep decline in water production.

Fig. 3.4c shows a plot of cumulative gas production as a function of time for different initial water saturations. After 1000 days, the dry model (i.e., $S_{wI} = 0$) has produced 5500 (SMCM) (standard thousand cubic meters) of gas. In contrast, the fully water saturated model (i.e., $S_{wI} = 1$) has produced just 3600 SMCM of gas in the same time. The time at which 3500 SMCM is produced increases with increasing initial water saturation and ranges from 500 (with $S_{wI} = 0$) to 950 (with $S_{wI} = 1$) days. The increase in time with increasing initial water saturation is again due to an associated reduction in gas relative permeability.

To explore the potential role of water saturation on land surface subsidence, it is worth to look at the variation in simulated fluid pressures. Fig. 3.4d shows plots of mean fluid pressure, $\hat{P}$, as a function of time for different initial water saturations, found from

$$\hat{P}(t) = \frac{2}{R^2 - r_w^2} \int_{r_w}^{R} rP(r,t)dr \tag{3.26}$$

Lower mean fluid pressures imply an increase in effective stress, which will lead to an increase in ground-surface subsidence. Fig. 3.4d shows that the decline in fluid pressure after 1000 days of production reduces with increasing initial wa-

ter saturation. But these fluid pressure reductions do not correspond to the same quantity of gas produced (recall Fig. 3.4c).

Fig. 3.5a shows a plot of water saturation against radial distance as a function of time for the case when $S_{wI} = 1$. It can be seen that the reduction in pressure at the well-bore leads to a drying-front that propagates out from the well. This occurs because the reduction in pressure gives rise to gas desorption from the coal-matrix, which in turn displaces water contained within the fractures into the well-bore.

Fig. 3.5b shows a plot of fluid pressure against radial distance as a function of time for the case when $S_{wI} = 1$. Here it can be seen that a pressure front moves out from the production well at a similar rate to the aforementioned drying front. Once the pressure front reaches the reservoir boundary, the pressure reduces across the reservoir in a relatively uniform manner. This leads to a corresponding spatially uniform decrease in water saturation (Fig. 3.5a). Reinspection of Fig. 3.4a suggests that the aforementioned second rise in gas production also corresponds with when the pressure front reaches the reservoir boundary.

Relating back to the effect of water saturation on land-surface subsidence, Fig. 3.5c shows a plot of fluid pressure against radial distance from each of the different initial water saturations studied at the exact time at which 3500 SMCM of gas is produced (recall Fig. 3.4c). Here it can be seen that initial water saturation has a negligible effect on the pressure distribution within a CBM reservoir for a fixed volume of gas produced after 1000 days of production. The main reason for this is that the initial fracture porosity is very small and consequently the volume of water contained within the fractures is trivial compared to the total volume of gas.

3.4 Conclusions

The model for CBM production developed in Chapter 2 has been extended to account for the presence of water in the fracture porosity. This led to the need to solve three coupled non-linear partial differential equations using the MATLAB solver, ODE15s. The capability to incorporate water was tested by comparing numerical results for methane gas production rate to published results obtained using the commercial software packages GEM and ECLIPSE. The case study due to Ye et al. (2014), from Chapter 2, was then extended to look at the effect of initial water saturation on gas production and reservoir pressure draw-down.

The presence of water in the fracture porosity was found to reduce gas production rates. This was due to the reduced gas relative permeability that occurs as a consequence of water saturation. However, water saturation was also found to delay the propagation of pressure change from the well-bore. Furthermore, it was found that the pressure distribution within a CBM reservoir, after a specified quantity of gas is produced, is insensitive to initial water saturation. An explanation for this is that the quantity of water that can be stored in the fracture space is very small as compared to the standard volume of gas that can be stored in an adsorbed phase within the coal matrix.

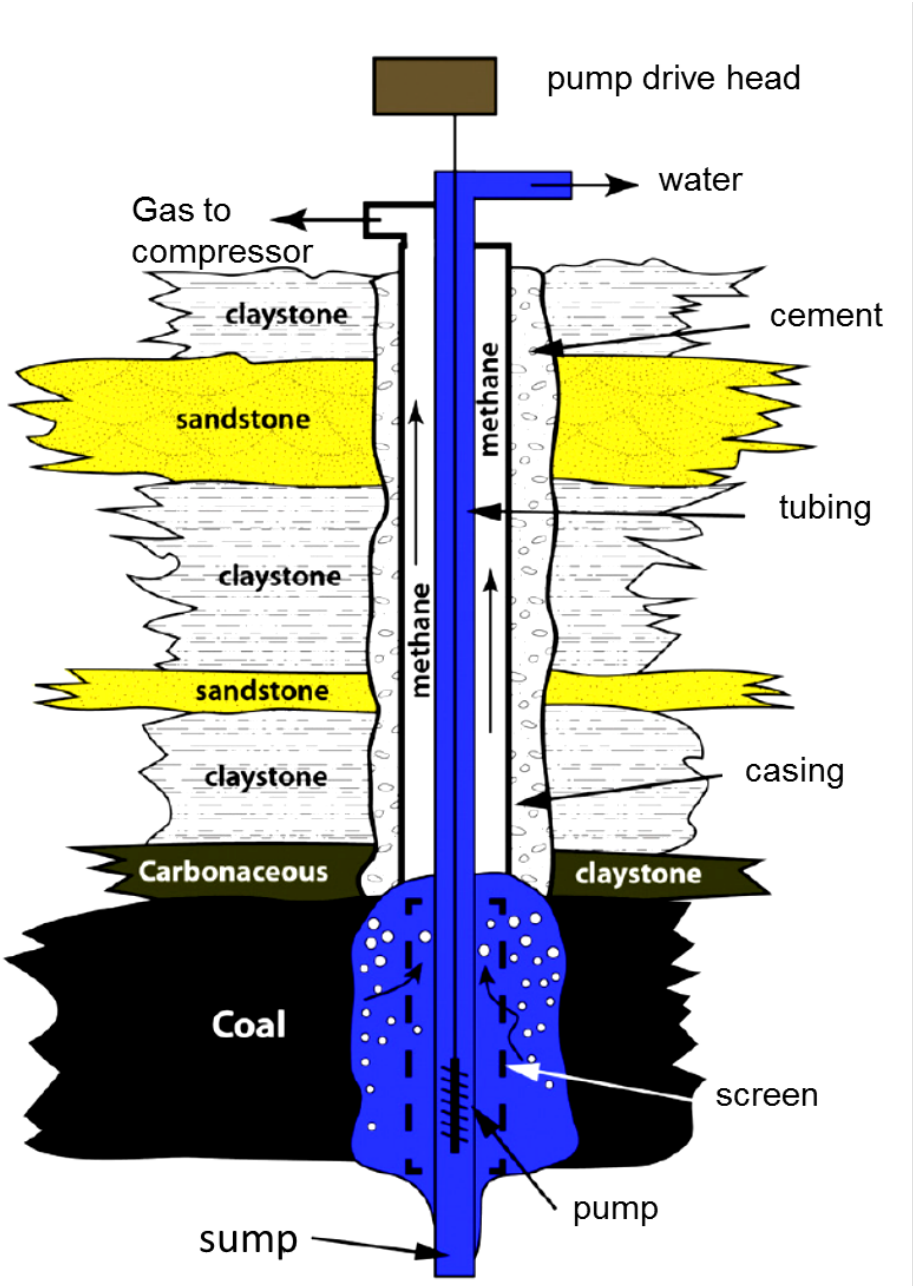

Figure 3.2: Schematic diagram illustrating CBM producing reservoir with methane gas and water migrating through a vertical well (after Moore, 2012).

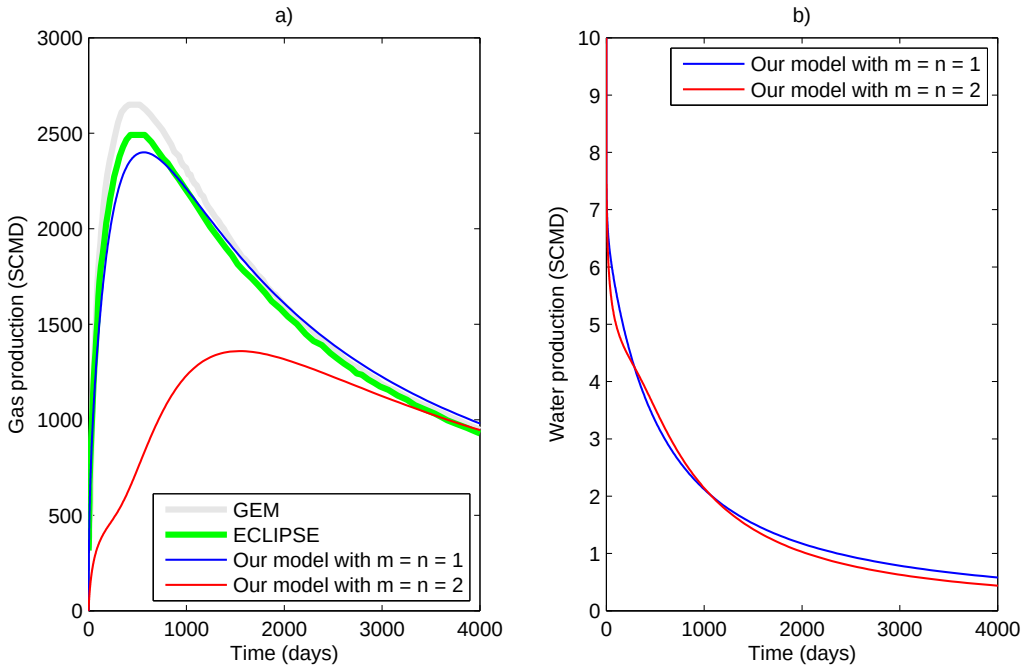

Figure 3.3: Comparison of our model results with those from GEM and ECLIPSE as presented by Mora and Wattenbarger (2009). The model with $m = n = 1$ assumes that relative permeability is a linear function of water saturation. The model with $m = n = 2$ assumes that relative permeability is a quadratic function of water saturation. The SPE acronym, SCMD, stands for Standard Cubic Metres per Day.

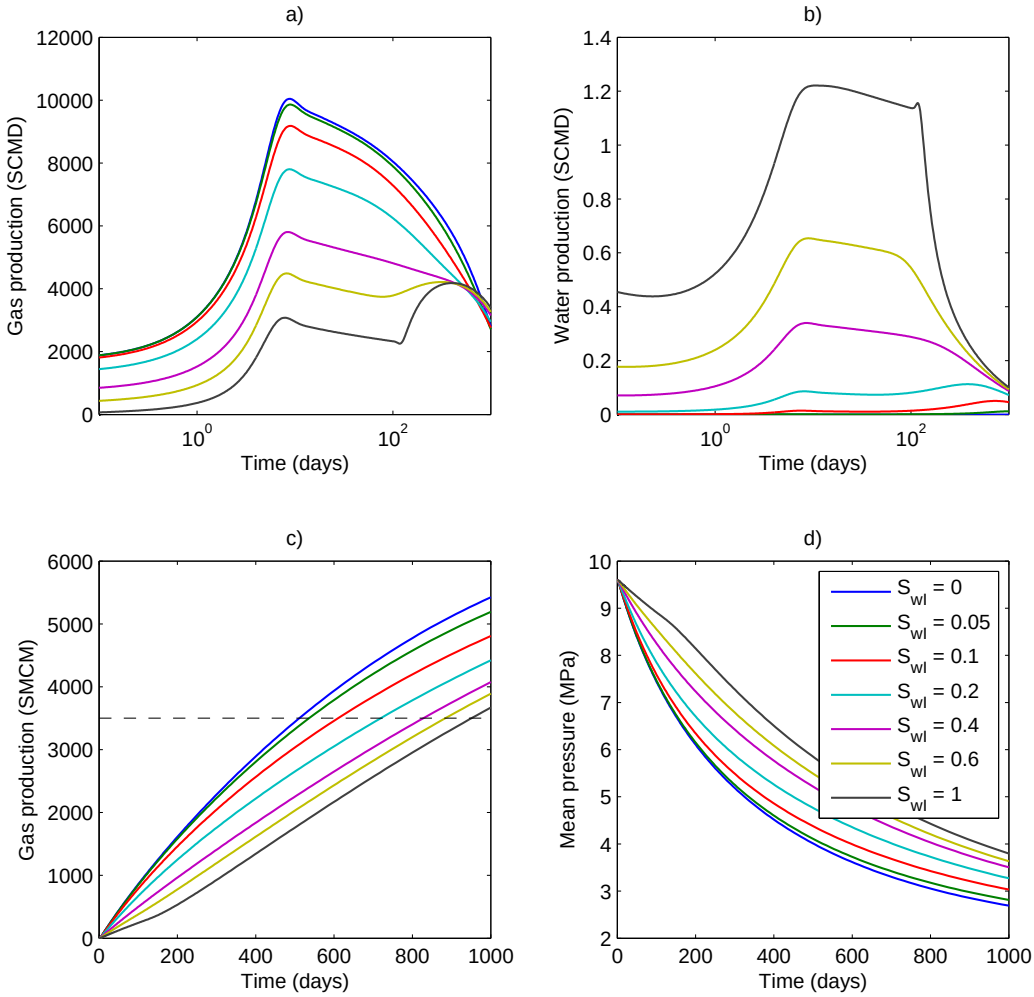

Figure 3.4: Numerical model results based on Case 1 of Ye et al. (2014) but with varying initial water saturations. a) Plot of gas production rate. b) Plot of water production rate. c) Plot of cumulative gas production. The black dashed line indicates a gas volume of 3500 SMCM. d) Plot of mean reservoir pressure. The SPE acronyms, SCMD and SMCM, stand for Standard Cubic Meters per Day and Standard Thousand Cubic Metres, respectively.

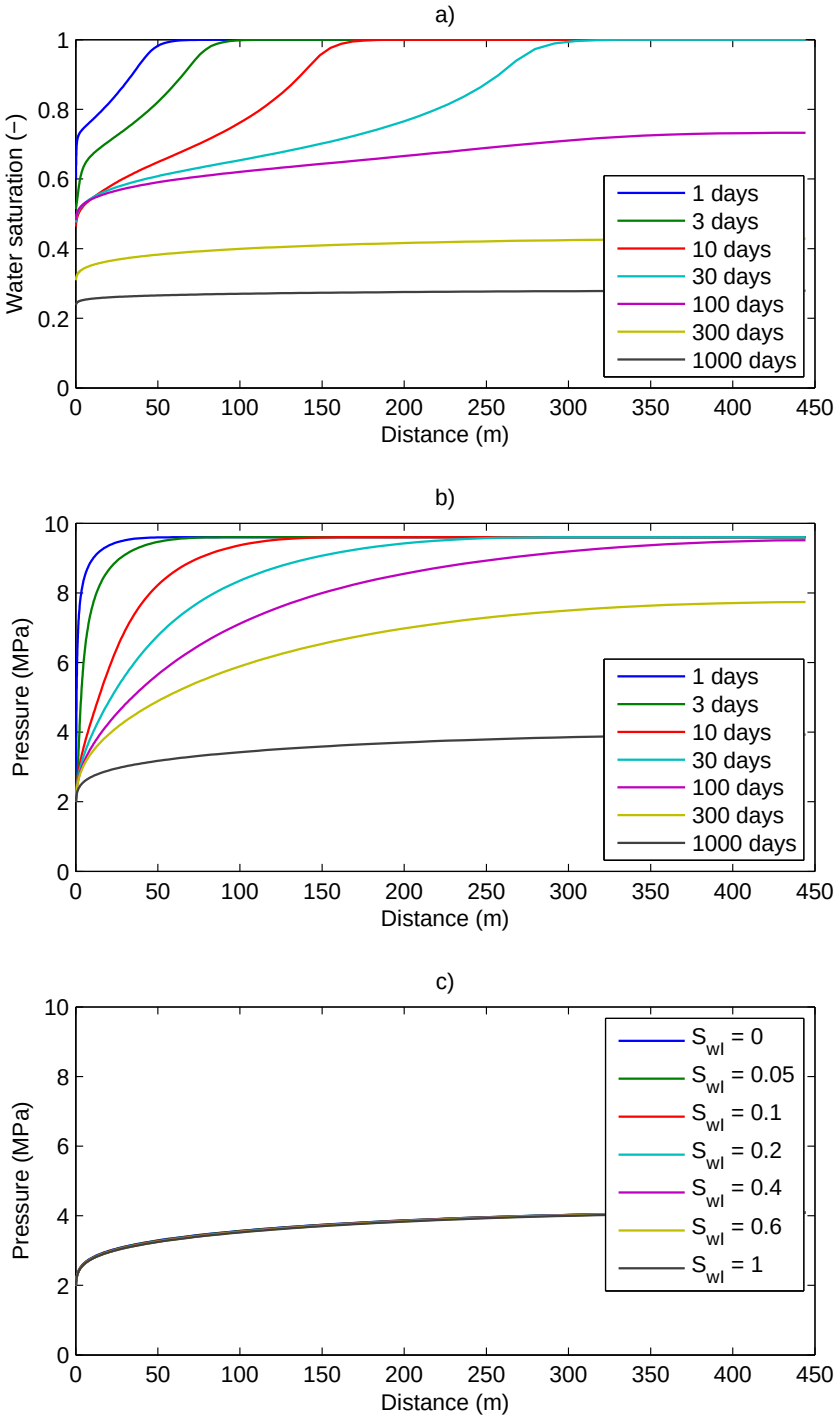

Figure 3.5: Numerical model results based on Case 1 of Ye et al. (2014) but with varying initial water saturations. a) Plot of water saturation against radial distance at different times for the $S_{wI} = 1$ scenario. b) Plot of fluid pressure against radial distance at different times for the $S_{wI} = 1$ scenario. c) Plot of fluid pressure against radial distance after 3500 MSCM of gas has been produced with different initial water saturations.

Chapter 4

Subsidence due to fluid production from a cylindrical confined aquifer

Summary

This chapter describes the steps involved in developing an analytical model to quantify ground surface subsidence caused by groundwater withdrawal from a confined aquifer with radial symmetry.

The advancement in this chapter is the presentation of an analytical model to quantify ground surface subsidence caused by groundwater pumping from a confined aquifer with radial symmetry. The closed-form equation accounts for an approximate distribution within the aquifer and a complete 3-D stress distribution in the computational domain. The final equation is effective and efficient as the existing analytical solution but much more comfortable to implement than the previous analytical formulation recently proposed in the literature.

4.1 Introduction

Before looking at models to describe ground surface subsidence due to coal-bed methane production it is conducive to first consider the more simple problem of ground surface subsidence due to groundwater production. Ground surface subsidence due to groundwater production has been a significant problem around the world for many decades (Gambolati and Teatini, 2015). When water is produced from an aquifer, the pressure within the aquifer is reduced, leading to a reduction in effective stress, which results in subsidence at the ground surface. Many attempts have been made to develop analytical models to forecast subsidence rates as a consequence of groundwater production.

Early models assumed radial symmetry around a groundwater production well. These models then either assumed that strain occurred only in the vertical direction (uniaxial strain) (Verruijt, 1969; Bear and Corapcioglu, 1981a) or that incremental vertical total stress is zero (Verruijt, 1969; Bear and Corapcioglu, 1981b). Verruijt (1969) argues that the zero incremental vertical total stress model is analogous to assuming that the aquifer is overlain by a soft clay overburden, which offers negligible resistance to displacement. Both approaches lead to the elegant result that subsidence, at any point on the ground surface, is linearly proportional to the change in pressure in the aquifer immediately below.

However, the uniaxial strain model overestimates subsidence at the ground surface because it neglects the way the surrounding geological media distributes deformation laterally away from the aquifer of concern (Wu et al., 2018a). The zero incremental vertical total stress model also overestimates subsidence at the ground surface because it neglects the vertical resistance of the overburden.

Geertsma (1973) developed an alternative analytical solution whereby the three-dimensional stress distribution is resolved without invoking uniaxial strain or zero incremental vertical total stress assumptions. Specifically, Geertsma (1973) considered the stress, strain and displacement around a cylindrical region of uniform pressure change. In particular, Geertsma (1973) derived a closed-form equation to calculate the ground surface subsidence (induced by the pressure change) immediately above the center of this cylindrical region.

Geertsma's closed-from equation can be related to the ground surface subsidence immediately above a production well at the center of a cylindrical confined aquifer. However, the assumption of uniform pressure leads to an underestimate in ground surface subsidence in this context. This is because the drawdown in pressure at the production well is much more significant than at the far-field of the aquifer (Wu et al., 2018a).

Selvadurai and Kim (2015) sought to extend the analytical solution of Geertsma (1973) to allow for a non-uniform pressure distribution controlled by fluid production rate, fluid viscosity and aquifer permeability. However, the resulting equation for ground surface subsidence at the production well is significantly more complicated to evaluate, rendering it beyond application for most practical purposes.

More recently, Pujades et al. (2017) developed a numerical model to look at subsidence above a production well in an unconfined aquifer. They found that the zero incremental vertical total stress model was effective at estimating the subsidence far away from the production well. But close to the production well, the zero incremental vertical total stress model significantly overestimates the subsidence. Pujades et al. (2017) then derived an empirical correction factor based on studying

a sensitivity analysis of their numerical model. However, a limitation of their numerical model was that the model domain was restricted to the extent of the aquifer. Therefore their model was unable to properly account for how fluid production induced deformations propagate out into laterally and vertically extensive geological formations surrounding the aquifer region.

In this chapter, we build on the work of Geertsma (1973) to develop a closed-form equation for ground surface subsidence due to constant rate production of a viscous fluid from a cylindrical aquifer of finite permeability. This is achieved by application of the principle of superposition. Results from the new analytical solution are compared with equivalent results from a set of finite element simulations obtained using COMSOL Multiphysics v5.4.

A version of this chapter is presented in the following article:

Jayeoba, A., Mathias, S. A., Nielsen, S., Vilarrasa, V., & Bjørnarå, T. I. (2019). Closed-form equation for subsidence due to fluid production from a cylindrical confined aquifer. Journal of Hydrology, 573, 964-969.

4.2 Mathematical model

The mathematical model in this chapter is developed as follows. An analytical solution for the pressure distribution around a production well within a confined aquifer is presented. The original analytical solution of Geertsma (1973), for ground surface subsidence due to a cylindrical uniform pressure change, is presented. It is then shown how to incorporate non-uniform pressure distributions, resulting from constant rate production of a viscous fluid from a cylindrical aquifer of finite permeability, using the principle of superposition. A closed-form equation is then derived

to calculate the ground surface subsidence directly above the production well.

4.2.1 Pressure distribution in a confined aquifer

Consider constant-rate single-phase fluid production from a vertically oriented and fully completed production well, of infinitesimally small radius, located in the center of a homogenous, isotropic, cylindrical and confined aquifer (see Fig. 4.1a). The pressure distribution, P [$\mathrm{ML^{-1}T^{-2}}$], within the aquifer can be found from (Theis, 1935; Dake, 1983; Mijic et al., 2013)

$$P(r,t) = \begin{cases} P_i - \dfrac{Q\mu}{4\pi kH}\mathrm{E}_1\left(\dfrac{S\mu r^2}{4kt}\right), & 0 < t < t_c \\ \\ P_i - \dfrac{Q\mu}{4\pi kH}\left[\ln\left(\dfrac{R^2}{r^2}\right) + \dfrac{r^2}{R^2} - \dfrac{3}{2} + \dfrac{4kt}{S\mu R^2}\right] F(R-r), & t > t_c \end{cases} \tag{4.1}$$

where t [T] is time, P_i [$\mathrm{ML^{-1}T^{-2}}$] is the uniform initial pressure of the aquifer prior to commencement of fluid production, Q [$\mathrm{L^3T^{-1}}$] is the constant fluid production rate, μ [$\mathrm{ML^{-1}T^{-1}}$] is the dynamic viscosity of the fluid, k [$\mathrm{L^2}$] is the permeability of the aquifer, H [L] is the thickness of the aquifer, r [L] is radial distance from the production well, S [$\mathrm{M^{-1}LT^2}$] is the specific storage coefficient of the aquifer, R [L] is the radial extent of the aquifer, $F(x)$ denotes the Heaviside step function, $\mathrm{E}_1(x) = -\mathrm{Ei}(-x)$ and $\mathrm{Ei}(x)$ is the exponential integral function and t_c [T] is the characteristic time at which the pressure front, caused by the initiation of fluid production, reaches the boundary of the confined aquifer at $r = R$.

Eq. (4.1) is exact for $t \gg t_c$ and $t \ll t_c$ but also works as an accurate approximation for $t < t_c$ and $t > t_c$. However, Eq. (4.1) is not valid in the immediate region around t_c. However, this is of little consequence for our subsequent results. The ex-

act solution to this problem is provided by Van Everdingen (1949). However, their solution is provided as a Laplace transform, which requires numerical inversion, and is therefore not suitable for our subsequent analysis.

Note that the above set of equations represents a flow model, which has been uncoupled from the associated geomechanical processes. However, a good approximation for the pressure distribution, from a fully coupled flow model, can be obtained using a specific storage coefficient derived assuming zero lateral strain (Gambolati et al., 2000). A recent demonstration was provided by (Andersen et al., 2017). Analogous to Eq. (7.90) of Jaeger et al. (2009, p. 189) and Eq. (6a) of Gambolati et al. (2000), such an expression takes the form

$$S = \frac{\phi}{K_f} + \frac{(1-\alpha)(\alpha-\phi)}{K} + \alpha^2 C_m \tag{4.2}$$

where ϕ [-] is the porosity, K_f [$\mathrm{ML^{-1}T^{-2}}$] is the bulk modulus of the fluid, α [-] is the Biot coefficient, K [$\mathrm{ML^{-1}T^{-2}}$] is the bulk modulus of the rock and C_m [$\mathrm{M^{-1}LT^2}$] is the vertical (oedometric) bulk compressibility as measured in an oedometer with lateral expansion precluded, found from (Fjær et al., 2008, p.394)

$$C_m = \frac{1}{3K}\left(\frac{1+\nu}{1-\nu}\right) \tag{4.3}$$

where ν [-] is Poisson's ratio.

The drawdown of the piezometric surface within the aquifer, s [L], can be found from

$$s = \frac{P_i - P}{\rho g} \tag{4.4}$$

The characteristic time, t_c, can be thought of as the time at which $P = P_i$ at $r = R$ for the $t > t_c$ expression given in Eq. (4.1). It follows that

$$t_c = \frac{S\mu R^2}{8k} \tag{4.5}$$

4.2.2 Ground surface subsidence due to a cylindrical uniform pressure change

The geological material surrounding the aquifer is assumed to be homogenous, isotropic, impermeable and semi-infinite. Furthermore, the elastic properties of the surrounding material are assumed to be the same as those of the confined aquifer.

When the change in fluid pressure within the aquifer can be assumed uniform, Eq. (4.1) reduces to

$$P = P_i - \frac{Qt}{\pi HSR^2}, \quad 0 \leq r \leq R \tag{4.6}$$

and the subsidence at the surface directly above the production well, w [L], can be found from (Geertsma, 1973; Fjær et al., 2008, p. 405)

$$w = 2C_m H\alpha(P_i - P)(1-\nu)\left(1 - \frac{D}{\sqrt{D^2+R^2}}\right) \tag{4.7}$$

where D [L] is the depth of the center of the aquifer from the ground surface.

Substituting Eq. (4.6) into Eq. (4.7) leads to

$$w = \frac{2C_m\alpha(1-\nu)Qt}{\pi SR^2}\left(1 - \frac{D}{\sqrt{D^2+R^2}}\right) \tag{4.8}$$

Geertsma (1973) also derived analytical solutions for displacement in the radial and vertical directions, $u_r(r,z)$ [L] and $u_z(r,z)$ [L], respectively, normal total stress in the radial, angular and vertical directions, $\tau_{rr}(r,z)$ [$\mathrm{ML^{-1}T^{-2}}$], $\tau_{\theta\theta}(r,z)$ [$\mathrm{ML^{-1}T^{-2}}$] and $\tau_{zz}(r,z)$ [$\mathrm{ML^{-1}T^{-2}}$], respectively, and the stress, $\tau_{rz}(r,z)$ [$\mathrm{ML^{-1}T^{-2}}$] for this case. Note that z [L] is depth from the ground surface and r [L] is, again, the horizontal distance from the center of the well. In this way it can be understood that $w = -u_z(0,0)$ (see Fig. 4.1b). These analytical solutions are substantially more complicated to evaluate as compared to Eq. (4.7) because they involve numerical

approximations of several integral expressions. Nevertheless, all the mathematical expressions needed to determine these analytical solutions are presented in Appendix D5 of Fjær et al. (2008).

Because the problem being solved is a linear elastic problem, all the analytical solutions presented in Appendix D5 are linearly proportional to $P - P_i$. It is therefore useful to define the following auxiliary terms:

$$\tilde{w}(R) = \frac{w}{P - P_i}, \quad \tilde{u}_j(r,z,R) = \frac{u_j(r,z,R)}{P - P_i}, \quad \tilde{\tau}_{ij}(r,z,R) = \frac{\tau_{ij}(r,z)}{P - P_i} \tag{4.9}$$

where j is r for radial direction and z for vertical direction and the w, u_j and τ_{ij} terms in Eq. (4.9) hereafter specifically relate to the expressions presented in Appendix D5 of Fjær et al. (2008). Note that we are also identifying these expressions are functions of the radius of the uniform pressure cylinder, R, which corresponds to the radius of the confined aquifer in this case. For example, from Eq. (4.7),

$$\tilde{w}(R) = -2C_m H\alpha(1-\nu)\left(1 - \frac{D}{\sqrt{D^2+R^2}}\right) \tag{4.10}$$

4.2.3 Ground surface subsidence due to production of a viscous fluid

The analytical solutions presented by Geertsma (1973) explicitly assumes that the pressure within the aquifer is uniform. However, it is possible to derive approximate solutions to allow for non-uniform pressures by discretising the pressure distribution and applying the principle of superposition as follows:

Let $r \in [0,R]$ be discretized into N, not necessarily equally spaced, points located at r_k where $k = 1,2,3,\ldots,N$ (see Fig. 4.1c). In this way it can be said that:

$$w \approx \sum_{k=2}^{N} \tilde{w}(r_{k-1/2})(P_{k-1} - P_k) \tag{4.11}$$

$$u_j(r,z) \approx \sum_{k=2}^{N} \tilde{u}_j(r,z,r_{k-1/2})(P_{k-1}-P_k) \tag{4.12}$$

$$\tau_{ij}(r,z) \approx \sum_{k=2}^{N} \tilde{\tau}_{ij}(r,z,r_{k-1/2})(P_{k-1}-P_k) \tag{4.13}$$

where

$$r_{k-1/2} = \frac{r_k + r_{k-1}}{2} \tag{4.14}$$

4.2.4 Closed-form equation for subsidence above the production well

The series expansion of the $\mathrm{E}_1(x)$ function takes the form (Cooper and Jacob, 1946)

$$\mathrm{E}_1\left(\frac{S\mu r^2}{4kt}\right) = -\gamma - \ln\left(\frac{S\mu r^2}{4kt}\right) + O\left(\frac{S\mu r^2}{4kt}\right) \tag{4.15}$$

where $\gamma = 0.5772$ is known as the Euler-Mascheroni constant.

It follows that Eq. (4.1) can be written as (considering Cooper and Jacob, 1946)

$$P(r,t) = \begin{cases} P_i - \dfrac{Q\mu}{4\pi kH}\ln\left(\dfrac{r_e^2}{r^2}\right)F(r_e-r) + O\left(\dfrac{S\mu r^2}{4kt}\right), & 0 < t < t_c \\ \\ P_i - \dfrac{Q\mu}{4\pi kH}\left[\ln\left(\dfrac{R^2}{r^2}\right) + \dfrac{r^2}{R^2} - \dfrac{3}{2} + \dfrac{4kt}{S\mu R^2}\right]F(R-r), & t > t_c \end{cases} \tag{4.16}$$

where r_e [L] can be thought of as the radius of influence of the production well, found from

$$r_e = \sqrt{\frac{4kte^{-\gamma}}{S\mu}} \tag{4.17}$$

Because of the simple forms of Eqs. (4.16) and (4.7), an exact solution for w can be obtained by considering

$$w = \int_0^R \tilde{w}(r)\frac{dP}{dr}dr \tag{4.18}$$

Differentiating Eq. (4.16) with respect to r leads to

$$\frac{dP}{dr} = \frac{Q\mu}{2\pi kH} \begin{cases} \dfrac{1}{r}F(r_e - r) + O\left(\dfrac{S\mu r}{4kt}\right), & 0 < t < t_c \\ \left(\dfrac{1}{r} - \dfrac{r}{R^2}\right)F(R-r) + \left(\dfrac{2kt}{S\mu R^2} - \dfrac{1}{4}\right)\delta(R-r), & t > t_c \end{cases} \tag{4.19}$$

where $\delta(x)$ is the Dirac delta function.

It follows that

$$w_D = \begin{cases} 4\ln\left[\dfrac{1}{2}\left(1 + \sqrt{1 + \dfrac{\varepsilon e^{-\gamma t_D}}{2}}\right)\right], & 0 < t_D < 1 \\ \left(1 - \dfrac{1}{\sqrt{1+\varepsilon}}\right)(t_{0D} + t_D), & t_D > 1 \end{cases} \tag{4.20}$$

where

$$t_{0D} = \left(1 - \frac{1}{\sqrt{1+\varepsilon}}\right)^{-1}\left[4\ln\left(\frac{1+\sqrt{1+\varepsilon}}{2}\right) + \frac{4+5\varepsilon}{\varepsilon\sqrt{1+\varepsilon}} - \frac{4}{\varepsilon} - 3\right] \tag{4.21}$$

and

$$w_D = \frac{4\pi kw}{Q\mu C_m \alpha(1-\nu)}, \quad t_D = \frac{8kt}{S\mu R^2}, \quad \varepsilon = \frac{R^2}{D^2} \tag{4.22}$$

It can be seen that the deviation of Eq. (4.20) from the original solution for a uniform pressure distribution, Eq. (4.8), is controlled by the value of t_D. When $t_D \gg t_{0D}$, Eq. (4.20) reduces to Eq. (4.8). High t_D values imply high permeability, long production duration, low compressibility, low viscosity and/or small aquifer radius. From Eq. (4.21), it can be shown that $t_{0D} < 1$ when $\varepsilon < 3.453$. It follows that if $t_D > 1$, ground surface subsidence can be calculated to a reasonable accuracy using a uniform pressure distribution providing the radius of the aquifer is a lot less than 1.858 times the depth of the aquifer below the ground surface. This further implies that, for many practical purposes, ground surface subsidence is insensitive

to production fluid viscosity and aquifer permeability when the aquifer radius is less than the aquifer depth.

4.3 Finite element modeling

Results from the analytical solution were compared with results from four equivalent finite element (FE) simulations, described by the parameter values given in Table 4.1. These simulations were obtained using COMSOL Multiphysics v5.4.

Cases 1 and 3 in Table 4.1 are relatively shallow scenarios with the aquifers situated at a depth of 200 m. In contrast, Cases 2 and 4 are deeper scenarios with the aquifers situated at a depth of 1000 m. Cases 1 and 2 are based on the Berea sandstone properties presented in Table 7.2 of Jaeger et al. (2009). Cases 3 and 4 are based on a softer rock with a Bulk modulus an order of magnitude less than that for the Berea sandstone.

The FE simulations involved full hydro-mechanical coupling such that changes in fluid pressure result in changes in volume of the porous material and deformation whilst concomitant changes in stress results in a change in fluid pressure. Fluid production is specified as an outward mass flux on a vertical well segment along the radial symmetry axis. Since the formation surrounding the aquifer is assumed to be impervious, the aquifer has no-flow boundary conditions on all other boundaries. To simulate an infinitely large domain outside of the aquifer, the lateral and lower sides of the formation surrounding the aquifer is padded with infinite element domains (boundary condition in COMSOL that commonly applied to problems in which the domain extend is so large that it can be considered as infinity). These domains have a geometrical scaling corresponding to an extent of several hundred kilometers,

enough for the stress perturbation (caused by fluid production) not to reach the outer boundary of the computational model. The associated boundaries are treated as zero deformation boundaries. In contrast, the free surface upper boundary is treated as a zero traction boundary.

Pressure dissipation is fast in nearly incompressible fluids and formations. Since the aquifer is confined, there are no particularly large gradients in the solution for the fluid pressure or the displacement that require a particularly fine computational grid. The mesh used therefore consists of a fairly uniform grid with a maximum grid size of 125 meters, mainly to ensure a high resolution in the output for presentation of the results.

The FE models were constructed using COMSOL's core functionality and did not require the use of any additional application packages. The relevant equations used are described in Sections 3 and 4 of Bjørnarå (2018). Spatial discretisation was achieved using default quadratic Lagrange elements. Solution was achieved using COMSOL's direct solver, MUMPS (MUltifrontal Massively Parallel sparse direct Solver).

4.4 Results

Fig. 4.2 shows plots of drawdown and ground surface subsidence as a function of radial distance from the production well for different times. The results from the finite element simulations are shown as circular dots. The results from the analytical solution are shown as solid lines. Drawdown was calculated using Eq. (4.1) and subsidence was calculated using Eq. (4.12). To perform the superposition, $r \in [R \times 10^{-3}, R]$ was discretised into 100 logarithmically spaced points. Logarithimic

spacing is required to properly capture the steep pressure gradients that occur close to the production well. Also shown, as circular markers, are values of subsidence directly above the production well, calculated using the closed-form equation given by Eq. (4.20).

The results from the fully coupled hydro-mechanical finite element simulations and the analytical solution are very similar, confirming that the uniaxial strain assumption involved in the definition of storativity, S, in Eq. (4.2) is appropriate in this context, as previously shown by Gambolati et al. (2000). The results from the closed-form equation, given by Eq. (4.20), correspond increasingly well with Eq. (4.12) with increasing time. This is to be expected because the associated approximation of the pressure profile, given by Eq. (4.16), assumes that $t_D \gg 1$. Despite this shortcoming, Eq. (4.20) provides very close estimates of the subsidence calculated by Eq. (4.12). The advantage of Eq. (4.20) is that it is significantly more straightforward to evaluate, as compared to Eq. (4.12).

Looking at Fig. 4.2a it can be seen that the radius of influence moves out from the well until just after 30 days, when it reaches the aquifer boundary, at a radial distance of 3000 m. After this point, pressure across the aquifer increases in a relatively uniform fashion. After 300 days of water production, the drawdown in the aquifer ranges from 8 to 12 m. For the shallow case (i.e., Fig. 4.2b), the subsidence above the well reaches a maximum value of just over 0.6 mm. This appears relatively uniform throughout the confined aquifer. The subsidence then decreases to zero at 1000 m from the edge of the aquifer. For the deeper case, the maximum subsidence is reduced but subsidence persists much further away from the aquifer boundary (see Fig. 4.2c).

The softer rock scenarios, Cases 3 and 4, lead to less drawdown in the aquifer (see Fig. 4.2d). However, this is compensated for by a greater level of subsidence at the ground surface (compare Figs. 4.2b and e and 4.2c and f). It is also noted that the radius of influence takes longer to reach the aquifer boundary. This is due to the reduction in t_c caused by the reduction in bulk modulus (recall Eq. (4.5)). The non-uniform pressure profile in the aquifer is clearly pronounced in the surface subsidence profile for the shallow scenario depicted in Fig. 4.2e. However, the subsidence profile is much smoother at 1000 m depth (see Fig. 4.2f).

4.5 Conclusions

Geertsma (1973) provided an analytical solution, which can be used to calculate the ground surface subsidence due to a cylindrical uniform pressure change. In this chapter, the principle of superposition was used to build on the work of Geertsma (1973) to develop an analytical solution for ground surface subsidence due to constant rate production of a viscous fluid from a cylindrical aquifer of finite permeability. Results from the analytical solution were verified by comparison with a set of fully coupled hydro-mechanical finite element simulations.

The analytical solution based on the principle of superposition requires a priori discretisation of the pressure distribution. However, using Geertsma's closed-form equation to describe ground surface subsidence directly above the center of the cylindrical uniform pressure change, it was also possible to derive a simple closed-form equation to describe ground surface subsidence directly above the production well (or uplift directly above an injection well) within the aforementioned aquifer. The resulting equation relates a dimensionless subsidence to a dimension-

Table 4.1: Parameter values used to obtain the results presented in Fig. 4.2.

Parameter	Case 1	Case 2	Case 3	Case 4
Depth of aquifer, D (m)	200	1000	200	1000
Radius of aquifer, R (m)	3000	3000	3000	3000
Aquifer thickness, H (m)	100	100	100	100
Production rate, Q ($m^3 day^{-1}$)	100	100	100	100
Bulk modulus, K (GPa)	8.0	8.0	0.8	0.8
Poisson's ratio, ν (-)	0.2	0.2	0.2	0.2
Biot coefficient, α (-)	0.8	0.8	0.8	0.8
Porosity, ϕ (-)	0.19	0.19	0.19	0.19
Permeability, k (m^2)	190×10^{-15}	190×10^{-15}	190×10^{-15}	190×10^{-15}
Fluid density, ρ (kg m^{-3})	1000	1000	1000	1000
Dynamic viscosity, μ (Pa s)	10^{-3}	10^{-3}	10^{-3}	10^{-3}
Fluid modulus, K_f (GPa)	2.1	2.1	2.1	2.1
Aspect ratio, $\varepsilon = R^2/D^2$ (-)	225	9	225	9
Value of t_D at 300 days (-)	29.30	29.30	6.872	6.872

less time, with just one free dimensionless parameter, which represents the ratio of the aquifer radial extent to the aquifer depth. Furthermore, the equation shows that, for many practical purposes, ground surface subsidence is insensitive to production fluid viscosity and aquifer permeability when the aquifer radius is less than the aquifer depth below the ground surface.

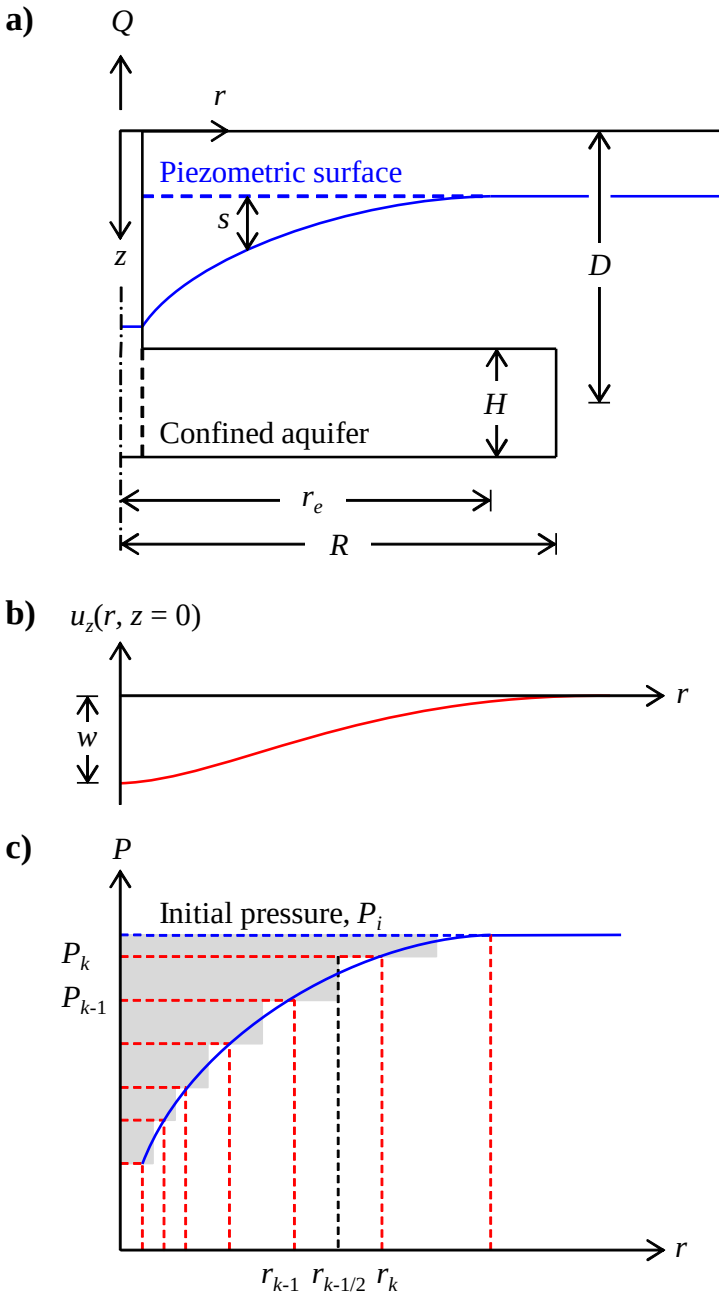

Figure 4.1: Schematic diagrams showing: a) The production well and its relation to the confined aquifer and surrounding semi-infinite geological formation. b) The maximum subsidence above the production well and the vertical displacement, $u_z(r,z)$, at the ground surface (i.e., $z=0$). c) How the pressure is discretised to apply the principle of superposition for Eqs. (4.11) to (4.13).

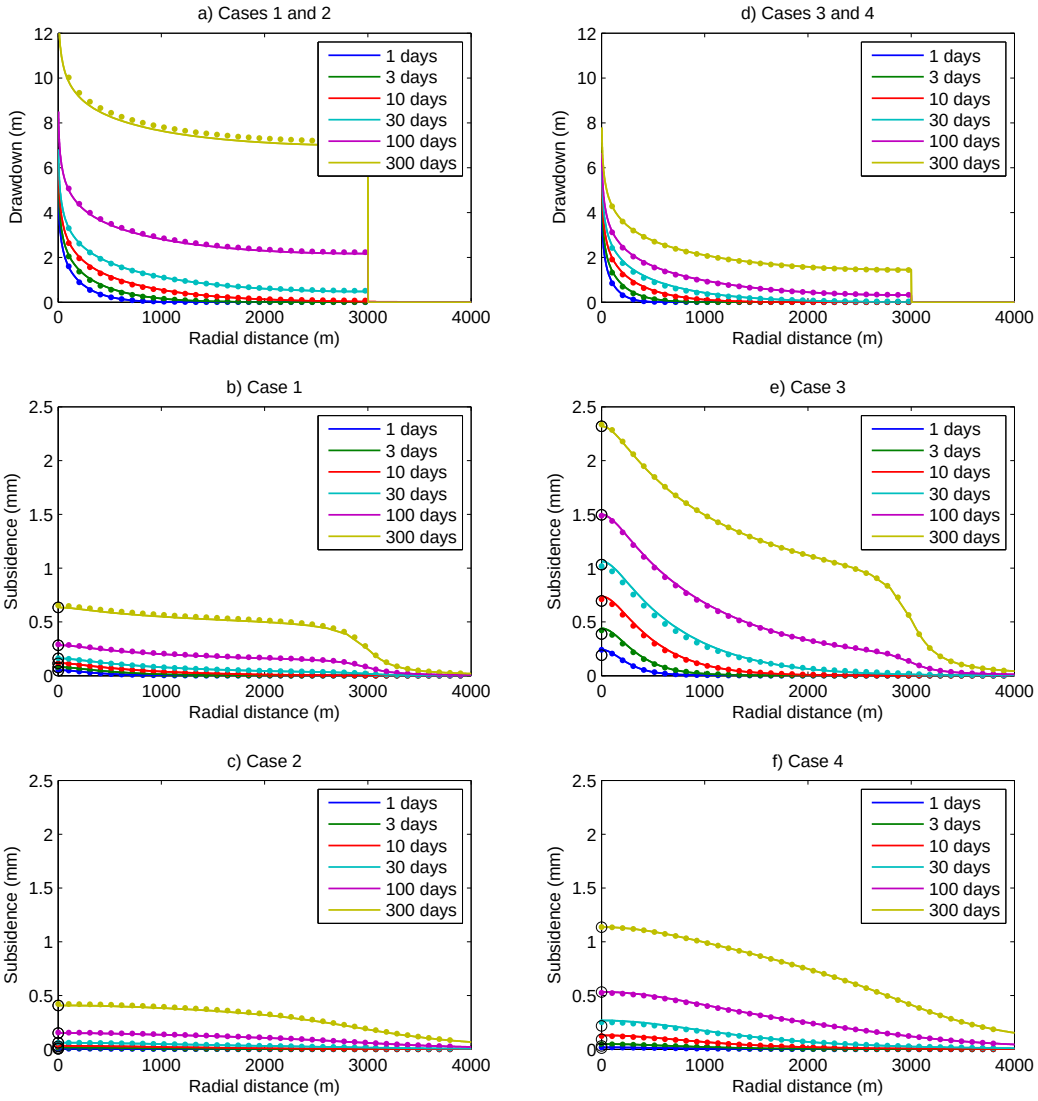

Figure 4.2: Plots of drawdown (s) and subsidence ($-u_z(r,0)$) for Cases 1 to 4 as indicated by the subtitles. The solid lines were determined using Eq. (4.12). The circular dots were determined using the finite element simulations. The subsidence values directly above the production well (w), as calculated using Eq. (4.20), are presented as black circular markers.

Chapter 5

Subsidence due to coal bed methane production

Summary

This chapter describes the coupling of single- and two-phase fluid flow models developed in chapters 2 and 3 with the analytical ground surface subsidence derived in chapter 4. The primary objective of the work was to build a semi-analytical model to investigate ground surface subsidence around CBM producing wells.

The model performed well at exploring ground surface subsidence around CBM production wells. However, the model is not robust in its current state. This is because the assumption that the producing CBM formation is hydraulically isolated from the surrounding formations is not often valid. Realistically, there are hydraulic interactions between most CBM formation and its surrounding aquifers. This implies that the developed CBM model will mostly underestimate ground surface subsidence in this context. Future work should focus on improving the model through coupling the CBM model developed with a regional scale aquifer model.

The main advancement in this chapter are as follow:

- Development of a semi-analytical solution for ground surface subsidence above a CBM production well. The advantage of this model over the existing analytical and numerical models are: (1) It is effective, efficient, and more accurate than the existing models. This is because it incorporates all the limitations of the existing models, (2) It is less computational expense and gives a much faster solution, (3) It allows more parametric analysis to be conducted, thereby provides a platform to have a deeper understanding of the physical problem.

- Derivation of a simplified analytical solution within the CBM reservoir under the assumption of uniform pressure. The model is effective at predicting ground surface subsidence for a given gas production volume and efficient in conducting sensitivity analysis.

- The study presents a wider sensitivity analysis to gain insight into the parameters controlling ground surface subsidence resulting from CBM production compared to the existing models.

- The study shows that initial water saturation has no influence on ground surface subsidence for a given gas production volume.

- The research work shows that a combination of certain parameters can lead to reservoir pressure being less important when comparing from site to site. The groups are classified into four namely: (1) The ratio of initial reservoir pressure to Langmuir pressure constant, (2) The ratio of the Langmuir pressure constant for coal swelling strain to the Langmuir pressure constant, (3) The

ratio of the volume of gas produced to the product of the mass of the coalbed and Langmuir volume constant, and (4) The ratio of the product of Langmuir pressure constant and Biot coefficient to the product of Young's modulus and Langmuir volumetric strain constant.

- The study reveals that initial permeability and cleat compressibility are insignificant when considering ground surface subsidence due to a given gas production volume.

5.1 Introduction

In this chapter, the fluid flow model developed in Chapters 2 and 3, in conjunction with the ground surface subsidence model presented in Chapter 4, is used to simulate ground surface subsidence above a coalbed methane (CBM) production well. The phenomenon of ground surface subsidence associated with the withdrawal of ground fluid (geothermal fluid extraction, water, oil, and gas production) can have a significant negative impact on infrastructure, natural resources, and environment (Geertsma, 1973; Ferronato et al., 2001; Pineda and Sheng, 2014; Schmid et al., 2014).

CBM extraction involves producing groundwater from CBM reservoirs at a rate sufficient to decrease the pressure within the reservoir, such that methane adsorbed to the inner surface of coal particles is released and migrates to the production well as gaseous methane. Economically feasible CBM reservoirs are typically located at depths of more than 200 m (Commonwealth of Australia, 2014b), where pressure is high enough to trap the gas as an adsorbed phase within a CBM formation.

Compaction occurs as methane and water are extracted from a CBM formation. A CBM formation comprises a solid phase (coal matrix domain) and a pore-space (fracture domain) filled with fluid. During CBM production, water is pumped from the CBM formation, which lowers the reservoir pressure and induces desorption of methane from the coal matrix. The desorbed methane then diffuses through micropores to the fracture domain and subsequently flows to the well-bore. During these processes, the extraction of water and gas can induce deformation within the coal (McKee et al., 1988; Palmer and Mansoori, 1996), and volumetric changes of the coal matrix and cleat system (Commonwealth of Australia, 2014a; Pineda and Sheng, 2014). This, in turn, may lead to ground surface subsidence.

There have been many studies seeking to investigate the environmental impact of CBM extraction (Rice et al., 2002; Jackson and Reddy, 2007; Okotie and Moore, 2011; Mooney, 2011; Liu et al., 2012; Hamawand et al., 2013). However, there are relatively few studies seeking to quantify possible ground surface subsidence effects due to CBM extraction (Pitman et al., 2003; Batley and Kookana, 2012; Hamawand et al., 2013).

Fanchi (2002) coupled a black oil simulator with a CBM algorithm and uniaxial compaction model to investigate ground surface subsidence due to CBM production. Their focus was on the Fruitland coal formation in San Juan, United States of America. However, their model is likely to have underestimated ground surface subsidence because they assumed porosity and permeability were constant throughout. In practice, CBM formation porosity and permeability are highly sensitive to effective stress changes, giving rise to large rock deformations during gas production (Chin et al., 2000). In contrast, their uniaxial compaction model is limited to

one-dimensional strain and is therefore likely to lead to an overestimate in ground surface subsidence because it ignores the lateral distribution of strain within the overburden above the CBM reservoir (Wu et al., 2018a).

Chamani and Rasouli (2011) studied production-induced stress, displacement, and ground surface subsidence due to CBM extraction in the San Juan Basin, United States of America, using a three-dimensional finite element model, which overcomes the limitation of the uniaxial compaction model. However, their model also assumed constant porosity and permeability. Furthermore, their model did not account for desorption shrinkage strain. Consequently, their model was also likely to underestimate ground surface subsidence. Note that shrinkage leads to greater levels of ground surface subsidence in formations that possess shrinkage such as coal and shale than formations without shrinkage (Commonwealth of Australia, 2014a).

Freij-Ayoub (2012) coupled their fluid flow model with the geomechanical model, FLAC3D, to examine the possibilities of land surface subsidence as a result of CBM extraction in the Gippsland Basin in Victoria, Australia. However, they also assumed a constant porosity and permeability within the CBM formation.

Brown et al. (2014) sought to quantify land surface subsidence due to CBM extraction within the Surat Basin Australia using the aforementioned analytical solution of Geertsma (1973) (see Chapter 4). The study analyzed three regions and predicted the maximum surface deformation to be approximately 0.1 m. However, the assumption of uniform pressure change adopted in Geertsma's model may have resulted in an underestimate in surface deformation because the pressure gradient at the vicinity of the production well is higher than the pressure gradient at the far-edge of the reservoir (Wu et al., 2018a).

In a recent article, Wu et al. (2018a) compared the suitability of the analytical solution of Geertsma (1973), the uniaxial compaction model, and a three dimensional hydro-mechanical model for modelling ground surface subsidence due to CBM extraction. They found that Geertsma's model underestimates ground surface subsidence induced by CBM extraction because the model ignores the pressure gradient within the CBM formation. The uniaxial compaction model is restricted to one-dimensional strain, thereby ignoring the lateral extent of the CBM reservoir and treated the overlying formations as soft clay overburden, which offers negligible resistance to displacement, which in turn leads to an overestimate in ground surface subsidence. Wu et al. (2018a), therefore, recommends the use of a fully coupled three-dimensional hydro-mechanical models. However, such models are computationally expensive, and more straightforward methods remain desirable (Du and Olson, 2001).

This chapter aims to develop a semi-analytical solution for ground surface subsidence above a CBM production well, which will be effective, efficient, more accurate, and straightforward to implement than the existing analytical and numerical models. In order to achieve the aims of this study, the pressure distribution from the CBM model developed in Chapters 2 and 3 are used to derive an effective pressure to drive the semi-analytical solution for ground surface subsidence developed in Chapter 4. A sensitivity analysis is then performed to investigate how different model parameters affect ground surface subsidence during CBM production.

5.2 Methodology for simulating ground surface subsidence

In the previous chapter, a semi-analytical solution for displacement around a groundwater production well within a cylindrical confined aquifer was developed by applying the principle of superposition to the analytical solution of Geertsma (1973) for displacement around a cylindrical disk of raised uniform pressure. The driving force of displacement was due to pore-pressure induced changes in porosity within the aquifer.

A similar approach can be adopted for looking at displacement around a CBM well. However, pore-pressure induced changes in porosity are slightly more complicated in this case due to the swelling effect of adsorbed methane.

To understand this further, consider the modified form of Hooke's law used by Shi and Durucan (2004) to derive Eq. (2.14):

$$d\varepsilon = \frac{(1+\nu)}{E} d\boldsymbol{\tau} - \frac{\nu}{E}\text{trace}(d\boldsymbol{\tau})\mathbf{I} - \frac{\alpha dP}{3K}\mathbf{I} - \frac{d\varepsilon_s}{3}\mathbf{I} \tag{5.1}$$

where ε_s is found from Eq. (2.15) and K [$\text{ML}^{-1}\text{T}^{-2}$] is the bulk modulus found from $K = E/[3(1-2\nu)]$.

Let P_s be an effective pressure that accounts for both the pore-pressure and the swelling strain associated with methane adsorption, defined by

$$P_s \equiv P + K\varepsilon_s/\alpha \tag{5.2}$$

It can therefore be said

$$d\varepsilon = \frac{(1+\nu)}{E} d\boldsymbol{\tau} - \frac{\nu}{E}\text{trace}(d\boldsymbol{\tau})\mathbf{I} - \frac{\alpha dP_s}{3K}\mathbf{I} \tag{5.3}$$

Note that when $d\varepsilon_s = 0$, $dP_s = dP$. It is therefore clear that the analytical solution of Geertsma (1973) should be driven by P_s as opposed to P when studying displacement around a CBM well.

5.3 Conceptual model

Consider a fully penetrated CBM production well of radius r_w [L] situated at the centre of a homogeneous, isotropic, cylindrical, and confined coalbed methane reservoir of radial extent r_c [L] and formation thickness H [L]. Low permeability geological materials surround the CBM reservoir with the assumption that the surrounding geological materials are homogeneous, isotropic, impermeable, and semi-infinite (Fig. 5.1). It is also assumed that the elastic properties of the confined CBM reservoir is a continuum, Darcy's law can describe the rate of water and/or gas flow through the coal fracture domain, and the coalbed reservoir contains ideal gas under isothermal conditions. Since the surrounding materials are considered impervious, the CBM reservoir has no-flow boundary conditions on all other boundaries. The CBM reservoir has its overburden zone extended up to the surface while the lateral and underburden extend to a large area extent enough for the stress perturbation caused by CBM production not to reach the outer boundaries (zero deformation boundary).

The mass conservation statements for methane and water in the CBM reservoir given in chapter 3 as:

$$\frac{(\phi\rho_g S_g)}{\partial t} + \rho_c \frac{\partial s}{\partial t} = -\frac{1}{r}\frac{\partial (r\rho_g q_g)}{\partial r} \tag{5.4}$$

$$\frac{(\phi\rho_w S_w)}{\partial t} = -\frac{1}{r}\frac{\partial (r\rho_w q_w)}{\partial r} \tag{5.5}$$

where ϕ [-] is the cleat porosity, ρ_g [ML^{-3}] is the methane density in the cleats, ρ_w [ML^{-3}] is the density of water in the cleats, P [$ML^{-1}T^{-2}$] is pressure, t [T] is time, ρ_c [ML^{-3}] is the density of the coal-bed, s [-] is the mass of adsorbed methane per unit mass of coal-bed, q_g [LT^{-1}] is the volumetric flux of methane, q_w [LT^{-1}] is the volumetric flux of water, S_g [-] and S_w [-] are volume fractions of the fracture porosity containing gaseous methane and water, respectively (referred to hereafter as the gas and water saturations, respectively) and r [L] is radial distance from the methane production well.

Note: ρ_g, s, q_g, q_w and ρ_w are defined in Eqs (2.2), (2.6), (2.10), (3.3), (3.4) and (3.12), respectively.

Consider the mathematical model for CBM production in Chapters 2 and 3 (Referred to Eqs (5.4) and (5.5)). Given Eq. (4.12) from the previous chapter, if $r \in [0,R]$ is discretized into N, not necessarily equally spaced, points located at r_k where $k = 1,2,3,\ldots,N$, the vertical displacement, $u_z(r,z)$, at any point within overburden above a CBM reservoir can be determined from

$$u_z(r,z) \approx \sum_{k=2}^{N} \tilde{u}_z(r,z,r_{k-1/2})(P_{s,k-1} - P_{s,k}) \tag{5.6}$$

where $\tilde{u}_z(r,z,r_{k-1/2})(P_{s,k-1} - P_{s,k})$ is obtained using the analytical solution of Geertsma (1973) (as reported in Appendix D5 of Fjær et al. (2008)) for displacement around a cylindrical disk of radius $r_{k-1/2}$, which is subject to a uniform effective pressure change of $(P_{s,k-1} - P_{s,k})$.

5.4 Uniform pressure simplified model

If we assume that the pressure within the CBM formation is uniform and that the porosity of the formation is negligibly small, the model significantly simplifies and a closed-form analytical solution between maximum subsidence and produced gas volume can be obtained.

Under such cirmcumstances the maximum subsidence, w [L], is found from (recall Eq. (4.7))

$$w = 2C_m H \alpha \Delta P_s (1-\nu)\left(1 - \frac{D}{\sqrt{D^2+R^2}}\right) \tag{5.7}$$

where (recall Eqs. (2.15) and (5.2))

$$\Delta P_s = P_I - P + \frac{K\varepsilon_L}{\alpha}\left(\frac{P_I}{P_{L,\varepsilon}+P_I} - \frac{P}{P_{L,\varepsilon}+P}\right) \tag{5.8}$$

The volume of gas produced, V_g [L^3], is found from (recall Eq. (2.9))

$$V_g = M_c V_L \left(\frac{P_I}{P_L+P_I} - \frac{P}{P_L+P}\right) \tag{5.9}$$

where M_c [M] is the mass of the coalbed, found from

$$M_c = \pi R^2 H \tag{5.10}$$

Note that Eq. (5.9) can be solved for pressure as follows

$$P = \left(\frac{M_c V_L P_I - V_g(P_L+P_I)}{M_c V_L P_L + V_g(P_L+P_I)}\right) P_L \tag{5.11}$$

5.4.1 Dimensionless transformation

Further insight into parameteric controls on subsidence in this context can be gained by applying the following dimensionless transformations:

$$w_D = \left(1 - \frac{D}{\sqrt{D^2+R^2}}\right)^{-1} \frac{3w}{2H(1+\nu)\varepsilon_L} \tag{5.12}$$

$$p_I = \frac{P_I}{P_L}, \quad p_{L,\varepsilon} = \frac{P_{L,\varepsilon}}{P_L}, \quad v_g = \frac{V_g}{M_c V_L}, \quad \gamma = \frac{\alpha P_L}{K\varepsilon_L} \tag{5.13}$$

such that the above set of equations reduce to

$$w_D = \left(\frac{\gamma(1+p_I)^2}{1+(1+p_I)v_g} + \frac{p_{L,\varepsilon}(1+p_I)^2}{(p_{L,\varepsilon}+p_I)^2 + (p_{L,\varepsilon}-1)(p_{L,\varepsilon}+p_I)(1+p_I)v_g}\right) v_g \tag{5.14}$$

Note that when

$$\lim_{p_{L,\varepsilon}\to 1} w_D = \left(\frac{\gamma(1+p_I)^2}{1+(1+p_I)v_g} + 1\right) v_g \tag{5.15}$$

5.5 Results

Fig. 5.2a shows a plot of water saturation against radial distance at different times for the case when the initial water saturation, $S_{wI} = 1$, as previously shown in Fig. 3.5 except assuming a formation thickness of 20 m and a formation depth of 80 m. As discussed in Section 3.3.2, the pressure drawdown at the well-bore gives rise to a drying-front that spreads out from the well. The reason is that the reduction in pressure provokes gas desorption from the coal-matrix, which increases with increasing gas relative permeability as production progresses. This, in turn, dislodges water contained within the fracture into the well-bore.

As previously shown in Fig. 3.5b, Fig. 5.2b presents a plot of pressure distribution at different times. Again the formation thickness and formation depth are assumed to be 20 m and 80 m, respectively. Here it can be seen that pressure loss due to production is substantial near the well-bore, which leads to large pressure gradients around the well-bore vicinity with pressure decreasing with distance from

the well-bore. The extension of the pressure front towards the reservoir boundary increases with increasing production time. Once the pressure front reaches the reservoir boundary, the pressure reduces across the reservoir in a relatively uniform manner.

Fig. 5.2c shows a plot of subsidence at the land surface against radial distance as a function of time for the case when $S_{wI} = 1$, again with a formation thickness of 20 m and a formation depth of 80 m. It can be observed that ground surface subsidence increases with increasing time of fluid production. This occurs because the pressure drawdown increases with increasing time of production (Fig. 5.2b), which invariably increases gas desorption from the coal-matrix.

The maximum ground surface subsidence occurs immediately above the well-bore (Fig. 5.2c). Ground surface subsidence decreases with radial distance from the well-bore. This is because the maximum pore pressure occurs immediately above the well-bore. This, in turn, leads to the maximum effective stress occurring in that region, which in turn leads to maximum compaction within the CBM reservoir. Besides, the gas in this region further desorbs and the coal matrix shrinks, further exacerbating the volumetric changes in the coal matrix.

Fig. 5.3 shows results looking at sensitivity to initial water saturation. Fig. 5.3a shows a plot of cumulative gas production as a function of time for different initial water saturations, as previously shown in Fig. 3.4 except assuming a formation thickness of 20 m. It can be seen that gas production increases with decreasing initial water saturation and increasing production time. This occurs because a decrease in initial water saturation is associated with an increase in gas relative permeability.

Fig. 5.3b presents a plot of maximum ground surface subsidence as a function of

time for different initial water saturations. It can be observed that, for a given time, subsidence increases with decreasing initial water saturation. As previously shown in Fig. 3.4d, the decline in the mean pressures implies an increase in effective stress, which leads to an increase in ground surface subsidence. This is because the reduction in mean pressure gives rise to compaction and gas desorption in the coal matrix. As production progresses, the gas relative permeability, which has an inverse relationship with initial water saturation, increases. With the desorption of more gas, the effective stress in the CBM reservoir increases, which in turn leads to a decrease in the volume of the CBM reservoir through compaction and shrinkage.

Fig. 5.3c shows a plot of mean pressure against gas production volume for different initial water saturation. Here it can be seen that initial water saturation has no effect on the mean pressure after a given specific volume of gas has been produced. As stated in Section 3.3.2, the reason is that the initial fracture porosity is very small compared to the volume of the coal-matrix (Moore, 2012). Therefore, the volume of initial water saturation residing within the fracture domain is insignificant compared to the total volume of gas in the CBM reservoir.

Note that the final values of gas production studied for each initial water saturation are the final gas production values achieved after 1000 days of production (see Fig. 5.3a). This is also the case for all the subsequent similar figures presented in this chapter thereafter.

Fig. 5.3d presents a plot of maximum ground surface subsidence against cumulative gas production for different initial water saturations. It can be observed that initial water saturation has an insignificant effect on ground surface subsidence for a given gas production volume. As discussed earlier, the reason is that the volume of

the initial fracture porosity that contains the initial water saturation is comparatively small in comparison to the volume of gas stored within the coal-matrix.

Reservoir depth is a known important factor controlling ground surface subsidence due to subsurface fluid production (Gambolati et al., 2006). To explore the effects of CBM reservoir depth on ground surface subsidence, the simulation presented in Fig. 5.2c was repeated for a range of alternative burial depths. Fig. 5.4 shows plots of ground surface subsidence as a function of radial distance from the well-bore after different production times. The subsidence results are again based on Case 1 of Ye et al. (2014) with initial water saturation, S_{wI}=1, at various depths assuming a formation thickness of 20 m. Four different CBM reservoir burial depths are considered:: 80 m, 200 m, 500 m, and 1000 m. From a practical perspective, methane is typically extracted from CBM reservoirs located at depths ranging between 200 m and 1000 m, with CBM reservoir pressures expected to range between 3 MPa and 10 MPa (Commonwealth of Australia, 2014b; Pineda and Sheng, 2014; Towler et al., 2016). Such a range represents an optimal region in terms of high gas content and practical values of coal bed permeability (Moore, 2012) (while gas content increases with depth, permeability tends to decrease with depth). CBM reservoirs located at depths below 200 m tend not to be sufficiently pressured to enable adequate absorption of gas within the coal matrix. However, at greater burial depths with high temperature, gas content decreases due to the higher reservoir temperature (Moore, 2012). Nevertheless, the burial depth of 80 m is considered within the sensitivity analysis for comparison.

Fig. 5.4a presents a plot of ground surface subsidence as a function of time when the CBM reservoir is located at a depth of 80 m. It can be seen that ground

surface subsidence increases with increasing time of production. However, these effects generally decrease with distance from the well-bore. Fig. 5.4d shows the results when depth increases to 1000 m. Here it can be seen that ground surface subsidence effects become less pronounced with reservoir depth compared to when the reservoir depth is 80 m. For instance, ground surface subsidence at a reservoir depth of 80 m after 1000 days of production reduces by 90% when the reservoir depth is 1000 m for the same period of production. This occurs because the deformation within the CBM reservoir, resulting from gas production, is laterally distributed by the overburden with the rate of distribution increasing with increasing overburden thickness. Geomechanical properties will also control the transmission or attenuation of the reservoir displacement up to the land surface (Christensen et al., 1988).

To explore further the impact of CBM reservoir depth on ground surface subsidence, the simulation presented in Fig. 5.4 is normalized to fit within a single graph. This is achieved by plotting normalized subsidence against normalized radial distance. It can be seen that normalized subsidence decreases with increasing reservoir depth after a specific time of production. For instance, normalized subsidence decreases by approximately 8%, after 1000 days of production, by increasing the reservoir depth from 80 m to 1000 m. The same trend of result is observed after 10 days of production where the normalized subsidence decreases by approximately 91%. However, it can be observed that the uncertainty in the reservoir depth reduces with increasing time.

The percentage decrease in subsidence when the reservoir depth increases from 80 m to 1000 m after 1000 days of production is approximately 8%. However, for

300, 100, 30, and 10 days of production, the percentage decreases in subsidence are approximately 40%, 72%, 82%, and 91%, respectively. It shows that the effect of reservoir depth is not that significant when looking at normalized ground surface subsidence after 1000 days of production.

Fig. 5.6 presents results from a sensitivity analysis around the dry-gas scenarios of Ye et al. (2014) studied in Chapter 2, assuming a formation thickness 20 m and a formation depth of 80 m. Subplots (a) and (b) show plots of gas production changes with time. Subplot (c) and (d) show plots of maximum subsidence against production time and subplots (e) and (f) present plots of maximum subsidence against gas production volume. Initial permeability can be seen to have a significant impact on gas production volume and ground surface subsidence at a given time. Wu et al. (2018a) analyzed the permeability sensitivity by plotting subsidence as a function of depth. The authors observed that higher coal bed permeability leads to larger ground surface subsidence.

Figs. 5.6a, c, and e show results looking at sensitivity to initial permeability of coal beds as indicated in the legends. Note that cleat compressibility was set at 0.1 MPa^{-1}. Coal bed permeability has been recognized as the most significant parameter which controls the fluid flow rate in the reservoir. This is because a large coal permeability results in a higher gas rate due to higher drainage efficiency (Wu et al., 2018b). It is also one of the most uncertain parameters in the study of subsidence due to CBM production. The reason is that coal bed permeability is stress-dependent. It can change during gas extraction due to changes in effective stress and coal shrinkage (Wu et al., 2018a). As discussed earlier, an increase in effective stress will induce a decrease in coal permeability. However, coal shrinkage

will invoke an increase in permeability.

It is clear from Fig. 5.6a that an increase in initial permeability of coal bed leads to a higher volume of gas production at a specific time of production. After 1000 days of gas production, the maximum gas production is around 60 SMMCM for the coal bed with an initial permeability of 5 mD, while the volume of gas produced is approximately 13 SMMCM when the initial permeability of the coal bed is 0.1 mD. This is because the developed cleat network controls fluid mobility in the CBM reservoir. A possible explanation is that gas production from a coal bed with higher initial permeability will attain critical desorption pressure earlier than that with smaller initial permeability. Furthermore, coal beds with higher initial permeability will have larger cleat aperture, which will further increase desorption rate (Remner et al., 1986; Wei and Zhang, 2010; Moore, 2012), and consequently have the potential to drain larger areas, for a given production time, than reservoirs with smaller initial permeability.

During gas production in a CBM reservoir, a region of reduced pressure is created. As production continues, the region increases radially, and gas desorption will only manifest within that region. The rate of propagation of this region increases with increased permeability. Since pressure-transient wave propagates faster in more permeable coals (Remner et al., 1986; Wan et al., 2016; Xu et al., 2017), more gas will tend to desorb in coalbed reservoirs with more significant coal permeability, which will, in turn, enhance gas production rates and cumulative gas production.

Fig. 5.6c shows similar trends as Fig. 5.6a. Here, it can be seen that higher initial coal permeability produces larger subsidence due to gas production and maximum subsidence increases with increasing time of production. When the initial

coal permeability is 0.1 mD, the corresponding maximum subsidence is roughly 13 mm; however, the maximum subsidence is approximately six times higher when the initial coal permeability is 5 mD. This occurs because the production of gas from the coal bed leads to pore pressure drawdown, which in turn causes more gas desorption from the coal matrix. The depressurization can cause compaction of the CBM reservoir, especially in the region of the well, which is further aided by matrix shrinkage. This, in turn, leads to subsidence of the land surface.

However, larger initial coal permeability permits higher gas production and more gas desorption. This, in turn, results in a greater depleted region around the vicinity of the well-bore and subsequently leads to larger ground surface subsidence than that with smaller initial coal permeability at a specific time. This result is consistent with the study of Wu et al. (2018a). Interestingly, the relationship between subsidence as a function of gas production volume is independent of initial coal permeability, as shown in Fig. 5.6e.

Figs. 5.6b, d, and f show results looking at sensitivity to cleat volume compressibility, c_f, of coal beds as indicated in the legends, assuming an initial permeability of 1 mD. c_f is an essential parameter in coal bed reservoirs because it controls the sensitivity of both porosity and permeability to changes in effective stress.

In order to investigate gas production volume change with respect to time of production, gas production volume is determined using different c_f values for each production time step. It can be seen from Fig. 5.6b, that gas production volume increases dramatically with increasing time of production. Gas production volume increases from 8.2 SMMCM to 59.9 SMMCM with production time from 100 days to 1000 days when c_f is 0.3 MPa^{-1}, which is about 630% change in gas produc-

tion volume. It can also be seen that gas production volume, for a given production time, increases with increasing c_f. For instance, the gas production volume increases from 32.7 SMMCM to 59.9 SMMCM when c_f changes from 0.03 MPa^{-1} to 0.3 MPa^{-1} after 1000 days of production. This represents an 83% increase in gas production volume.

It can be seen from Fig. 5.6d that maximum subsidence increases significantly with increasing production time for different c_f values. Maximum subsidence increases from 20.6 mm to 65.7 mm with production time from 100 days to 1000 days for c_f of 0.3 MPa^{-1}, which is approximately 219% increment in maximum subsidence. Furthermore, maximum subsidence increases with increasing c_f after a specific time of production. For instance, after 1000 days of production, it increases from 40.7 mm to 65.7 mm when c_f increases from 0.03 MPa^{-1} to 0.3 MPa^{-1}, which is roughly 61%.

Fig. 5.6f shows plots of maximum subsidence against gas production volume for different c_f values. It can be seen that maximum subsidence increases with increasing c_f. An increment of c_f from 0.03 MPa^{-1} to 0.3 MPa^{-1} significantly increases the maximum subsidence from 37.8 mm to 43.3 mm, representing 14.6% incremental increase, after 30 SMMSM volume of gas has been produced. Interestingly, the influence of c_f on the relationship between subsidence as a function of gas production volume vanishes as the volume of gas produced increases.

To better understand the impacts of initial permeability and c_f on subsidence, the simulations presented in Fig. 5.6 were repeated for a range of different formation depth values. The results are also compared to results from the analytical solution in Eq. (5.14).

Fig. 5.7 presents results from a sensitivity analysis around the dry-gas scenario of Ye et al. (2014) studied in Chapter 2, assuming a formation thickness of 20 m. Results from the analytical solution are shown as thick green lines. Figs. 5.7a and c show results looking at sensitivity to the initial permeability of coal beds, as indicated in the legend at different formation depths. As stated earlier, c_f is assumed to be 0.1 MPa^{-1}. Fig. 5.7a shows plots of maximum subsidence against gas production volume for different initial permeabilities. It can be observed that the relationship between maximum subsidence and gas production volume is independent of the initial permeability irrespective of the formation depth. Formation depth also influences the subsidence, which decreases with increasing formation depth. When 80 SMMCM of gas has been produced, the maximum subsidence when the formation depth is 80 m is 75.60 mm. However, it decreases to 23.07 mm (about 70% reduction) when the formation depth is 500 m.

To further investigate the effect of initial permeability on subsidence after a specific volume of gas has been produced, Fig. 5.7c presents plots of normalized subsidence against gas production volume at different initial permeability in conjunction with results from the aforementioned analytical solution. It can be seen that the initial permeability does not affect subsidence after a fixed volume of gas has been produced. Furthermore, there is a close correspondence between the analytical solution and the numerical model when the formation depth is 500 m. This shows that the influence of formation depth on surface subsidence decreases with increasing depth.

Figs. 5.7b and d show results looking at sensitivity to c_f and formation depths, assuming an initial permeability of 1 mD. It can be seen that the influence of c_f on

the relationship between maximum subsidence and gas production volume reduces with increasing formation depth. Of interest is that at a formation depth of 500 m, the maximum subsidence relationship with gas production volume is independent of c_f. Fig. 5.7d shows plot of normalized subsidence against gas production volume for different c_f, assuming different formation depths. It can be seen that the effects of c_f on subsidence decreases with increasing depth. The subsidence curves for each c_f values converge at a formation depth of 500 m and are very similar to the results from the analytical solution.

Of particular interest is that the analytical solution given in Eq. (5.14) has proven to be effective at predicting the subsidence estimated by the numerical model for all of the scenarios studied. This suggests that the pressure distribution within the CBM reservoir is not the only important parameter controlling ground surface subsidence, as previously considered by Wu et al. (2018a). There are other important parameters and certain combinations of values that can lead to reservoir pressure being less important when comparing one CBM reservoir to another. Fig. 5.8 shows a plot of w_D as a function of v_d for different values of γ and p_I using Eq. (5.14) whilst assuming $p_{L,\varepsilon} = 1$. Note that for the Case 1 parameters of Ye et al. (2014) used for the study above, $\gamma = 0.0506$ and $p_I = 0.483$. Increases in γ and p_I lead to an increase in deviation from a one-to-one correspondence between w_D and v_d. This is because increasing γ or p_I leads to greater importance in coal-matrix shrinkage due to gas desorption.

5.6 Conclusions

The objective of this study was to investigate possible land surface subsidence associated with CBM extraction. The pressure distribution from the numerical finite difference single and two-phase CBM flow models developed in chapters 2 and 3 were used to derive an effective pressure to drive the semi-analytical solution for ground surface subsidence developed in chapter 4.

A simplified analytical solution for maximum ground surface subsidence was derived, assuming that the pressure distribution within the reservoir is uniform (recall Eq. (5.14)). Dimensionless transformation revealed that four essential parameter groups control ground surface subsidence including (1) the ratio of initial reservoir pressure to Langmuir pressure constant, p_I; (2) the ratio of the Langmuir pressure constant for coal swelling strain to the Langmuir pressure constant, $p_{L,\varepsilon}$; (3) the ratio of the volume of gas produced to the product of the mass of the coalbed and Langmuir volume constant, v_g; and (4) the ratio of the product of Langmuir pressure constant and Biot coefficient to the product of Young's modulus and Langmuir volumetric strain constant, γ.

The results showed that the presence of water in the cleats was found to have no influence on ground surface subsidence for a given gas production volume. The reason was that the initial fracture porosity, where the initial water saturation resides, is very small compared to the volume of the coal matrix, where most of the gas storage is present.

Sensitivity analysis showed that overburden thickness influenced ground surface subsidence. It was also shown that an increase in initial coal permeability and cleat volume compressibility leads to an increase in ground surface subsidence for a given

time. However, these parameters were found not to be significant when considering ground surface subsidence due to a given gas production volume.

The sensitivity analysis also showed that the simplified analytical solution is effective at predicting ground surface subsidence for a given gas production volume, predicted by the numerical model, for all of the scenarios studied. This suggests that pressure distribution within a CBM reservoir is not the only essential parameters for determining ground surface subsidence. There are other important parameters as well, and certain combinations of values can lead to reservoir pressure being less critical when comparing one site to another.

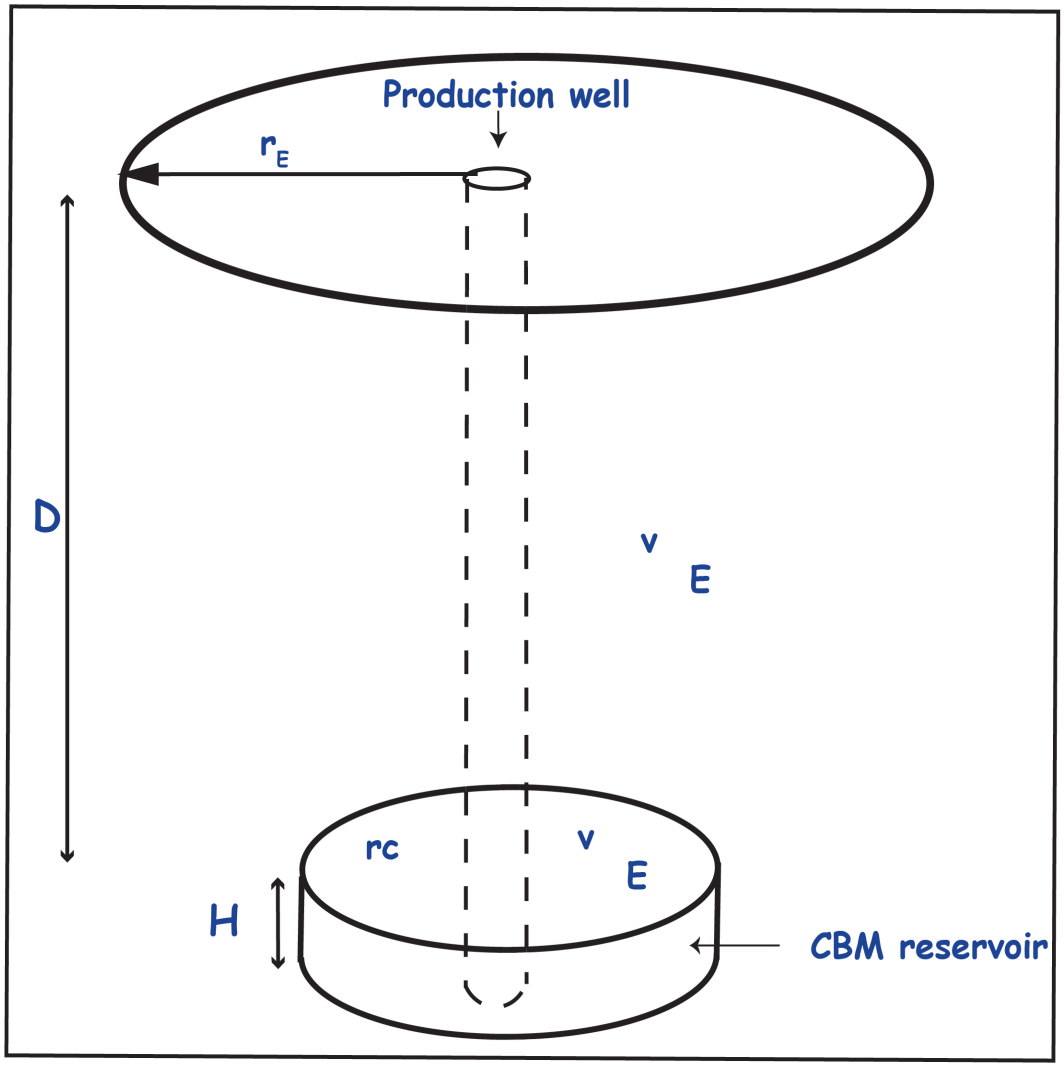

Figure 5.1: Schematic diagram of a homogeneous, isotropic, cylindrical, and confined coalbed methane reservoir embedded within a homogeneous, isotropic, and impermeable geological materials with production well.

.

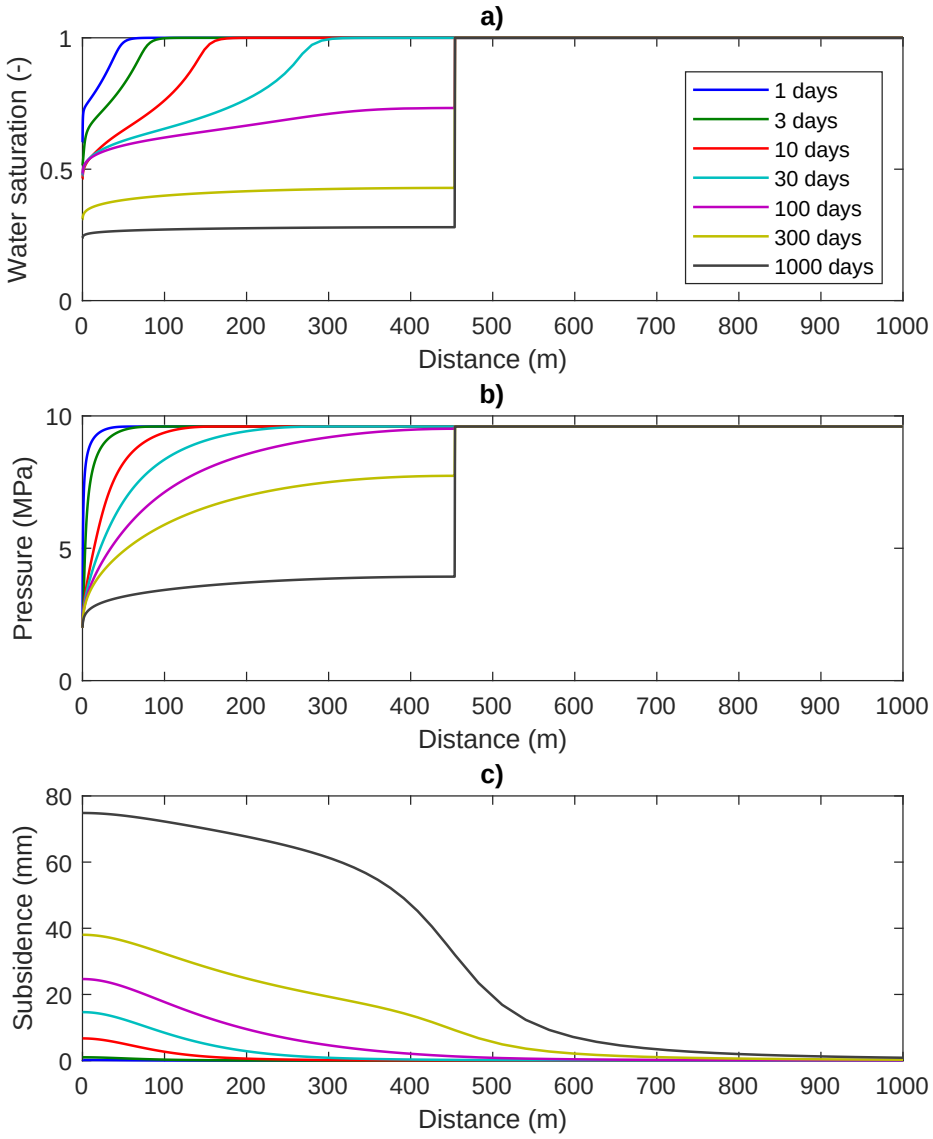

Figure 5.2: Numerical model results based on Case 1 of Ye et al. (2014) but with initial water saturation, $S_{wI} = 1$, and assuming a formation thickness of 20 m and a formation depth of 80 m. a) Plot of water saturation against radial distance at different times as previously shown in Fig. 3.5. b) Plot of fluid pressure against radial distance at different times as previously shown in Fig. 3.5. c) Plot of subsidence at the land surface against radial distance at different times.

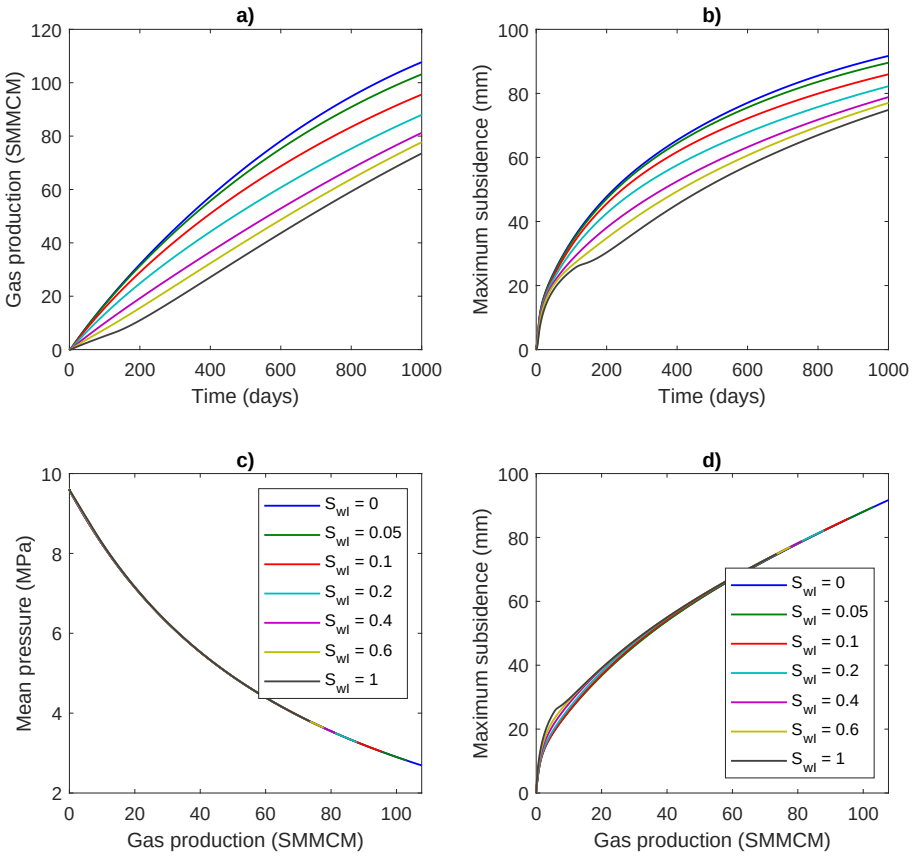

Figure 5.3: Numerical model results based on Case 1 of Ye et al. (2014) but with varying initial water saturations (as shown in the legends, assuming a formation thickness of 20 m and a formation depth of 80 m. a) Plot of cumulative gas production rate against time as previously shown in Fig. 3.4 except assuming the formation thickness is 20m. b) Plot of maximum ground surface subsidence against time. c) Plot of cumulative gas production against mean reservoir pressure. d) Plot of cumulative gas production against maximum ground surface subsidence. The SPE acronym, SMMCM, stands for Standard Million Cubic Metres.

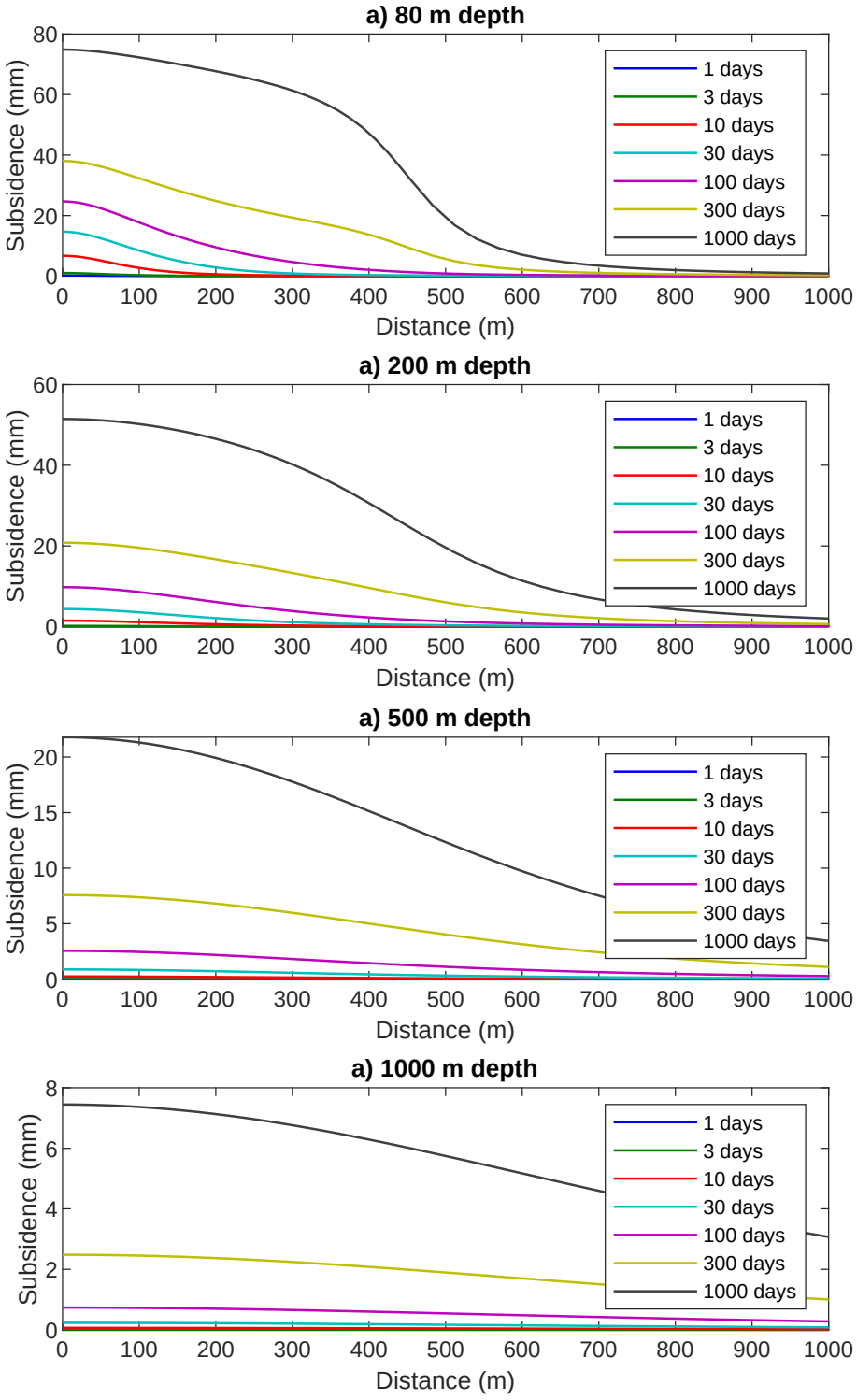

Figure 5.4: Subsidence results based on Case 1 of Ye et al. (2014) with initial water saturation, $S_{wI} = 1$, at various depths assuming a formation thickness of 20 m.

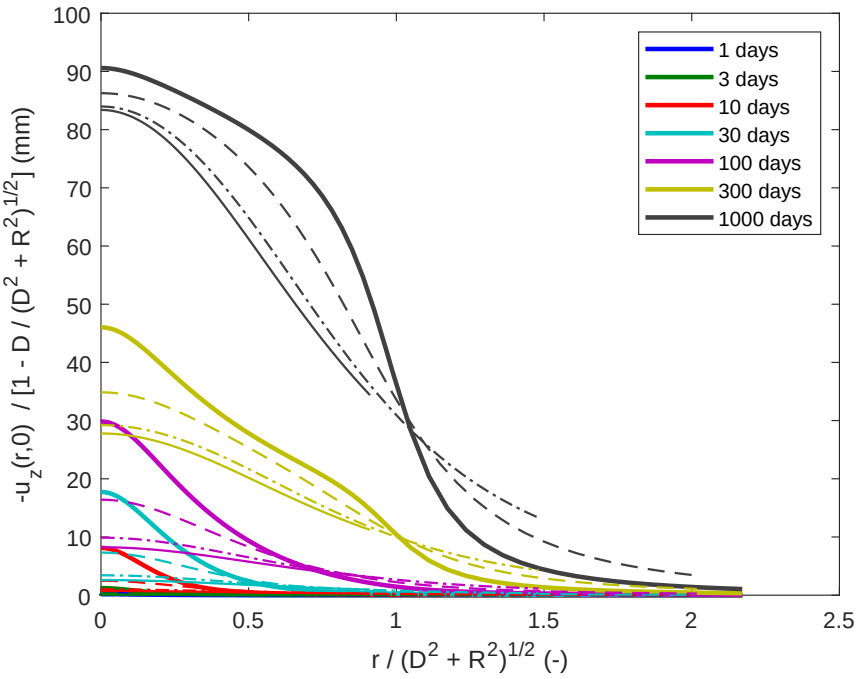

Figure 5.5: The results from Fig. 5.4 normalised to fit on a single graph. The thick solid lines, dashed lines, dash-dot lines and thin solid lines are from simulations assuming reservoir depths of 80, 200, 500 and 1000 m, respectively.

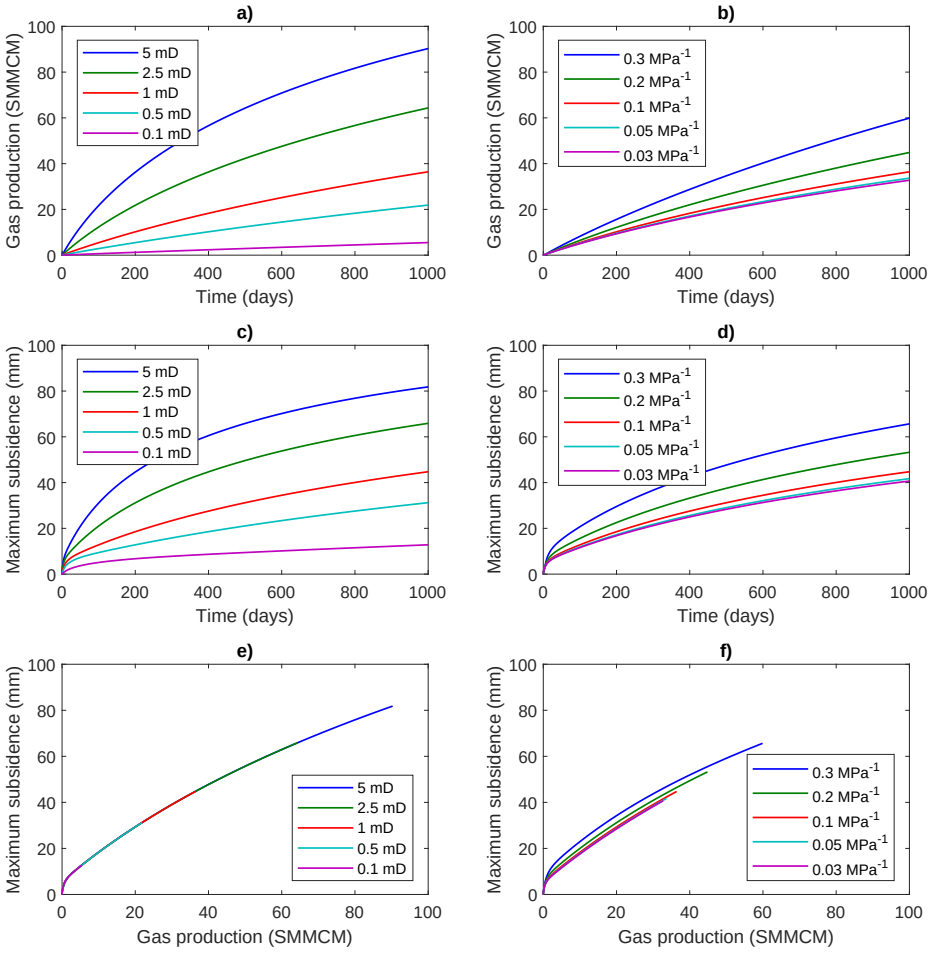

Figure 5.6: Sensitivity analysis around the dry-gas scenario of Ye et al. (2014) studied in Chapter 2, assuming a formation thickness of 20 m and a formation depth of 80 m. a), c) and e) look at sensitivity to initial permeability (as indicated in the legends) assuming a cleat compressibility of 0.1 MPa^{-1}. b), d) and f) look at sensitivity to cleat compressibility (as indicated in the legends) assuming an initial permeability of 1 mD.

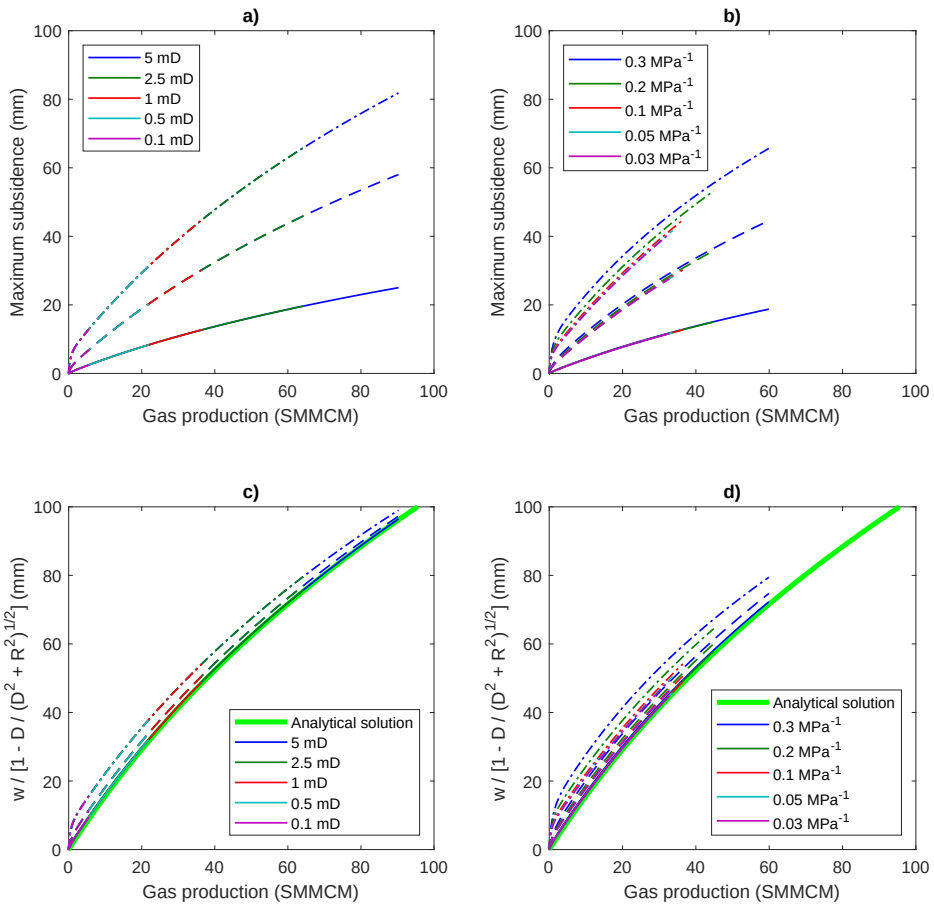

Figure 5.7: Sensitivity analysis around the dry-gas scenario of Ye et al. (2014) studied in Chapter 2, assuming a formation thickness of 20 m. The dash-dot lines, dashed lines and solid lines represent models assuming formation depths of 80 m, 200 m and 500 m, respectively. Results from the analytical solution given in Eq. (5.14) are shown as thick green lines. a) and c) look at sensitivity to initial permeability (as indicated in the legends) assuming a cleat compressibility of 0.1 MPa^{-1}. b) and d) look at sensitivity to cleat compressibility (as indicated in the legends) assuming an initial permeability of 1 mD.

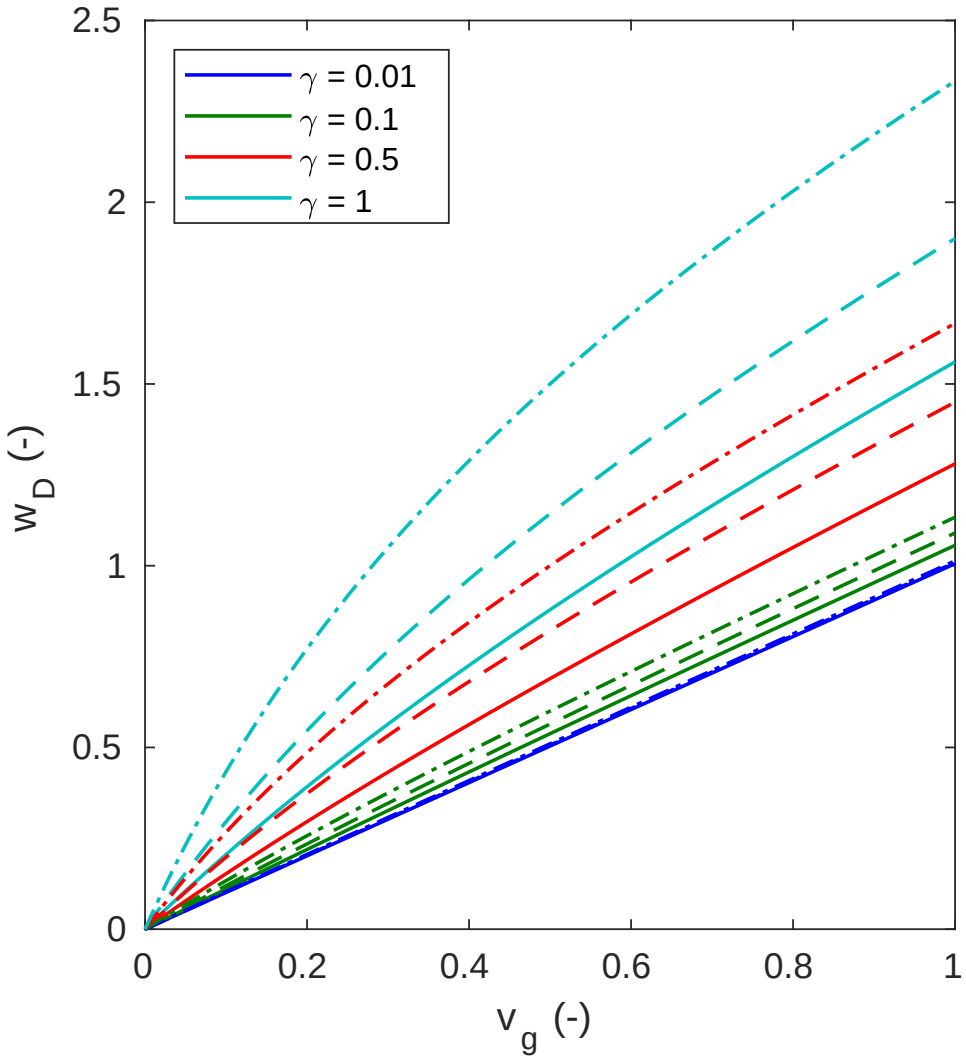

Figure 5.8: Plot of dimensionless maximums subsidence, w_D, against dimensionless gas production volume, v_g, for different values of dimensionless Langmuir isotherm pressure, γ, as indicated in the legend. The solid lines assume $p_I = 0.08$, the dashed lines assume $p_I = 0.5$ and the dashed-dot lines assume $p_I = 1.0$. The results were obtained using Eq. (5.14) with $p_{L,\varepsilon} = 1$.

Chapter 6

Summary and conclusions

Demand for energy and subsequent decline in conventional gas resources worldwide continues to motivate improved understanding of unconventional gas resources such as coalbed methane (CBM). During CBM extraction, water is pumped from a CBM reservoir to reduce the reservoir pressure and induce desorption of CBM from the reservoir. There have many previous studies seeking to investigate the environmental impact of CBM extraction associated with gas leakage, water quality, and well failure. However, this thesis focuses on the numerical modeling of CBM extraction induced ground surface subsidence.

In Chapter 2, governing equations describing methane production from a CBM reservoir in the absence of water were presented. These equations using a method of lines approach (MoL) whereby the partial differential equations (PDE) were discretized in space to form a coupled set of non-linear ordinary differential equations (ODE) with respect to time, which were in turn solved using the MATLAB ODE solver, ODE15s. A model verification was performed by re-simulating relevant numerical results from a published study due to Ye et al. (2014). There was good

agreement between our model results and those from the literature. Following on from this, the model was calibrated to observed gas production data from the Horseshoe Canyon coalfield in Canada, as a demonstration of the practical application of our developed numerical model.

In Chapter 3, the model for CBM production developed in Chapter 2 was extended to account for the presence of water in the fracture porosity. This led to the need to solve three coupled non-linear partial differential equations using the MATLAB solver, ODE15s. The capability to incorporate water was tested by comparing numerical results for methane gas production rate to published results obtained using the commercial software packages GEM and ECLIPSE. The case study due to Ye et al. (2014), from Chapter 2, was then extended to look at the effect of initial water saturation on gas production and reservoir pressure drawdown.

The effect of water on gas production and pressure distribution in the presence of stress-dependent porosity and permeability was explored by varying the initial water saturation used for one of the case studies developed in Chapter 2. The results showed that for a given time, gas production rates reduce with increasing initial water saturation. In contrast, water production rates increase with increasing initial water saturation. This is because higher initial water saturations lead to smaller initial relative permeabilities for gas. The potential role of initial water saturation on ground surface subsidence was investigated by studying the associated spatial distributions of fluid pressure. It was found that, for a given time, the mean fluid pressure within the reservoir reduces with increasing initial water saturation. However, the spatial distribution of fluid pressure, for a given volume of produced gas, was found to be insensitive to initial water saturation. This can be attributed to the

fact that the volume of water stored in the cleats of the coalbed is very small as compared to the volume of gas stored within the coal matrix.

In chapter 4, a closed-form equation for ground surface subsidence due to constant rate of production of water from a cylindrical aquifer of finite permeability was developed. This was achieved by applying the principle of superposition to an existing analytical solution due to Geertsma (1973), which looks at ground surface subsidence above a cylindrical region of uniform pressure change. The results from our new analytical solution were verified by comparison with the results from a set of fully coupled hydro-mechanical finite element (FE) simulations, which were obtained using COMSOL Multiphysics v5.4.

In Chapter 5, the pressure distribution from the numerical finite difference single and two-phase CBM flow models developed in Chapters 2 and 3 were used to derive an effective pressure to drive the semi-analytical solution for ground surface subsidence developed in Chapter 4.

A simplified analytical solution for maximum ground surface subsidence was derived, assuming that the pressure distribution within the reservoir is uniform (recall Eq. (5.14)). Dimensionless transformation revealed that four important parameter groups control ground surface subsidence including (1) the ratio of initial reservoir pressure to Langmuir pressure constant, p_I; (2) the ratio of the Langmuir pressure constant for coal swelling strain to the Langmuir pressure constant, $p_{L,\varepsilon}$; (3) the ratio of the volume of gas produced to the product of the mass of the coalbed and Langmuir volume constant, v_g; and (4) the ratio of the product of Langmuir pressure constant and Biot coefficient to the product of Young's modulus and Langmuir volumetric strain constant, γ.

The results showed that the presence of water in the cleats was found to have no influence on ground surface subsidence for a given gas production volume. The reason was that the initial fracture porosity, where the initial water saturation resides, is very small compared to the volume of the coal matrix, where most of the gas storage is present.

Sensitivity analysis showed that overburden thickness influenced ground surface subsidence. It was also shown that an increase in initial coal permeability and cleat volume compressibility leads to an increase in ground surface subsidence for a given time. However, these parameters were found not to be significant when considering ground surface subsidence due to a given gas production volume.

The sensitivity analysis also showed that the simplified analytical solution is effective at predicting ground surface subsidence for a given gas production volume, predicted by the numerical model, for all of the scenarios studied. This suggests that pressure distribution within a CBM reservoir is not the only important parameters for determining ground surface subsidence. The amount of observed subsidence due to CBM production can also be controlled by the relationship between the rock mechanics and sorption parameters.

A significant limitation of this work concerns the simplifying assumption that the producing CBM formation is hydraulically isolated from the surrounding overburden and under-burden. Such an assumption implies that the water being produced is solely derived from the fracture porosity within the CBM formation. Such a situation is considered an ideal CBM reservoir for gas companies because pressure reduction, needed for gas desorption, can be achieved with minimal energy requirements (Commonwealth of Australia, 2014b). However, this assumption is

often invalid. The implications are that much more water needs to be produced to achieve desired pressure reductions within the CBM formation because water will leak into the CBM formation from surrounding aquifers. This, in turn, implies that our model will be underestimating subsidence in this context. Recommended further work should look at coupling the CBM model developed in this thesis with regional scale aquifer models. This will enable the effect of aquifer connectivity on ground surface subsidence to be further explored.

Appendix A

Gas viscosity

The semi-empirical relationship for calculating the viscosity of gases as presented by Lee et al. (1996) as reported by Ahmed (2001) is given as

$$\mu_g = 10^{-4} K \exp\left[X\left(\frac{\rho_g}{62.4}\right)^Y\right] \tag{A.1}$$

where

$$K = \frac{(9.4 + 0.02M_a)T^{1.5}}{209 + 19M_a + T} \tag{A.2}$$

$$X = 3.5 + \frac{986}{T} + 0.01M_a \tag{A.3}$$

$$Y = 2.4 - 0.2X \tag{A.4}$$

Where:

M_a is the apparent molecular weight of the gas mixture.

ρ_g is the gas density at reservoir pressure and temperature, lb/ft^3.

T is the reservoir pressure, ^{o}R.

References

Addis, M. (1997, January). The stress-depletion response of reservoirs. In *Society of Petroleum Engineers annual Technical Conference.* Paper presented at the 1997 Society of Petroleum Engineers annual Technical Conference and Exhibition, San Antonio, 5-8 October(pp. 55-65). https://doi.org/10.2118/38720-MS

Al-Jubori, A., Johnston, S., Boyer, C., Lambert, S. W., Bustos, O. A., Pashin, J. C., Wray, A. (2009). Coalbed methane: clean energy for the world. *Oilfield Review, 21*(2), 4-13.

Ahmed, T. (2001). *Reservoir engineering handbook*. (2nd Edition). Oxford, United Kingdom: Gulf Professional Publishing.

Amaziane, B., Jurak, M., & Zgaljic-Keko, A. (2012, September). Modeling compositional compressible two-phase flow in porous media by the concept of the global pressure. *In ECMOR XIII-13th European Conference on the Mathematics of Oil Recovery (pp. cp-307)*. European Association of Geoscientists & Engineers.

Aminian, K., Ameri, S., Bhavsar, A. B., & Lakshminarayanan, S. (2005, September). Type Curves for Production Prediction and Evaluation of Coalbed Methane Reservoirs. In *SPE Eastern Regional Meeting*. https://doi.org/10.2118/97957-MS

Andersen, O., Nilsen, H. M., Gasda, S. (2017). Modeling geomechanical impact of

fluid storage in poroelastic media using precomputed response functions. *Computational Geosciences, 21,* 1135–1156. DOI 10.1007/s10596-017-9674-8

Arri, L. E., Yee, D., Morgan, W. D., & Jeansonne, M. W. (1992, January). Modeling coalbed methane production with binary gas sorption. In SPE rocky mountain regional meeting. Society of Petroleum Engineers.

Ayoub, J., Colson, L., Hinkel, J., Johnston, D., & Levine, J. (1991). Learning to produce coalbed methane. *Oilfield Review, 3*(1), 27-40.

Balla, L. (1989). Mathematical modeling of methane flow in a borehole coal mining system. *Transport in porous media, 4(2)*, 199-212.

Batley, G. E., & Kookana, R. S. (2012). Environmental issues associated with coal seam gas recovery: managing the fracking boom. *Environmental Chemistry, 9*(5), 425-428. https://doi.org/10.1071/EN12136

Batzle, M., & Wang, Z. (1992). Seismic properties of pore fluids. *Geophysics, 57*(11), 1396-1408. doi:10.1190/1.1443207

Bear, J., & Corapcioglu, M. Y. (1981a). Mathematical model for regional land subsidence due to pumping: 1. Integrated aquifer subsidence equations based on vertical displacement only. *Water Resources Research, 17,* 937–946.

Bear, J., & Corapcioglu, M. Y. (1981b). Mathematical model for regional land subsidence due to pumping: 2. Integrated aquifer subsidence equations for vertical and horizontal displacements. *Water Resources Research, 17,* 947-958.

Bertrand, F., Cerfontaine, B., & Collin, F. (2017). A fully coupled hydro-mechanical

model for the modeling of coalbed methane recovery. *Journal of Natural Gas Science and Engineering, 46*, 307-325.

Biot, M. A. (1941). General theory of three dimensional consolidation. *Journal of Applied Physics, 12*(2), 155-164. doi:10.1063/1.1712886

Bishop, R. E., Lampe, D. J., Okey, B. W., Wilber, T., & Arnowitt, M. (2012). " Fracking:" A Roundtable. *Journal of Appalachian Studies, 18*(1/2), 31-47. Retrieved from https://www.jstor.org/stable/23337707

Bjørnarå, T. I. (2018). *Model development for efficient simulation of CO2 storage.* Unpublished PhD Thesis. The University of Bergen. Retrieved from http://hdl.handle.net/1956/17695

Bourgeat, A., Jurak, M., & Smaï, F. (2013). On persistent primary variables for numerical modeling of gas migration in a nuclear waste repository. *Computational geosciences, 17*(2), 287-305.

Brooks, R. H., Corey, A. T. (1966). Properties of porous media affecting fluid flow. *Journal of the Irrigation and Drainage Division, 92*(2), 61-90.

Brown, N. J., Woods, A.W., Neufeld, J. A., & Richardson, C. (2014). *Constraining Surface Deformation Predictions Resulting from Coal Seam Gas Extraction*. Record 2014/14. Geoscience Australia, Canberra. http://dx.doi.org/10.11636/Record.2014.044

Bumb, A. C., & McKee, C. R. (1988). Gas-Well Testing in the Presence of Desorption for Coalbed Methane and Devonian Shale. *Society of Petroleum Engineers Formation Evaluation, 3*(01), 179–185. DOI: 10.2118/15227-PA.

Calderhead, A. I., Therrien, R., Rivera, A., Martel, R., Garfias, J. (2011). Simulating pumping-induced regional land subsidence with the use of InSAR and field data in the Toluca Valley, Mexico. *Advances in Water Resources, 34*(1), 83-97. https://doi.org/10.1016/j.advwatres.2010.09.017

Celaya, E. A., Aguirrezabala, J. A., & Chatzipantelidis, P. (2014). Implementation of an Adaptive BDF2 Formula and Comparison with the MATLAB Ode15s. *Procedia Computer Science, 29*, 1014-1026.

Chamani, A. and Rasouli, V. (2011). Simulation of Depletion-induced Surface Subsidence in a Coal Seam. In APCBM (Ed), *Asia Pacific Coalbed Methane Symposium*. Paper presented at the 3rd Asia Pacific Coalbed Methane Symposium, Brisbane, Australia, 3-6 May. http://hdl.handle.net/20.500.11937/14262

Chen, C., Pei, S., Jiao, J. (2003). Land subsidence caused by groundwater exploitation in Suzhou City, China. *Hydrogeology Journal, 11*(2), 275-287. DOI 10.1007/s10040-002-0225-5

Chen, Z., Liu, J., Pan, Z., Connell, L. D., Elsworth, D. (2012). Influence of the effective stress coefficient and sorption-induced strain on the evolution of coal permeability: model development and analysis. International Journal of Greenhouse Gas Control, 8, 101-110. Elsevier

Chen, Z., Liu, J., Kabir, A., Wang, J., & Pan, Z. (2013a). Impact of various parameters on the production of coalbed methane. *Society of Petroleum Engineers Journal, 18*(05), 910-923.

Chen, D., Pan, Z., Liu, J., & Connell, L. D. (2013b). An improved relative per-

meability model for coal reservoirs. International *Journal of Coal Geology, 109,* 45-57. https://doi.org/10.1016/j.coal.2013.02.002

Chin, L. Y., Raghavan, R., & Thomas, L. K. (2000). Fully Coupled Geomechanics and Fluid-Flow Analysis of Wells With Stress-Dependent Permeability. *Society of Petroleum Engineers Journal, 5*(01), 32-45.

Christensen, S. O., Janbu, N., & Jones, M. E. (1988). *Subsidence due to oil-gas production. Proceedings of International. Conference on Behaviour of Offshore Structures (BOSS '88), Trondheim, June 1988*. Norway. Vol. 1: Geotechnics, p. 143.

Christian, J. T., & Boehmer, J. W. (1970). Plane Strain Consolidation by Finite Elements. *Journal of the Soil Mechanics and Foundations Division, 96*(4), 1435-1457.

Commonwealth of Australia (2014a). *Monitoring and management of subsidence induced by coal seam gas extraction. Knowledge report*, prepared by Coffey Geotechics for the Department of the Environment, Commonwealth of Australia, Canberra. Retrieved from http://iesc.environment.gov.au

Commonwealth of Australia (2014b). *Subsidence from coal seam gas extraction in Australia. Background review.* Retrieved from http://iesc.environment.gov.au/index.html

Connell, L. D. (2009). Coupled flow and geomechanical processes during gas production from coal seams. *International Journal of Coal Geology, 79*(1-2), 18-28. https://doi.org/10.1016/j.coal.2009.03.008

Connell, L. D., & Detournay, C. (2009). Coupled flow and geomechanical processes during enhanced coal seam methane recovery through CO2 sequestration. *International Journal of Coal Geology, 77(1-2)*, 222-233.

Connell, L. D., Lu, M., Pan, Z. (2010). An analytical coal permeability model for tri-axial strain and stress conditions. International Journal of Coal Geology, 84(2), 103-114.

Cooper Jr, H. H., & Jacob, C. E. (1946). A generalized graphical method for evaluating formation constants and summarizing well-field history. *Eos, Transactions American Geophysical Union, 27*(4), 526-534.

Cui, X. and Bustin, R. M. (2005). Volumetric strain associated with methane desorption and its impact on coalbed gas production from deep coal seams. *AAPG Bulletin, 89*(9), 1181-1202. https://doi.org/10.1306/05110504114

Dahm, K. G., Guerra, K. L., Xu, P., & Drewes, J. E. (2011). Composite geochemical database for coalbed methane produced water quality in the Rocky Mountain region. *Environmental Science & Technology, 45*(18), 7655-7663. dx.doi.org/10.1021/es201021n

Dabbous, M. K., Reznik, A. A., Mody, B. G., Fulton, P. F., & Taber, J. J. (1976). Gas-water capillary pressure in coal at various overburden pressures. Society of Petroleum Engineers Journal, 16(05), 261-268.

Dake, L.P. (1983). Fundamentals of Reservoir Engineering. (Vol. 8). Oxford United Kingdom: Elsevier.

Durran, D. R. (2010). Numerical methods for fluid dynamics: With applications to geophysics (Vol. 32). Springer Science & Business Media.

Du, J., & Olson, J. E. (2001). A poroelastic reservoir model for predicting subsidence and mapping subsurface pressure fronts. *Journal of Petroleum Science and Engineering, 30*(3-4), 181-197. https://doi.org/10.1016/S0920-4105(01)00131-0

Durucan, S., Edwards, J. S. (1986). The effects of stress and fracturing on permeability of coal. *Mining Science and Technology, 3*(3), 205-216. https://doi.org/10.1016/S0167-9031(86)90357-9

Durucana, S., Ahsanb, M., Syeda, A., Shia, J. Q., & Korrea, A. (2013). Two phase relative permeability of gas and water in coal for enhanced coalbed methane recovery and CO2 storage. *Energy Procedia, 37,* 6730-6737.

Enever, J. R. E., Henning, A. (1997, May). The relationship between permeability and effective stress for Australian coal and its implications with respect to coalbed methane exploration and reservoir modelling. In *1997 international coalbed methane symposium*. Paper presented at the proceedings of the 1997 International Coalbed Methane Symposium, Bryant Conference Center, University of Alabama, Tuscaloosa, Alabama, U.S.A, 12-17 May (pp 13-22). Tuscaloosa, AL, USA: University of Alabama.

Esfandiari, R. S. (2017). Numerical Methods for Engineers and Scientists Using MATLAB®. *CRC Press*.

Espinoza, D. N., Pereira, J. M., Vandamme, M., Dangla, P., & Vidal-Gilbert, S. (2015). Desorption-induced shear failure of coal bed seams during gas depletion. *International Journal of Coal Geology, 137*, 142-151.

Fan, C., Elsworth, D., Li, S., Zhou, L., Yang, Z., & Song, Y. (2019). Thermo-hydro-mechanical-chemical couplings controlling CH4 production and CO2 sequestration in enhanced coalbed methane recovery. Energy, 173, 1054-1077.

Fanchi, J. R. (2002). *Estimating Subsidence During Coalbed Methane Production.* Paper presented at the Society of Petroleum Engineers Gas Technology Symposium, Calgary, Alberta, Canada, 30 April-2 May. https://doi.org/10.2118/75511-MS

Ferronato, M., Gambolati, G., Teatini, P., & Bau, D. (2001). Land surface uplift above compacting overconsolidated reservoirs. *International Journal of Solids and Structures, 38*(46-47), 8155-8169. https://doi.org/10.1016/S0020-7683(01)00122-6

Fjær, E., Holt, R. M., Horsrud, P., Raaen, A. M., & Risnes, R. (2008). *Petroleum Related Rock Mechanics* (2nd Ed.). (Vol.53). Oxford, United Kingdom: Elsevier.

Flores, R. M. (2004). Coalbed methane in the Powder River Basin, Wyoming and Montana: an assessment of the Tertiary–Upper Cretaceous coalbed methane total petroleum system. *US Geological survey digital data series dds-69-c, 2,* 56.

Fokker, P. (2002, January). *Subsidence prediction and inversion of subsidence data.* Paper presented at SPE/ISRM Rock Mechanics conference, Irving, Texas, 20-23 October. https://doi.org/10.2118/78227-MS

Fokker, P. A., & Orlic, B. (2006). Semi-analytic modelling of subsidence. *Mathematical Geology, 38*(5), 565-589. DOI: 10.1007/s11004-006-9034-z

Forth, R. A. (2004). Groundwater and geotechnical aspects of deep

excavations in Hong Kong. *Engineering Geology, 72*(3), 253-260. https://doi.org/10.1016/j.enggeo.2003.09.003

Fredrich, J. T., Arguello, J. G., Deitrick, G. L., & Rouffignac, E. P. (2000). Geomechanical Modeling of Reservoir Compaction, Surface Subsidence, and Casing Damage at the Belridge Diatomite Field. *Society of Petroleum Engineers Reservoir Evaluation & Engineering, 3*(4), 348-359. DOI:10.2118/65354-PA

Freij-Ayoub, R. (2012). *Numerical Simulation of the Production of Methane and Water from Coal Seams and the Associated Ground Surface Subsidence.* Paper presentated at the Socitey of Petroleum Engineers Asia Pacific Oil and Gas Conference and Exhibition, Perth, Australia, 22–24 October. https://doi.org/10.2118/158425-MS

Frost, C. D., Pearson, B. N., Ogle, K. M., Heffern, E. L., & Lyman, R. M. (2002). Sr isotope tracing of aquifer interactions in an area of accelerating coal-bed methane production, Powder River Basin, Wyoming. *Geology, 30*(10), 923-926. https://doi.org/10.1130/0091-7613(2002)030¡0923:SITOAI¿2.0.CO;2

Galloway, D. L., & Burbey, T. J. (2011). Regional land subsidence accompanying groundwater extraction. *Hydrogeology Journal, 19*(8), 1459-1486. https://doi.org/10.1007/s10040-011-0775-5

Galloway, D. L., and Sneed, M. (2013). Analysis and simulation of regional subsidence accompanying groundwater abstraction and compaction of susceptible aquifer systems in the USA. *Boletín de la Sociedad Geológica Mexicana, 65*(1), 123-136. Retrieved from http://www.redalyc.org/articulo.oa?id=94348265011

Gambolati, G. (1972). A three-dimensional model to compute land subsidence. *Hydrological Sciences Bulletin, 17*(2), 219-226. DOI:10.1080/02626667209493823

Gambolati, G., & Freeze, R. A. (1973). Mathematical simulation of the subsidence of Venice: 1. Theory. *Water Resources Research, 9*(3), 721-733. https://doi.org/10.1029/WR009i003p00721

Gambolati, G., & Teatini, P. (2015). Geomechanics of subsurface water withdrawal and injection. *Water Resources Research, 51,* 3922-3955. https://doi.org/10.1002/2014WR016841

Gambolati, G., Gatto, P., & Freeze, R. A. (1974). Mathematical simulation of the subsidence of Venice: 2. Results. *Water Resources Research, 10*(3), 563-577. https://doi.org/10.1029/WR010i003p00563

Gambolati G, Bau, D., Teatini, P., & Ferronato, M. (2000). Importance of poroelastic coupling in dynamically active aquifers of the Po river basin, Italy. *Water Resources Research, 36,* 2443-2459. https://doi.org/10.1029/2000WR900127

Gambolati, G., Teatini, P., & Ferronato, M. (2005). Anthropogenic land subsidence. *Encyclopedia of Hydrological Sciences, Vol.13*(1),160-178.

Gambolati, G., Teatini, P., & Ferronato, M. (2006). Anthropogenic land subsidence. In M.G. Anderson (Ed.), *Encyclopedia of Hydrological Sciences* (pp. 2443-2459). New Jersey: John Wiley & Sons, Ltd. https://doi.org/10.1002/0470848944.hsa164b

Geertsma, J. (1973). Land subsidence above compacting oil and gas reservoirs. *Journal of Petroleum Technology, 25*, 734-744. https://doi.org/10.2118/3730-PA

Gerami, S., Pooladi-Darvish, M., Morad, K., & Mattar, L. (2008). Type curves for dry CBM reservoirs with equilibrium desorption. *Journal of Canadian Petroleum Technology, 47*(7), 48-56. https://doi.org/10.2118/2007-011

Gilman, A.,and Beckaie, R. (2000). Flow of coal-bed methane to a gallery. *Transport in porous media, 41*(01), 1-16. https://doi.org/10.1023/A:1006754108197

Goudarzi, S., Mathias, S. A., & Gluyas, J. G. (2016). Simulation of three-component two-phase flow in porous media using method of lines. *Transport in Porous Media, 112*(1), 1-19. https://doi.org/10.1007/s11242-016-0639-5

Reservoir engineering in coal seams: Part 1-The physical process of gas storage and movement in coal seams. SPE Reservoir Engineering, 2(01), 28-34. Society of Petroleum Engineers

Gu, F., & Chalaturnyk, R. J. (2006). Numerical simulation of stress and strain due to gas sorption/desorption and their effects on in situ permeability of coalbeds. *Journal of Canadian Petroleum Technology, 45*(10). https://doi.org/10.2118/06-10-05

Gu, F., & Chalaturnyk, R. (2010). Permeability and porosity models considering anisotropy and discontinuity of coalbeds and application in coupled simulation. Journal of Petroleum Science and Engineering, 74(3-4), 113-131.

Gunter, W. D., Mavor, M. J., & Robinson, J. R. (2005, September). CO2 storage and enhanced methane production: field testing at Fenn-Big Valley, Alberta, Canada, with application. In *Greenhouse Gas Control Technologies 7*. Proceedings of the 7th International Conference on Greenhouse Gas Control Technology 5 Vancouver(Vol. 1, pp. 413-421). Vancouver, Canada: Elsevier Science Ltd.

Ham, Y., & Kantzas, A. (2008). Measurement of relative permeability of coal: approaches and limitations. In *CIPC/SPE gas technology symposium 2008 joint conference.* https://doi.org/10.2118/114994-MS

Hairer, E., Wanner, G., & Nørsett, S. P. (1993). Solving ordinary differential equations. *Springer*.

Hamawand, I., Yusaf, T., & Hamawand, S. G. (2013). Coal seam gas and associated water: a review paper. *Renewable and Sustainable Energy Reviews, 22,* 550-560. https://doi.org/10.1016/j.rser.2013.02.030

Haq, S., Hussain, A., & Uddin, M. (2012). On the numerical solution of nonlinear Burgers'-type equations using meshless method of lines. *Applied Mathematics and Computation, 218(11)*, 6280-6290.

Harada, Y., & Yamanouchi, T. (1983). Land subsidence in Saga Plain, Japan and its analysis by the quasi three-dimensional aquifer model. *Geotechnical Engineering, 14*(1), 23-54.

Hardwick, J. S., and Mathias, S. A. (2018). Masuda's sandstone core hydrate dissociation experiment revisited. *Chemical Engineering Science, 175*, 98-109.

Harpalani, S., & McPherson, M. J. (1986, January). Mechanism of methane flow through solid coal. In The 27th US Symposium on Rock Mechanics (USRMS). American Rock Mechanics Association.

Harpalani, S., & Schraufnagel, R. A. (1990, September). Influence of Matrix Shrinkage and Compressibility on Gas Production From Coalbed Methane Reservoirs'. In *SPE annual Technical Conference and Exhibition.* Paper presented at

the Society of Petroleum Engineers annual Technical Conference and Exhibition, New Orleans, 23-26 September. doi:10.2118/20729-MS

Harpalani, S., & Chen, G. (1995). Estimation of changes in fracture porosity of coal with gas emission. *Fuel, 74*(10), 1491-1498. https://doi.org/10.1016/0016-2361(95)00106-F

Harpalani, S., & Ouyang, S. (1996, June). A New Laboratory Technique to Estimate Gas Diffusion Characteristics of Naturally Fractured Reservoirs. In *2nd North American Rock Mechanics Symposium.* Paper Presented at the 2nd North American Rock Mechanics Symposium, Montreal, Canada, 19-21 June. Quebec: American Rock Mechanics Association.

Hower, T. L. (2003, January). Coalbed methane reservoir simulation: an evolving science. In SPE Annual Technical Conference and Exhibition. Society of Petroleum Engineers.

Hsi, J. P., & Small, J. C. (1992). Ground settlements and drawdown of the water table around an excavation. *Canadian Geotechnical Journal, 29*(5), 740-756. https://doi.org/10.1139/t92-082

Hsi, J. P., Carter, J. P., Small, J. C. (1994). Surface subsidence and drawdown of the water table due to pumping. *Geotechnique, 44*(3), 381-396. https://doi.org/10.1680/geot.1994.44.3.381

Hu, R. L., Yue, Z. Q., Wang, L. U., & Wang, S. J. (2004). Review on current status and challenging issues of land subsidence in China. *Engineering Geology, 76*(1-2), 65-77. https://doi.org/10.1016/j.enggeo.2004.06.006

Hwang, C., Morgenstern, N. R., Murray, D. W. (1971). On solutions of plane strain consolidation problems by finite element methods. *Canadian Geotechnical Journal, 8*(1), 109-118. https://doi.org/10.1139/t71-009

Ireson, A. M., Mathias, S. A., Wheater, H. S., Butler, A. P., & Finch, J. (2009). A model for flow in the chalk unsaturated zone incorporating progressive weathering. *Journal of Hydrology, 365(3-4)*, 244-260.

Izadi, G., Wang, S., Elsworth, D., Liu, J., Wu, Y., Pone, D. (2011). Permeability evolution of fluid-infiltrated coal containing discrete fractures. International Journal of Coal Geology, 85(2), 202-211.

Jaeger, J. C., Cook, N. G., & Zimmerman, R. (2009). *Fundamentals of Rock Mechanics*. (Fourth edition). Malden, U.S.A: Blackwell Publishing.

Jackson, R. E., & Reddy, K. J. (2007). Geochemistry of coalbed natural gas (CBNG) produced water in Powder River Basin, Wyoming: salinity and sodicity. *Water, air, and soil pollution, 184*(1-4), 49-61. https://doi.org/10.1007/s11270-007-9398-9

Jackson, R. E., Gorody, A. W., Mayer, B., Roy, J. W., Ryan, M. C., & Van Stempvoort, D. R. (2013). Groundwater protection and unconventional gas extraction: The critical need for field-based hydrogeological research. *Groundwater, 51*(4), 488-510. https://doi.org/10.1111/gwat.12074

Jayeoba, A., Mathias, S. A., Nielsen, S., Vilarrasa, V., & Bjørnarå, T. I. (2019). Closed-form equation for subsidence due to fluid production from a cylindrical confined aquifer. *Journal of Hydrology, 573*, 964-969. https://doi.org/10.1016/j.jhydrol.2019.03.041

Jones Jr, F. O. (1975). A laboratory study of the effects of confining pressure on fracture flow and storage capacity in carbonate rocks. *Journal of Petroleum Technology, 27(01)*, 21-27.

Ketelaar, V. G. (2009). *Satellite radar interferometry: Subsidence monitoring techniques* (Vol. 14). Berlin: Springer Science & Business Media.

King, G. R., Ertekin, T., & Schwerer, F. C. (1986). Numerical simulation of the transient behavior of coal-seam degasification wells. *SPE Formation Evaluation, 1(02)*, 165-183.

Kissell, F. N. (1972). The methane migration and storage characteristics of the Pittsburgh, Pocahontas No. 3, and Oklahoma Hartshorne coalbeds.

Kissell, F. N., & Edwards, J. C. (1975). Two-phase flow in coalbeds.

Kolesar, J. E., Ertekin, T., & Obut, S. T. (1990). The unsteady-state nature of sorption and diffusion phenomena in the micropore structure of coal: Part 1-Theory and mathematical formulation. SPE Formation Evaluation, 5(01), 81-88.

Kolesar, J. E., Ertekin, T., & Obut, S. T. (1990). The unsteady-state nature of sorption and diffusion phenomena in the micropore structure of coal: Part 2-Solution. *SPE Formation Evaluation, 5(01)*, 89-97.

Laubach, S.E., Marrett, R.A., Olson, J.E., Scott, A.R. (1998). Characteristics and origins of coal cleat: a review. *International Journal of Coal Geology, 35*(1), 175-207. https://doi.org/10.1016/S0166-5162(97)00012-8

Law, D. H. S., Van der Meer, L. G. H., & Gunter, W. D. (2002, April). Numerical simulator comparison study for enhanced coalbed methane recovery

processes. In *Part I: Pure Carbon Dioxide Injection, Paper SPE 75669 presented at the SPE Gas Technology Symposium, Calgary, Alberta, Canada, April.* https://doi.org/10.2118/75669-MS

Lee, A. L., Gonzalez, M. H., & Eakin, B. E. (1966). The viscosity of natural gases. *Journal of Petroleum Technology, 18*(08), 997-1000. https://doi.org/10.2118/1340-PA

Lee, H. S., Matthews, C. J., Braddock, R. D., Sander, G. C., & Gandola, F. (2004). A MATLAB method of lines template for transport equations. *Environmental Modelling & Software, 19(6)*, 603-614.

Levine, J. R. (1996). Model study of the influence of matrix shrinkage on absolute permeability of coal bed reservoirs. *Geological Society, London, Special Publications, 109*(1), 197-212. https://doi.org/10.1144/GSL.SP.1996.109.01.14

Lewis, R. W., & Schrefler, B. (1978). A fully coupled consolidation model of the subsidence of Venice. *Water Resources Research, 14*(2), 223-230. https://doi.org/10.1029/WR014i002p00223

Lewis, R. W., and Schrefler, B. A. (1998). *The finite element method in the static and dynamic deformation and consolidation of porous media*. New York, NY: John Wiley.

Lewis, R. W., & Sukirman, Y. (1994). Finite element modelling for simulating the surface subsidence above a compacting hydrocarbon reservoir. *International Journal for Numerical and Analytical Methods in Geomechanics, 18*(9), 619-639. https://doi.org/10.1002/nag.1610180904

Li, X., & Fang, Z. M. (2014). Current status and technical challenges of CO 2 storage in coal seams and enhanced coalbed methane recovery: an overview. *International Journal of Coal Science & Technology, 1*(1), 93-102. https://doi.org/10.1007/s40789-014-0002-9

Liu, S., & Harpalani, S. (2013). A new theoretical approach to model sorption-induced coal shrinkage or swelling. *AAPG bulletin, 97*(7), 1033-1049.

Li, S., Fan, C., Han, J., Luo, M., Yang, Z., & Bi, H. (2016). A fully coupled thermal-hydraulic-mechanical model with two-phase flow for coalbed methane extraction. *Journal of Natural Gas Science and Engineering, 33*, 324-336.

Liu, H. H., & Rutqvist, J. (2010). A new coal-permeability model: internal swelling stress and fracture–matrix interaction. Transport in Porous Media, 82(1), 157-171.

Liu, S., & Harpalani, S. (2014). Evaluation of in situ stress changes with gas depletion of coalbed methane reservoirs. *Journal of Geophysical Research: Solid Earth, 119*(8), 6263-6276. https://doi.org/10.1002/2014JB011228

Liu, J., Chen, Z., Elsworth, D., Miao, X., Mao, X. (2011). Evolution of coal permeability from stress-controlled to displacement-controlled swelling conditions. *Fuel, 90*(10), 2987-2997. https://doi.org/10.1016/j.fuel.2011.04.032

Liu, J., Chen, Z., Elsworth, D., Qu, H., & Chen, D. (2011). Interactions of multiple processes during CBM extraction: a critical review. International Journal of Coal Geology, 87(3-4), 175-189.

Liu, Q., Cheng, Y., Zhou, H., Guo, P., An, F., Chen, H. (2014). A mathemat-

ical model of coupled gas flow and coal deformation with gas diffusion and klinkenberg effects. *Rock Mechanics and Rock Engineering, 48*(03), 1163-1180. https://doi.org/10.1007/s00603-014-0594-9

Liu, S. Q., Sang, S. X., Li, Y. M., Li, M. X., Liu, H. H., & Zhang, J. G. (2012). Analysis on fracturing failure cause of coal bed methane well in south part of Qinshui Basin. *Coal Science and Technology, 6,* 031.

Loáiciga, H. A. (2012). Consolidation settlement in aquifers caused by pumping. *Journal of Geotechnical and Geoenvironmental Engineering, 139*(7), 1191-1204. https://doi.org/10.1061/(ASCE)GT.1943-5606.0000836

Lu, S., Cheng, Y., & Li, W. (2016). Model development and analysis of the evolution of coal permeability under different boundary conditions. *Journal of Natural Gas Science and Engineering, 31*, 129-138.

Ma, Q., Harpalani, S., Liu, S. (2011). A simplified permeability model for coalbed methane reservoirs based on matchstick strain and constant volume theory. International Journal of Coal Geology, 85(1), 43-48.

Ma, T., Rutqvist, J., Oldenburg, C. M., Liu, W., Chen, J. (2017a). Fully coupled two-phase flow and poromechanics modeling of coalbed methane recovery: impact of geomechanics on production rate. *Journal of Natural Gas Science and Engineering, 45,* 474-486. https://doi.org/10.1016/j.jngse.2017.05.024

Mahmoudpour, M., Khamehchiyan, M., Nikudel, M. R., Ghassemi, M. R. (2016). Numerical simulation and prediction of regional land subsidence caused by groundwater exploitation in the southwest plain of Tehran, Iran. *Engineering Geology, 201*, 6-28. https://doi.org/10.1016/j.enggeo.2015.12.004

Mathias, S. A., & Zimmerman, R. W. (2003). Laplace transform inversion for late-time behavior of groundwater flow problems. *Water Resources Research, 39*(10), 1283. https://doi.org/10.1029/2003WR002246

Mathias, S. A., Butler, A. P., Jackson, B. M., & Wheater, H. S. (2006). Transient simulations of flow and transport in the Chalk unsaturated zone. *Journal of Hydrology, 330(1-2)*, 10-28.

Mathias, S. A., Butler, A. P., & Zhan, H. (2008). Approximate solutions for Forchheimer flow to a well. *Journal of Hydraulic Engineering, 134*(9), 1318–1325. https://doi.org/10.1061/(ASCE)0733-9429(2008)134:9(1318)

Mathias, S. A., Butler, A. P., & Wheater, H. S. (2008). Modelling radioiodine transport across a capillary fringe. *Journal of environmental radioactivity, 99*(4), 716-729.

Mathias, S. A., Hardisty, P. E., Trudell, M. R., & Zimmerman, R. W. (2009). Approximate solutions for pressure buildup during CO 2 injection in brine aquifers. *Transport in Porous Media, 79(2)*, 265.

Mathias, S. A., Gluyas, J. G., de Miguel, G. J. G. M., Bryant, S. L., & Wilson, D. (2013). On relative permeability data uncertainty and CO2 injectivity estimation for brine aquifers. *International Journal of Greenhouse Gas Control, 12,* 200-212. https://doi.org/10.1016/j.ijggc.2012.09.017

Mathias, S. A., McElwaine, J. N., & Gluyas, J. G. (2014). Heat transport and pressure buildup during carbon dioxide injection into depleted gas reservoirs. *Journal of Fluid Mechanics, 756*, 89-109.

Mavor, M. J., & Vaughn, J. E. (1998). Increasing coal absolute permeability in the San Juan Basin fruitland formation. SPE Reservoir Evaluation & Engineering, 1(03), 201-206.

Mavor, M., Gunter, W., & Robinson, J. (2004, September). Alberta Multiwell Micro-Pilot Testing for CBM Properties, Enhanced Methane Recovery and CO2 Storage Potential. In *SPE Annual Technical Conference and Exhibition.* https://doi.org/10.2118/90256-MS

Mazzotti, M., Pini, R., & Storti, G. (2009). Enhanced coalbed methane recovery. *The Journal of Supercritical Fluids, 47*(3), 619-627. https://doi.org/10.1016/j.supflu.2008.08.013

McBeth, I., Reddy, K. J., & Skinner, Q. D. (2003). Chemistry of trace elements in coalbed methane product water. *Water Research, 37*(4), 884-890. https://doi.org/10.1016/S0043-1354(02)00382-2

McCann, G. D., & Wilts, C. H. (1951). *A mathematical analysis of the subsidence in the Long Beach-San Pedro Area. An Unpublished technical report from Institute of Technology, Pasadena, Califonia (pp. 119)*. Retrieved from http://resolver.caltech.edu/CaltechAUTHORS:20141013-140734512

McKee, C. R., and Bumb, A. C. (1987). Flow-testing coalbed methane production wells in the presence of water and gas. *SPE formation Evaluation, 2*(04), 599-608. https://doi.org/10.2118/14447-PA

McKee, C.R., Bumb, A.C., Koenig, R.A., and others. (1988). Stress-dependent permeability and porosity of coal and other geologic formations. *SPE formation evaluation, 3*(1), 81-91. https://doi.org/10.2118/12858-PA

McNamee, J. O. H. N., & Gibson, R. E. (1960). Displacement functions and linear transforms applied to diffusion through porous elastic media. *The Quarterly Journal of Mechanics and Applied Mathematics, 13*(1), 98-111. https://doi.org/10.1093/qjmam/13.1.98

Mijic, A., Mathias, S. A., & LaForce, T. C. (2013). Multiple well systems with non-Darcy flow. *Groundwater, 51*(4), 588-596. https://doi.org/10.1111/j.1745-6584.2012.00992.x

Mindlin, R. D., & Cheng, D. H. (1950). Thermoelastic stress in the semi-infinite solid. *Journal of Applied Physics, 21*(9), 931-933. https://doi.org/10.1063/1.1699786

Mitra, A., & Harpalani, S. (2007, October). Modeling Incremental Swelling of Coal Matrix with CO2 Injection in Coalbed Methane Reservoirs. In *Eastern Regional Meeting.* https://doi.org/10.2118/111184-MS

Mitra, A., Harpalani, S., & Liu, S. (2012). Laboratory measurement and modeling of coal permeability with continued methane production: Part 1–Laboratory results. *Fuel, 94,* 110-116. https://doi.org/10.1016/j.fuel.2011.10.052

Moffat, D. H., & Weale, K. E. (1955). Sorption by coal of methane at high pressures. Fuel, 34(4), 449-462.

Mooney, C. (2011). The truth about fracking. *Scientific American, 305*(5), 80-85. https://www.jstor.org/stable/10.2307/26002882

Moore, T. A. (2012). Coalbed methane: a review. *International Journal of Coal Geology, 101,* 36-81. https://doi.org/10.1016/j.coal.2012.05.011

Moore, R. L., Loftin, D. F., & Palmer, I. D. (2011, January). History matching and permeability increases of mature coalbed methane wells in San Juan Basin. *In SPE Asia pacific oil and gas conference and exhibition. Society of Petroleum Engineers*.

Mora, C. A., & Wattenbarger, R. A. (2009). Comparison of Computation Methods for CBM Performance. *Journal of Canadian Petroleum Technology, 48*(04), 42-48. https://doi.org/10.2118/2007-066

Nauroy, J. F. (2011). *Geomechanics applied to the petroleum industry*. Paris, France: Editions Technip.

Nelson, S. A. (2000). Subsidence: dissolution and human-related causes. University of Tulane, New Orlean, Louisiana. Retrieved from http://www.tulane.edu/ sanelson/geol204/subsidence.htm

Nghiem, L. D., Ren, T., Aziz, N., Porter, I., & Regmi, G. (2011). Treatment of coal seam gas produced water for beneficial use in Australia: a review of best practices. *Desalination and Water Treatment, 32*(1-3), 316-323. DOI: 10.5004/dwt.2011.2716

Okotie, V. U., & Moore, R. L. (2011). Well-production challenges and solutions in a mature, very-low-pressure coalbed-methane reservoir. *SPE Production & Operations, 26*(02), 149-161. https://doi.org/10.2118/137317-PA

Orr Jr., F. M. (2007). *Theory of Gas Injection Processes.* Copenhagen, Denmark: Tie-Line Publications.

Palmer, I. (2009). Permeability changes in coal: analytical modeling. International Journal of Coal Geology, 77(1), 119-126.

Palmer, I., & Mansoori, J. (1996, January). How permeability depends on stress and pore pressure in coalbeds: A new model. In *SPE annual technical conference* (pp. 557-564). https://doi.org/10.2118/36737-MS

Pan, Z., and Connell, L. D. (2012). Modelling permeability for coal reservoirs: a review of analytical models and testing data. International Journal of Coal Geology, 92, 1-44. Elsevier

Pashin, J. C. (2007). Hydrodynamics of coalbed methane reservoirs in the Black Warrior Basin: Key to understanding reservoir performance and environmental issues. *Applied Geochemistry, 22*(10), 2257-2272. https://doi.org/10.1016/j.apgeochem.2007.04.009

Patz, M. J., Ready, K. J., & Skinner, Q. D. (2004). Chemistry of coalbed methane discharge water interacting with semi-arid ephemeral stream channels. *Journal of the American Water Resources Association, 40*(5), 1247-1255. https://doi.org/10.1111/j.1752-1688.2004.tb01583.x

Pekot, L. J., Reeves, S. R. (2003). Modeling the effects of matrix shrinkage and differential swelling on coalbed methane recovery and carbon sequestration. In Paper 0328, proc. 2003 International Coalbed Methane Symposium. University of Alabama.

Phien-Wej, N., Giao, P. H., Nutalaya, P. (2006). Land subsidence in Bangkok, Thailand. *Engineering geology, 82*(4), 187-201. https://doi.org/10.1016/j.enggeo.2005.10.004

Pillalamarry, M., Harpalani, S., Liu, S. (2011). Gas diffusion behavior of coal and its impact on production from coalbed methane reservoirs. *International Journal of Coal Geology, 86*(4), 342-348. https://doi.org/10.1016/j.coal.2011.03.007

Pineda, J. A., & Sheng, D. (2014). Coal Seam Gas extraction and their potential effects on surface subsidence: an overview. *In 7th International Congress on Environmental Geotechnics: iceg2014* (p. 370). Engineers Australia.

Pitman, J. K., Pashin, J. C., Hatch, J. R., & Goldhaber, M. B. (2003). Origin of minerals in joint and cleat systems of the Pottsville Formation, Black Warrior basin, Alabama: implications for coalbed methane generation and production. *AAPG bulletin, 87*(5), 713-731. https://doi.org/10.1306/01140301055

Poland, J. F. (1984). Guidebook to studies of land subsidence due to ground-water withdrawal. In *Studies and reports in hydrology* (No. 40). UNESCO.

Poland, J. F., & Davis, G. H. (1969). Land subsidence due to withdrawal of fluids. *Reviews in engineering geology, 2,* 187-270.

Poulsen, B. A., & Shen, B. (2013). Subsidence risk assessment of decommissioned bord-and-pillar collieries. *International Journal of Rock Mechanics and Mining Sciences, 60,* 312-320. https://doi.org/10.1016/j.ijrmms.2013.01.014

Price, H. S., McCulloch, R. C., Edwards, J. C., & Kissell, F. N. (1973). Computer model study of methane migration in coal beds. CIM BULLETIN, 66(737), 103-112.

Pujades, E., De Simone, S., Carrera, J., Vazquez-Sune, E., & Jurado, A. (2017). Settlements around pumping wells: Analysis of influential factors

and a simple calculation procedure. J*ournal of Hydrology, 548*, 225–236. https://doi.org/10.1016/j.jhydrol.2017.02.040

Reeves, S. R. (2005). The Coal-Seq project: key results from field, laboratory, and modeling studies. In *Greenhouse Gas Control Technologies 7* (pp. 1399-1403). https://doi.org/10.1016/B978-008044704-9/50155-5

Reeves, S., & Pekot, L. (2001). *Advanced reservoir modeling in desorption-controlled reservoirs.* Paper SPE 71090 presented at the SPE Rocky Mountain Petroleum Technology Conference, Keystone, Colorado, 21–23 May. https://doi.org/10.2118/71090-MS

Remner, D. J., Ertekin, T., Sung, W., & King, G. R. (1986). A parametric study of the effects of coal seam properties on gas drainage efficiency. *SPE Reservoir Engineering, 1*(06), 633-646. https://doi.org/10.2118/13366-PA

Ren, W., Wang, H., Shi, J., Sun, F., Li, Y., Wang, Z., ... & Xu, Z. (2013, November). Desorption And Transport Mechanisms Of Gas Through Coal Matrix Pores And Gas Production Forecasting. In *2013 SPE Unconventional Resources Conference & Exhibition-Asia Pacific* Brinsbane, Australia, 11-13 November. https://doi.org/10.2118/166999-MS

Rice, C. A., Bartos, T. T., & Ellis, M. S. (2002, July). Chemical and isotopic composition of water in the Fort Union and Wasatch formations of the Powder River Basin, Wyoming and Montana: Implications for coalbed methane development. *In Rocky Mountain section AAPG convention* (pp. 53-70). Denevet, Colorado: Rocky Mountain Association of Geologists. Retrieved from http://archives.datapages.com/data/rmag/CBM2/rice.htm

Roadifer, R. D., Moore, T. R., Raterman, K. T., Farnan, R. A., & Crabtree, B. J. (2003, January). Coalbed Methane Parametric Study: What's Really Important to Production and When?. In *SPE Annual Technical Conference and Exhibition*. Denver, Colorado, 5-8 October. http://dx.doi.org/10.2118/84425-MS

Robertson, E. P., and Christiansen, R. L. (2006). *A permeability model for coal and other fractured, sorptive-elastic media* (No. INL/CON-06-11830). Idaho National Laboratory (INL).

Robertson, E. P., & Christiansen, R. L. (2007). Modeling laboratory permeability in coal using sorption-induced-strain data. SPE (Society of Petroleum Engineers) Reservoir Evaluation and Engineering, 10(3).

Robertson, E. P., Christiansen, R. L., and others (2008). A permeability model for coal and other fractured, sorptive-elastic media. *Society of Petroleum Engineers Journal, 13*(03), 314-324.

Rutqvist, J., & Stephansson, O. (2003). The role of hydromechanical coupling in fractured rock engineering. *Hydrogeology Journal, 11*(1), 7-40. https://doi.org/10.1007/s10040-002-0241-5

Sandhu, R. S., and Wilson, E. L. (1969). Finite-element analysis of seepage in elastic media. *Journal of the Engineering Mechanics Division, 95*(3), 641-652. Retrieved from https://cedb.asce.org/CEDBsearch/record.jsp?dockey=0016342

Saurabh, S., Harpalani, S., & Singh, V. K. (2016). Implications of stress redistribution and rock failure with continued gas depletion in coalbed methane reservoirs. *International Journal of Coal Geology, 162*, 183-192.

Saxena, S. K. (1979). *Evaluation and prediction of subsidence*. New York U.S.A.: American Society of Civil Engineers

Sawyer, W. K., Paul, G. W., & Schraufnagel, R. A. (1990, January). Development and application of a 3-D coalbed simulator. In Annual technical meeting. Petroleum Society of Canada.

Schmid, W., Hanson, R. T., Leake, S. A., Hughes, J. D., & Niswonger, R. G. (2014). Feedback of land subsidence on the movement and conjunctive use of water resources. *Environmental modelling & software, 62*, 253-270. https://doi.org/10.1016/j.envsoft.2014.08.006

Schraufnagel, R. (1993). Coalbed methane production. *Hydrocarbons from coal, AAPG Studies in Geology, 33*, pp. 341-359.

Schiesser, W. E. (2012). The numerical method of line nuys: integration of partial differential equations. Elsevier.

Segall, P. (1992). Induced stresses due to fluid extraction from axisymmetric reservoirs. *Pure and Applied Geophysics, 139*(3-4), 535-560. https://doi.org/10.1007/BF00879950

Seidle, J. (2011). *Fundamentals of coalbed methane reservoir engineering*. Tulsa, Oklahoma: PennWell Books.

Seidle, J. P., & Arri, L. E. (1990, January). Use of conventional reservoir models for coalbed methane simulation. In CIM/SPE International Technical Meeting. Society of Petroleum Engineers.

Seidle, J. R., Huitt, L. G. (1995, January). Experimental measurement of coal matrix shrinkage due to gas desorption and implications for cleat permeability increases. In *International meeting on petroleum Engineering* (pp. 575-582). https://doi.org/10.2118/30010-MS

Seidle, J. P., Jeansonne, M. W., Erickson, D. J. (1992). Application of matchstick geometry to stress dependent permeability in coals. In *SPE rocky mountain regional meeting*. Society of Petroleum Engineers.

Selvadurai, A. P. S., & Kim, J. (2015). Ground subsidence due to uniform fluid extraction over a circular region within an aquifer. *Advances in Water Resources, 78*, 50-59. https://doi.org/10.1016/j.advwatres.2015.01.015

Shampine, L. F., & Reichelt, M. W. (1997). The matlab ode suite. *SIAM journal on scientific computing, 18(1)*, 1-22.

Shampine, L. F., Gladwell, I., Shampine, L., & Thompson, S. (2003). Solving ODEs with matlab. *Cambridge university press.*

Sharaf, A. A., & Bakodah, H. O. (2005). A good spatial discretisation in the method of lines. *Applied mathematics and computation, 171(2)*, 1253-1263.

Shen, B., Alehossein, H., Poulsen, B., Huddlestone-Jolmes, C., & Zhou, B. (2010). *Collingwood park mine remediation - subsidence control using fly ash backfilling, 1-227.* (Report EP 105068). CSIRO Earth Science and Resource Engineering.

Shen, J., Qin, Y., Wang, G. X., Fu, X., Wei, C., & Lei, B. (2011). Relative permeabilities of gas and water for different rank coals. *International Journal of Coal Geology, 86*(2-3), 266-275. https://doi.org/10.1016/j.coal.2011.03.001

Ji-Quan, S., & Sevket, D. (2003, October). Gas storage and flow in coalbed reservoirs: Implementation of a Bidisperse pore model for gas diffusion in coal matrix. In *SPE Annual Technical Conference and Exhibition.* Society of Petroleum Engineers.

Shi, J. Q., Durucan, S. (2004). Drawdown induced changes in permeability of coalbeds: A new interpretation of the reservoir response to primary recovery. *Transport in porous media, 56*(1), 1-16. https://doi.org/10.1023/B:TIPM.0000018398.19928.5a

Shi, J. Q., Durucan, S. (2005). A model for changes in coalbed permeability during primary and enhanced methane recovery. *SPE Reservoir Evaluation & Engineering, 8*(04), 291-299. https://doi.org/10.2118/87230-PA

Shi, J. Q., & Durucan, S. (2005). CO2 storage in deep unminable coal seams. *Oil & gas science and technology, 60*(3), 547-558. https://doi.org/10.2516/ogst:2005037

Shi, J. Q., & Durucan, S. (2005). Gas Storage and Flow in Coalbed Reservoirs: Implementation of a Bidisperse Pore Model for Gas Diffusion in Coal Matrix. SPE Reservoir Evaluation & Engineering, 8(02), 169-175.

Shi, J. Q., Pan, Z., & Durucan, S. (2014). Analytical models for coal permeability changes during coalbed methane recovery: Model comparison and performance evaluation. International Journal of Coal Geology, 136, 17-24.

Shi, J. Q., Rubio, R. M., & Durucan, S. (2016). An improved void-resistance model for abandoned coal mine gas reservoirs. *International Journal of Coal Geology, 165,* 257-264. https://doi.org/10.1016/j.coal.2016.09.001

Singh, V. K. (2014). Assessment of sudden permeability uptick with depletion in coal bed. *In Retrieved from Southern Illinois University, Carbondale, Open SIUC, Paper 1503*.

Siriwardane, H., Haljasmaa, I., McLendon, R., Irdi, G., Soong, Y., Bromhal, G. (2009). Influence of carbon dioxide on coal permeability determined by pressure transient methods. *International Journal of Coal Geology, 77*(1), 109-118. https://doi.org/10.1016/j.coal.2008.08.006

Small, J. C., Booker, J. R., Davis, E. H. (1976). Elasto-plastic consolidation of soil. *International Journal of Solids and Structures, 12*(6), 431-448. https://doi.org/10.1016/0020-7683(76)90020-2

Snow, D. T. (1968). Rock fracture spacings, openings, and porosities. *Journal of Soil Mechanics & Foundations Division, ASCE, 94*(1), 73–91. Retrieved from https://trid.trb.org/view/126926

Somerton, W. H., Söylemezoğlu, I. M., Dudley, R. C. (1975, June). Effect of stress on permeability of coal. In *International Journal of Rock Mechanics and Mining Sciences & Geomechanics Abstracts* (Vol. 12, No. 5-6, pp. 129-145). https://doi.org/10.1016/0148-9062(75)91244-9

Sparks, D. P., McLendon, T. H., Saulsberry, J. L., Lambert, S. W. (1995). The effects of stress on coalbed reservoir performance, Black Warrior Basin, USA. In *Society of Petroleum Engineers. Annual technical conference* (pp. 339-351). https://doi.org/10.2118/30734-MS

Sroka, A., & Hejmanowski, R. (2006, May). Subsidence prediction caused by the oil and gas development. In *Proceedings 12th FIG Symposium, Baden*.

Stearns, M., Tindall, J. A., Cronin, G., Friedel, M. J., & Bergquist, E. (2005). Effects of coal-bed methane discharge waters on the vegetation and soil ecosystem in Powder River Basin, Wyoming. *Water, Air, and Soil Pollution, 168*(1-4), 33-57. https://doi.org/10.1007/s11270-005-0588-z

Sun, Z., Li, X., Shi, J., Yu, P., Huang, L., Xia, J., ... & Feng, D. (2017). A semi-analytical model for drainage and desorption area expansion during coal-bed methane production. *Fuel, 204,* 214-226. https://doi.org/10.1016/j.fuel.2017.05.047

Sung, W., Ertekin, T., & Schwerer, F. C. (1986, January). The development, testing, and application of a comprehensive coal seam degasification model. In SPE Unconventional Gas Technology Symposium. Society of Petroleum Engineers.

Teatini, P., Gambolati, G., Ferronato, M., Settari, A. T., & Walters, D. (2011). Land uplift due to subsurface fluid injection. *Journal of Geodynamics, 51*(1), 1-16. https://doi.org/10.1016/j.jog.2010.06.001

Terzaghi, K. (1925). Principles of soil mechanics. *Engineering News-Record, 95*(19-27), 19-32.

Thararoop, P., Karpyn, Z. T., Ertekin, T. (2012). Development of a multi-mechanistic, dual-porosity, dual-permeability, numerical flow model for coalbed methane reservoirs. *Journal of Natural Gas Science and Engineering, 8,* 121-131. https://doi.org/10.1016/j.jngse.2012.01.004

Theis, C. V. (1935). The relation between the lowering of the piezometric surface and the rate and duration of discharge of a well using ground-

water storage. *EOS, Transactions American Geophysical Union, 16*, 519–524. https://doi.org/10.1029/TR016i002p00519

Thimons, E. D., Kissell, F. N. (1973). Diffusion of methane through coal. *Fuel, 52*(4), 274-280. https://doi.org/10.1016/0016-2361(73)90057-4

Touzani, R., Alessio, L., Kuzmichev, D., & Buoy, R. (2017). Finite element solution for a coal-bed methane reservoir model. Mathematics and Computers in Simulation, 137, 448-461. https://doi.org/10.1016/j.matcom.2017.01.005

Towler, B., Firouzi, M., Underschultz, J., Rifkin, W., Garnett, A., Schultz, H., ... & Witt, K. (2016). An overview of the coal seam gas developments in Queensland. *Journal of Natural Gas Science and Engineering, 31*, 249-271. https://doi.org/10.1016/j.jngse.2016.02.040

Tuncay, K. and Corapcioglu, M.Y. (1995). Effective stress principle for saturated fractured porous media. *Water Resources Research, 31*(12), 3101-3106. https://doi.org/10.1029/95WR02764

Underground COAL. (2013). Permeability: Degree of fracturing. Outburst, overview, definitions. Underground COAl website http://www.undergroundcoal.com.au/outburst/fracturing.aspx (accesssed 08 December 2018).

Unsal, E., Matthäi, S. K., & Blunt, M. J. (2010). Simulation of multiphase flow in fractured reservoirs using a fracture-only model with transfer functions. *Computational Geosciences, 14*(4), 527-538.

Van Bergen, F., Pagnier, H., & Krzystolik, P. (2006, June). Field experiment of

CO2-ECBM in the Upper Silesian Basin of Poland. In *Proceedings of the 8th International Conference on Greenhouse Gas Control Technologies, Trondheim, Norway.*

Van Everdingen, A. F., & Hurst, W. (1949). The application of the Laplace transformation to flow problems in reservoirs. *Journal of Petroleum Technology, 1*(12), 305-324. https://doi.org/10.2118/949305-G

Van Genuchten, M. T. (1980). A closed-form equation for predicting the hydraulic conductivity of unsaturated soils 1. *Soil science society of America journal, 44*(5), 892-898. doi:10.2136/sssaj1980.03615995004400050002x

Verruijt, A. (1969). Elastic storage of aquifers. *Flow through porous media, 1*, 331-376.

Vohralík, M., & Wheeler, M. F. (2013). A posteriori error estimates, stopping criteria, and adaptivity for two-phase flows. *Computational Geosciences, 17(5)*, 789-812.

Wang, G. X., Massarotto, P., Rudolph, V. (2009). An improved permeability model of coal for coalbed methane recovery and CO 2 geosequestration. International Journal of Coal Geology, 77(1), 127-136.

Wan, Y., Liu, Y., Ouyang, W., Liu, W., & Han, G. (2016). Desorption area and pressure-drop region of wells in a homogeneous coalbed. *Journal of Natural Gas Science and Engineering, 28*, 1-14. https://doi.org/10.1016/j.jngse.2015.11.026

Wang, G. G., Zhang, X., Wei, X., Fu, X., Jiang, B., & Qin, Y. (2011). A review on

transport of coal seam gas and its impact on coalbed methane recovery. Frontiers of Chemical Science and Engineering, 5(2), 139-161.

Wang, K., Zang, J., Wang, G., & Zhou, A. (2014). Anisotropic permeability evolution of coal with effective stress variation and gas sorption: model development and analysis. *International Journal of Coal Geology, 130*, 53-65.

Wang, Y., Zhang, M. S., Hu, F. S., Dong, Y., & Yu, K. (2018). A Coupled One- Dimensional Numerical Simulation of the Land Subsidence Process in a Multilayer Aquifer System due to Hydraulic Head Variation in the Pumped Layer. *Geofluids*, 2018. https://doi.org/10.1155/2018/4083439

Warren, J.E., Root, P J., et al. (1963). The behavior of naturally fractured reservoirs. *Society of Petroleum Engineers Journal, 3*(3), 245-255. https://doi.org/10.2118/426-PA

Wei, X. R., Wang, G. X., Massarotto, P., Golding, S. D., & Rudolph, V. (2007). A Review on Recent Advances in the Numerical Simulation for Coalbed-Methane-Recovery Process. SPE Reservoir Evaluation & Engineering, 10(06), 657-666.

Wei, Z., and Zhang, D. (2010). Coupled fluid-flow and geomechanics for triple-porosity/dual-permeability modeling of coalbed methane recovery. *International Journal of Rock Mechanics and Mining Sciences, 47*(8), 1242-1253. https://doi.org/10.1016/j.ijrmms.2010.08.020

Wen, Z., Huang, G., & Zhan, H. (2009). A numerical solution for non-Darcian flow to a well in a confined aquifer using the power law function. *Journal of Hydrology, 364(1-2)*, 99-106.

Wong, S., Law, D., Deng, X., Robinson, J., Kadatz, B., Gunter, W. D., ... & Fan, Z. (2006, June). Enhanced coalbed methane, micropilot test at south qinshui, shanxi, china. In *Proceedings of the 8th International Conference on Greenhouse Gas Control Technologies, Trondheim, Norway*.

Wouwer, A. V., Saucez, P., Schiesser, W. E., & Thompson, S. (2005). A MATLAB implementation of upwind finite differences and adaptive grids in the method of lines. Journal of computational and applied mathematics, 183(2), 245-258.

Wu, Y., Liu, J., Elsworth, D., Miao, X., & Mao, X. (2010). Development of anisotropic permeability during coalbed methane production. Journal of Natural Gas Science and Engineering, 2(4), 197-210.

Wu, J., Shi, X., Ye, S., Xue, Y., Zhang, Y., Wei, Z., Fang, Z. (2010). Numerical simulation of viscoelastoplastic land subsidence due to groundwater overdrafting in Shanghai, China. *Journal of Hydrologic Engineering, 15*(3), 223-236. https://doi.org/10.1061/(ASCE)HE.1943-5584.0000172

Wu, G., Jia, S., Wu, B., & Yang, D. (2018a). A discussion on analytical and numerical modelling of the land subsidence induced by coal seam gas extraction. *Environmental Earth Sciences, 77,* 353.

Wu, Y., Pan, Z., Zhang, D., Lu, Z., & Connell, L. D. (2018b). Evaluation of gas production from multiple coal seams: A simulation study and economics. *International Journal of Mining Science and Technology, 28*(3), 359-371. https://doi.org/10.1007/s12665-018-7526-z

Xu, H., Tang, D. Z., Tang, S. H., Zhao, J. L., Meng, Y. J., & Tao, S. (2014). A dynamic prediction model for gas-water effective permeability based on coalbed

methane production data. *International Journal of Coal Geology, 121,* 44-52. https://doi.org/10.1016/j.coal.2013.11.008

Xu, B., Li, X., Ren, W., Chen, D., Chen, L., & Bai, Y. (2017). Dewatering rate optimization for coal-bed methane well based on the characteristics of pressure propagation. *Fuel, 188,* 11-18. https://doi.org/10.1016/j.fuel.2016.09.067

Yamaguchi, S., Oha, K., Fujioka, M., Nako, M., & Muto, S. (2006). Field experiment of Japan CO2 sequestration in coal seams project (JCOP). In *Proceedings of the 8th International Conference on Greenhouse Gas Technologies, Trondheim, Norway*.

Ye, Z., Chen, D., Wang, J. G. (2014). Evaluation of the non-Darcy effect in coalbed methane production. *Fuel, 121,* 1-10. https://doi.org/10.1016/j.fuel.2013.12.019

Young, G. B. C. (1998). Computer modeling and simulation of coalbed methane resources. I*nternational Journal of Coal Geology, 35*(1-4), 369-379.

Zhang, H., Liu, J., Elsworth, D. (2008). How sorption-induced matrix deformation affects gas flow in coal seams: a new FE model. *International Journal of Rock Mechanics and Mining Sciences, 45*(08), 1226-1236. https://doi.org/10.1016/j.ijrmms.2007.11.007

Zhang, J., Feng, Q., Zhang, X., Wen, S., Zhai, Y. (2015). Relative permeability of coal: a review. *Transport in Porous Media, 106*(3), 563-594. https://doi.org/10.1007/s11242-014-0414-4

Zhou, F. (2012). History matching and production prediction of a horizontal

coalbed methane well. *Journal of Petroleum Science and Engineering, 96,* 22-36. https://doi.org/10.1016/j.petrol.2012.08.013

Zhu, W.C., Liu, J. Sheng, J.C., Elsworth, D. (2007). Analysis of coupled gas flow and deformation process with desorption and Klinkenberg effects in coal seams. *International Journal of Rock Mechanics and Mining Sciences, 44*(7), 971-980. https://doi.org/10.1016/j.ijrmms.2006.11.008

Zhu, W. C., Wei, C. H., Liu, J., Qu, H. Y., & Elsworth, D. (2011). A model of coal–gas interaction under variable temperatures. International Journal of Coal Geology, 86(2-3), 213-221.